Cranfield University

Stephen Michael Topliss

Optical Fibre Long Period Grating Sensors with Nanostructured Coatings

Engineering Photonics Group,

School of Engineering

PhD Thesis

Supervisors: Dr. S.W.James, Prof. R.P.Tatam

June 2011

Cranfield University

Engineering Photonics Group,

School of Engineering

PhD Thesis

2011

Stephen Michael Topliss

Optical Fibre Long Period Grating Sensors with Nanostructured Coatings

Supervisors: Dr. S.W.James, Prof. R.P.Tatam

June 2011

This thesis is submitted in partial fulfillment of the requirement for the degree of Doctor of Philosophy

The dual resonant response of long period fibre gratings (LPG) operating near the phase matching turning point to the deposition of nanostructured coatings is explored. A broad range of LPGs have been fabricated with grating periods ranging from 80μm to 180μm, and these have been characterized with three different coating materials, ω-tricosensoic acid, undecyl-calix[4]resorcarene and tert-butyl-calix[8]arene carboxylic acid. The dual resonant response has been exploited with the construction of an LPG based sensor coated with a quinolinium dye forming a pH sensor. The wavelength response of this device was measured with a sensitivity of -0.55pH/nm.

Furthermore, length apodised phase shifted long period gratings have been characterized, and the effect on the dual resonant response has been recorded. Partial coating of this device has resulted in the observation of a bandgap feature in the wavelength response.

The use of calixarenes as a functional coating for long period fibre gratings is also investigated. Calixarene is applied in a thin layer with a thickness of several hundred nm's to the cladding of the fibre in the region containing the LPG sensor. The chemical sensing capabilities of a long period fibre grating sensor is presented for the detection of the volatile organic compounds; hexane, cyclohexane, benzene and toluene. The wavelength response was measured and the sensitivity to toluene vapour was recorded at 1600ppmv/nm. Using intensity detection of the central maxima in the wavelength response, the chemical selectivity is demonstrated showing sensitivity to toluene vapour over 13 times greater compared to hexane vapour.

PUBLICATIONS ARISING FROM THIS WORK:

Journals

1. Korposh, S., James, S.W., Lee, S-W., Topliss, S.M., Cheung, S.C.,Batty, W.J., Tatam, R.P., (2010) “Fiber optic long period grating sensors with a nanoassembled mesoporous film of SiO_2 nanoparticles” *Optics Express,* vol. 18, pp. 13227-13238
2. Topliss, S.M., James, S.W., Davis, F., Higson, S. P. J., Tatam, R.P., (2010) "Optical Fibre Long Period Grating based Selective Vapour Sensing of Volatile Organic Compounds” *Sensors & Actuators B: Chemical.* vol 143, no. 2, pp. 629-634
3. Cheung, C.S., Topliss, S.M., James, S.W., Tatam, R.P.,(2008) "Response of Fibre Optic Long Period Gratings operating near the Phase Matching Turning Point to the Deposition of Nanostructured Coatings” *Journal of the Optical Society of America B: Optical Physics.* vol 25, no. 6, pp. 897-902

Peer reviewed conferences

4. Korposh, S., Batty, W.J., Kodaira, S., Lee, S-W., James, S.W., Topliss, S.M., Tatam, R.P., (2010) “Ammonia sensing using a fibre optic long period grating with a porous nanostructured coating formed from silica nanospheres” Presented at the *4th European Workshop on Optical Fibre Sensors (EWOFS 10),* September 2010. Published in Proceedings of SPIE, vol. 7653, art. no. 76531D-1
5. Topliss, S.M., James, S.W., Davis, F., Higson, S. P. J., Tatam, R.P., (2009) "Species Selective Vapour Sensing of Organic Compounds using Dual Resonant Long Period Fibre Gratings with a Calixarene Coating” Presented at the *20th International Conference on Optical Fibre Sensors (OFS20),* October 2009. Published in Proceedings of SPIE, vol. 7503, art. no. 75031I
6. James, S.W., Topliss, S.M., Cheung, C.S., Tatam, R.P., (2009) "Response of fibre optic long period gratings operating near the phase matching turning point to the deposition of a nanostructured coating” Presented at the *20th International Conference on Optical Fibre Sensors (OFS20),* October 2009. Published in Proceedings of SPIE, vol. 7503, art. no. 750362

Other

7. Topliss, S.M., James, S.W., Davis, F., Tyrrell W. D., Tatam, R.P., (2008) “Long period gratings with nanostructured coatings operating near the phase matching turning point” Presented at *Photon08,* August 2008.

CONTENTS

ACKNOWLEDGEMENTS

I am indebted to Sammy Cheung for training me on the technology, and for always ensuring I had everything I needed. I would like to thank Steve James, my supervisor for giving me freedom in my work, and being a guiding light. His positive disposition was always a source of encouragement. My gratitude goes to the head of the group Ralph Tatam, for making it possible, and leading the way.

Thanks also to Frank Davis from Cranfield Health for giving me the special coating materials, the tetramer and octamer calixarenes, and for supplying me with a constant stream of useful references.

Not forgetting Edmon Chehura, my faithful friend. Jane Hodgkinson for help with calculations. Ricardo Correia for being my PC doctor. Steve Staines for fixing our kit. Wayne Tyrrell for doing some chemistry together. Matthew Partridge for conversations on monolayers. And my colleagues Renata, Tom, Helen, Jin, Ryadh and the rest of the team for their support.

For inspiration in getting started, the Advanced Technology Lectures at the Centre for Advanced Photonics and Electronics in Cambridge, and the Cambridge Science Festival.

I would like to thank the EPSRC for their funding of this PhD.

And finally the woman in my life, Jane. She is the woman behind me, she encouraged me to do what I wanted to do, and for spending our time and money in doing so.

S.M.Topliss

Freda Iris Topliss

5/3/1937 – 12/5/2009

Praise the Lord,

And pray in his name!

Tell everyone what he has done.

Psalm 105, 1 CEV

Edward Harold Wray Topliss

27/10/1912 – 2/8/2009

Be watchful, stand firm in your faith,

Be courageous, be strong.

Let all that you do be done in love.

1 Corinthians 16, 13-14 RSV

CHAPTER 1: INTRODUCTION.

1.1 DIFFRACTION GRATINGS IN OPTICAL FIBRE

Newton[a], Huygens, Young, Fresnel, Fraunhoffer, great names that have been associated with the observation and understanding of diffraction. This property of the wave nature of light can be seen in its purest form through a device known as the diffraction grating, which proves that light does not always travel in straight lines, Figure 1.1. The last two give their names to two forms of diffraction observed in the near field and far field respectively. The first gratings were constructed by Fraunhoffer, and consisted of two parallel screws with fine silver wires stretched between them, making a grating with a period of about 500μm, equal to the pitch of the screws[1]. Fraunhoffer then used a mechanism that ruled gratings using a diamond point on glass and this technique was improved upon by Rowland, who achieved gratings with pitches ranging from ~1μm to 0.25μm[1].

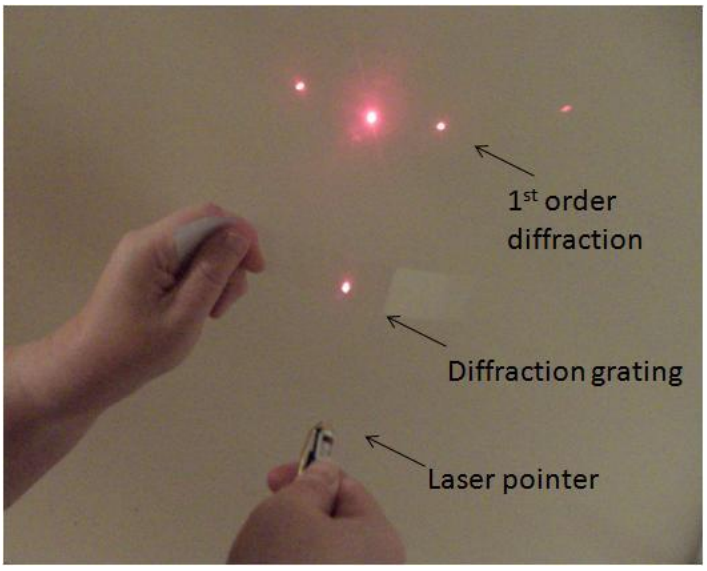

Figure 1.1 Diffraction demonstrated with a diffraction grating and a laser pointer. Light is bent as shown in the 1st order diffracted spot.

The optical fibre has been developed since the 1950s and Charles Kao and George Hockham at STL[b] in 1966 proposed optical fibres as a practical medium for guiding light over long distances[2]. Optical fibres allow light to travel around corners and this is

[a] Diffraction as observed by the broadening of a shadow cast by a thin wire by light[16]

[b] Standard Telecommunication Laboratories, Harlow, Essex, UK

demonstrated by the well known fibre optic lamp, Figure 1.2. Fibre optic cable has subsequently revolutionised data and voice communications.

Figure 1.2 Light guided in a fibre optic lamp. Light is bent along the curved trajectory of each fibre in the bundle.

In 1978, Ken Hill was the first to observe the effects of a diffraction grating in optical fibre[3]. The was a result of a standing wave pattern in the fibre that caused a permanent refractive index perturbation to be imprinted on the fibre core. Many years passed before these devices could be reproduced[4]. These devices have a pitch less than 1μm, and the resulting Fibre Bragg Grating has been exploited in sensor applications for measuring temperature and strain[17-20]. Since the light is tightly guided by the core, this has a positive and negative aspect. The advantage is this insulates the device from unwanted effects from contact with the sensor. The disadvantage is that one is unable to make a sensor that responds to the microenvironment surrounding the fibre.

1.2 LONG PERIOD FIBRE GRATINGS FOR SENSING

Long period gratings (LPGs), which have a pitch of typically several hundred microns, couple light into the evanescent field surrounding the fibre, so that the light can interact with the surrounding environment[5 6]. Increasing the evanescent field at the surface of the fibre is necessary to achieve sensing. One way of doing this is by using a long period grating. Here, changes in the refractive index of the ambient environment surrounding the fibre can be detected. This concept extends also to detecting changes in a thin coating directly applied to the cladding and has significance as a useful method for the interrogation of optical thin films.

Long period fibre gratings have a step modulation of the cores refractive index in the longitudinal axis of the fibre, Figure 1.3. In this way the effects of a diffraction grating are reproduced. Narrow wavelength bands are coupled into the cladding, and this creates drop outs in the transmission response of the fibre that can be monitored.

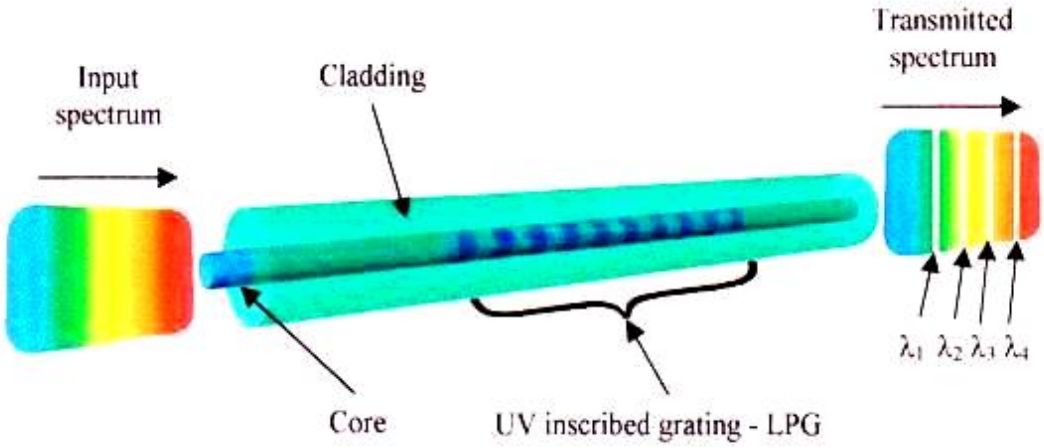

Figure 1.3 The long period grating. Coupling of light from the core to the cladding causes drop outs to appear in the transmitted spectrum[7].

The cladding modes interact with the change in the thickness or refractive index of the optical coating. Since the cladding is a waveguide, there are a discrete set of cladding modes that are supported in the cladding. With changes to the thickness or refractive index of the coating, one of the cladding modes can become partially guided by the optical coating. In this regime, the coupling of the cladding modes can experience a large change in wavelength and coupling strength. This corresponds to a large shift in wavelength or extinction ratio of the core modes attenuation bands. The wavelength or extinction ratio of the attenuation bands is monitored to perform sensing.

1.3 SENSING OF VOLATILE ORGANIC COMPOUNDS

Over the next forty years, the UK will be investing enormous sums of money in the deployment of low carbon power generation, accompanied with the development of the national grid. The carbon footprint extends to all forms of industrial activity, transport and domestic energy requirements. Carbon dioxide is the principal chemical species when considering greenhouse emissions and targets have been set in relation to this species alone. However, interest in the detection of the chemical species constituents in carbon emissions is sure to increase, especially if the legislation evolves in this direction.

Benzene and similar compounds can be emitted in car fuel exhaust systems. It has been reported that benzene and toluene are traffic associated volatile chemicals[8]. Already, analysis in the chemical species emissions from car exhaust gases has begun in the US.

Consequently, development of detection systems for such species may attract research capital over the coming decade. The types of detectors that can be deployed *in the field* overcome the limitation requiring a sample to be taken back to the laboratory, and the need for skilled personnel and complex scientific instrumentation using one of the techniques of mass spectrometry, chromatography, nuclear magnetic resonance, X-ray and IR technology for analysis[21 p570].

In-situ environmental monitoring involves the detection of organic pollutants in the atmosphere and contaminants in water and soil at a low concentration. The detection of organic aromatic compounds like benzene and toluene, which are by-products of the petrochemical industry and fossil fuel systems, is important because of the health risks resulting from their toxicity.

A study was conducted in Sweden of indoor house painters, investigating the negative health effects from exposure to volatile organic solvents. The investigation found that this led to respiratory problems with inflammation of the airways[11]. The MSDS[c] states that a maximum exposure to toluene in the air is 500ppmv (1.88g/m^3)[12]. At higher concentrations, a study reveals that changes to the bodies immune system occurs with exposure to concentrations above 19.2kppmv (72.5g/m^3)[13].

These levels are far higher than would normally be measured in outdoor and indoor working environments. The outdoor air quality at a kindergarten site in Germany was monitored and pollution resulting from heavy traffic pollution was measured for toluene at a mean level of 0.0075ppmv (28.3μg/m^3)[8]. A study at a number of photocopier centres in Taiwan measured the indoor air quality. The results showed a level of toluene concentration in the air up to 3.85ppmv (14.5mg/m^3)[9]. A further study of workers occupationally exposed to toluene showed an ambient air concentration for toluene of between 13ppmv (48.9mg/m^3) to 151 ppmv (568mg/m^3)[10].

Even so, there is also a need for gas detection in the monitoring of manufacturing processes and working environments since systems must be put in place that ensure the safe operating environment for employees.

[c] MSDS Material Safety Data Sheet

1.4 THESIS OBJECTIVES

Fundamental investigative work has been undertaken on long period fibre gratings operating at the phase matching turning point, also known as dual resonance. This has been achieved by controlling the grating pitch of the device to the region of 80μm to 180μm. The practical implications are that it will extend the performance envelope of long period gratings in terms of their sensitivity when deployed as sensors.

The exploitation of the phase matching turning point for long period grating sensors has not been reported widely. The closest reported to the work here is a biosensor using a long period grating with pitch of ~147μm, operating at the phase matching turning point. A polymer material was deposited using electrostatic self assembly, which responded to the concentration of streptavidin[14].

Furthermore, a long period grating with length apodised phase shifts has been investigated, giving for us unique results when used in conjunction with dual resonance. This work is of a practical nature requiring the fabrication of LPG sensors by UV exposure using the point by point technique, and coating the sensors using a Langmuir-Blodgett trough.

Another of the objectives of this work was to characterise different coating materials that became available for such sensors, especially in terms of species selectivity. These novel materials are calixarenes, which are nanoporous with pore sizes in the range 1-3nm, and selectively absorb organic molecules. The investigation procedure adopted here used the technique of injection of a volatile liquid into a chamber with the formation of vapour during its evaporation. With reference to the previous section, this technique allowed for toluene vapour concentrations from 3060ppmv (11.6g/m^3) up to 61200ppmv (231g/m^3) to be investigated.

The use of calixarenes as a functional coating for long period gratings has not been reported before. Calixarenes have been deposited on to the detectors of other sensor types, (e.g. SPR[d] and QCM[e]) but have not been deposited on fibre optic long period grating sensors. The closest identified in the literature deposits a calix[4]arene crown ether onto a Bragg reflector fabricated using an integrated optical device. A single monolayer is deposited and the functional group is not the calixarene moiety but is the crown ether which selectively absorbs potassium cations, and a change in wavelength of the reflection band is observed[15].

---

[d] Surface Plasmon Resonance

[e] Quartz Crystal Microbalance

Overall, this work therefore has been aimed at fabricating and characterizing fibre optic LPG chemical sensors, leading to low cost, chemically selective, reversible sensors which are stable under ambient conditions. The target analytes are benzene, toluene, hexane and cyclohexane, which constitute important chemical species when considering environmental pollution from petrochemicals. The results arising from this work on the species selectivity of the coatings and on dual resonance have been published at conferences and in journals, see the list of publications at the start of the thesis.

1.5 THESIS LAYOUT

The following chapter gives a description of the physics of long period gratings and the changes in their behaviour that occurs when a thin film is coated onto a cladding of the fibre.

Chapter three reports on three techniques for applying coatings to long period gratings, and reviews some topics in chemical sensing that have been reported in regard to these devices.

The next chapter, chapter four, describes the experimental apparatus used throughout the experimental sections of the thesis.

Chapter five gives an experimental investigation into the response of two long period gratings operating near the phase matching turning point. A pH sensing application is reported.

The next chapter, chapter six, is a systematic look at four long period gratings with differing periods between 80μm and 180μm, each coated with three different materials each with a unique refractive index. Some conclusions are drawn from the trends that are observed.

Chapter seven extends the performance of the device by looking at the effect of introducing phase shifts into the long period grating. The twin rejection bands that arise are investigated at the phase matching turning point. Partial coating of this device has led to some unique results.

Chapter eight explores the chemical sensing capabilities of long period gratings coated with a functional material, a calixarene. Dual resonance is exploited facilitating sensing of aromatic vapours. The response was found to be chemically selective.

Chapter nine compares long period gratings with two different calixarene coatings, and their chemical selectivity and kinetic response when sensing organic vapours.

The last chapter gives an overall interpretation of the results across the five experimental chapters, and the logical next steps in developing this work further.

1.6 REFERENCES

1. McKenzie, A. E. E. (1962), *"A second course on light "*, in Cambridge University Press, pp. 302.

2. Gowar, J. (1983), *"Optical Communication Systems"*, in Prentice-Hall International Series in Optoelectronics, pp. 3.

3. Hill, K. O., Fujii, Y., Johnson, D. C. and Kawasaki, B. S. (1978), "Photosensitivity in optical waveguides: Application to reflection filter fabrication", *Applied Physics Letters,* vol. 32, no. 10, pp. 647.

4. Kashyap, R. (1999), *Fiber Bragg Gratings,* Academic Press.

5. Bhatia, V. and Vengsarkar, A. M. (1996), "Optical fiber long-period grating sensors", *Optics Letters,* vol. 21, no. 9, pp. 692-694.

6. Patrick, H. J., Kersey, A. D., Bucholtz, F., Ewing, K. J., Judkins, J. B. and Vengsarkar, A. M. (1997), "Chemical sensor based on long-period fiber grating response to index of refraction", *Conference Proceedings - Lasers and Electro-Optics Society Annual Meeting-LEOS,* vol. 11, pp. 420.

7. Khaliq, S. (2003), *Fibre optic long period gratings for sensing applications*. PhD Thesis, Cranfield University, Cranfield, UK.

8. Rehwagen, M., Schlink, U., Herbarth, O. and Fritz, G. J. (1999), "Pollution profiles at different kindergarten sites in Leipzig, Germany", *Environmental toxicology,* vol. 14, no. 3, pp. 321-327.

9. Lee, C.W., Dai, Y. T., Chien, C. H. and Hsu, D. J. (2006), "Characteristics and health impacts of volatile organic compounds in photocopy centers", *Environmental research,* vol. 100, no. 2, pp. 139-149.

10. Angerer, J., Schildbach, M. and Krämer, A. (1997), "S-p-Toluylmercapturic acid in the urine of workers exposed to toluene: A new biomarker for toluene exposure", *Archives of Toxicology,* vol. 72, no. 2, pp. 119-123.

11. Wieslander, G., Norbäck, D. and Edling, C. (1997), "Airway symptoms among house painters in relation to exposure to volatile organic compounds (VOCs) - A longitudinal study", *Annals of Occupational Hygiene,* vol. 41, no. 2, pp. 155-166.

12. Baker, J. T. MSDS Number: T3913 toluene, 09/16/09.

13. Wichmann, G., Mühlenberg, J., Fischäder, G., Kulla, C., Rehwagen, M., Herbarth, O. and Lehmann, I. (2005), "An experimental model for the determination of

immunomodulating effects by volatile compounds", *Toxicology in Vitro,* vol. 19, no. 5, pp. 685-693.

14. Wang, Z., Heflin, J. R., Van Cott, K., Stolen, R. H., Ramachandran, S. and Ghalmi, S. (2009), "Biosensors employing ionic self-assembled multilayers adsorbed on long-period fiber gratings", *Sensors and Actuators, B: Chemical,* vol. 139, no. 2, pp. 618-623.

15. Oh, M. C., Kim, K. J., Lee, J. H., Chen, H. X. and Koh, K. N. (2006), "Polymeric waveguide biosensors with calixarene monolayer for detecting potassium ion concentration", *Applied Physics Letters,* vol. 89, no. 25.

16. Nelkon, M. (1954), *Light and Sound,* William Heinemann Ltd.

17. Rao, Y. J. (1999), "Recent progress in applications of in-fibre Bragg grating sensors", *Optics and Lasers in Engineering,* vol. 31, pp. 297-324.

18. James, S. W., Dockney, M. L. and Tatam, R. P. (1996), "Simultaneous independent strain and temperature measurement using in-fibre Bragg grating sensors", *Electronics Letters*, vol. 32, pp. 1133-1134.

19. Brady, G. P., Kalli, K., Webb, D. J., Jackson, D. A. Reekie, L., Archambault, J. L. (1997) "Simultaneous measurement of strain and temperature using the first- and second-order diffraction wavelengths of Bragg gratings", *IEE Proceedings: Optoelectronics*, vol. 144 pp. 156-161.

20. Frazão, O., Ferreira, L. A., Araujo, F. M., Santos, J. L. (2005) " Applications of Fiber Optic Grating Technology to Multi-Parameter Measurement", *Fibre and Integrated Optics,* vol. 24, no. 3-4, pp. 227-244.

21. Fraden, J. (2010) *Handbook of Modern Sensors : Physics, Designs and Applications,* Fourth Edition, Springer.

CHAPTER 2: THEORY OF LONG PERIOD FIBRE GRATINGS.

2.1 LONG PERIOD GRATINGS IN OPTICAL FIBRE

A diffraction grating is a periodic structure that causes light to diffract, due to the wave nature of light. A long period fibre grating is often structured as a square wave modulation[1; 2] of the refractive index of the core of the fibre, with a period ranging from tens of microns to several hundred microns. This phase modulation of the fundamental mode in the core causes the coupling of energy from the core mode to the cladding modes, at wavelengths that satisfy the phase matching condition[3].

$$\lambda_{(x)} = \frac{\left(n_{core} - n_{clad(x)}\right)\Lambda}{N} \tag{2.1}$$

where $\lambda_{(x)}$ represents the wavelength at which coupling occurs to the LP_{0x} mode, n_{core} is the effective refractive index of the mode propagating in the core of the fibre, $n_{clad(x)}$ is the effective index of the LP_{0x} cladding mode, N is an integer representing the order of diffraction and Λ is the period of the long period grating.

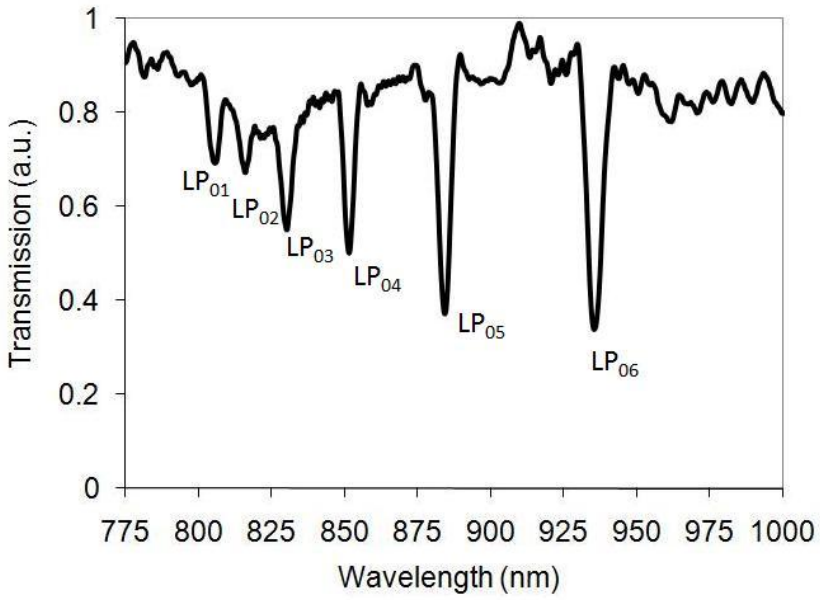

Figure 2.1 The transmission spectrum of a long period grating with a 400μm period, and length 35mm, fabricated using SM750 fibre. The attenuation bands in the spectrum are annotated with their cladding coupling modes.

The fibre cladding is also a waveguide and as such only supports a discrete or finite set of modes. Coupling occurs predominantly to the symmetric cladding modes, denoted

LP_{0x}, meaning that the energy distribution is of the form of concentric rings, where *x* denotes the number of rings.

In Figure 2.1, the extinction of the attenuations bands differ, with the power transfer from core to each cladding mode is determined by Equation 2.2. The power transmission (T) in the fibre[4]

$$T = 1 - \sin^2(\kappa^{(x)}L) \tag{2.2}$$

where $\kappa^{(x)}$ is the cross coupling coefficient of the *x*'th cladding mode, and L is the length of the grating. It can be seen from Equation 2.2 that if

$$\kappa^{(x)}L = \pi/2, 3\pi/2, 5\pi/2\ldots \tag{2.3}$$

then 100% of the light is coupled from the core to the cladding.

The cross coupling coefficient is partly dependent upon the index modulation in the core, Δn_{core}, and over-coupling can occur if the index modulation is increased beyond the optimum point. Likewise, the length of the grating can be optimized. However, this cannot be satisfied for all cladding modes simultaneously, so the grating should be optimized for the selected attenuation band in the chosen application.

2.2 COATINGS ON LONG PERIOD GRATINGS

The deposition of a thin film of the order of several hundred nanometres on the surface of the fibre cladding has been found to cause a change in the central wavelengths of the attenuation bands[5]. For coatings of higher refractive index than the cladding, the typical evolution of the LPG transmission spectrum with increasing coating thickness is shown in Figure 2.2, illustrating the important features.

The central wavelengths of the attenuation bands undergo a *relaxed* step change upon increasing the thickness of the coating, and the extinction of the bands becomes diminished, Figure 2.2. This step change is a result of the influence of the coating on the cladding waveguide, as the coating reaches a critical thickness. As the cladding mode field comprises a number of concentric rings, it has been stated that "*an outer-most lobe of the higher order cladding mode field is transferred from the cladding to the (coating)*"[6].

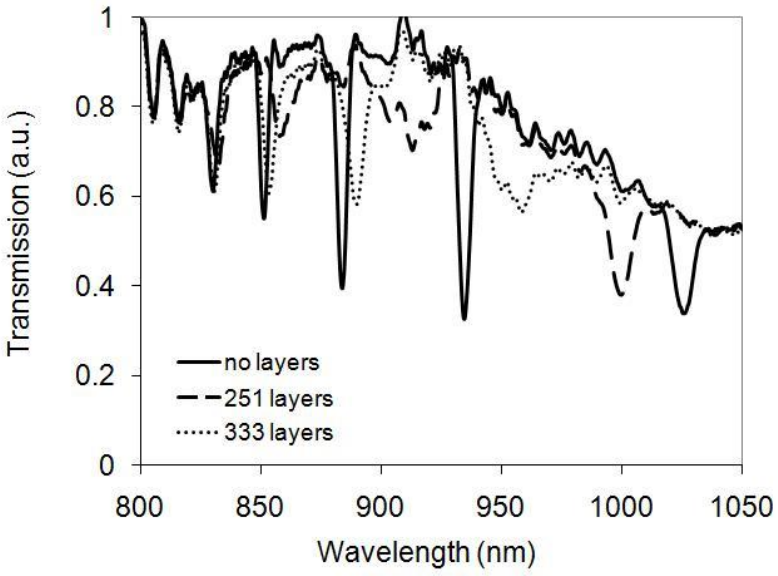

(a)

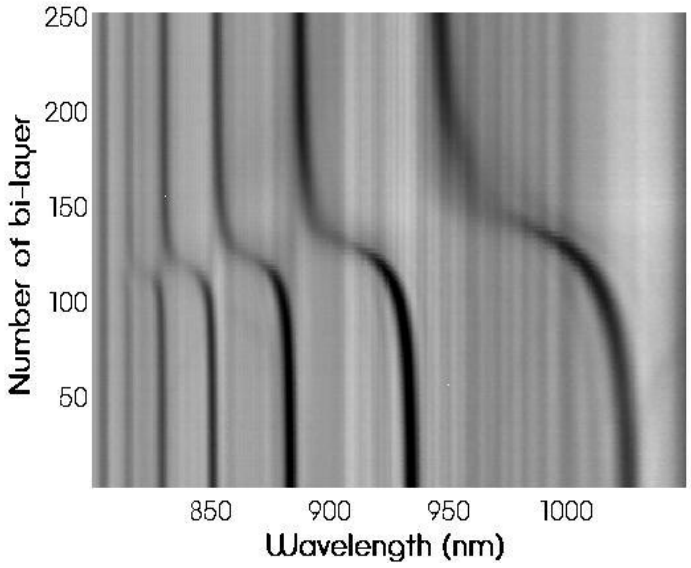

(b)

Figure 2.2 The spectral response of a long period grating with period 400μm to the deposition of a nanostructured coating[f]. The evolution of the spectrum (a) is shown in this grey scale plot (b) with darkness representing the degree of extinction of the attenuation band.

[f] 1-octadecyl-4-[2-(4-methoxy-naphthalene-1-yl)-vinyl]-quinolinium iodide, Cranfield reference APD173

At this point, a reorganisation takes place when one cladding mode is partially guided by the coating, with a higher order mode adopting the effective index of the mode that has now become guided by the coating. At greater coating thickness, the effective index of the mode guided by the coating starts to approach that of the bulk refractive index of the coating, once that cladding mode field becomes increasingly guided by the coating. The first thirteen cladding modes are shown in Figure 2.3, LP_{02} to $LP_{0\,13}$. As the cladding modes LP_{03}, LP_{06}, $LP_{0\,10}$ and $LP_{0\,13}$ become guided by the coating, the other cladding modes effective indices change in concert[7]. In this way, all the cladding modes effective indices increase as the coating thickness increases.

The term *(mode) transition* region has been used to denote the reorganisation that takes place. During the transition region, the attenuation band can diminish in extinction due to weaker coupling from the core to the cladding mode. Computer modelling reflects this if the effective refractive index of the cladding mode is considered as a complex number i.e. real and imaginary[7]. The imaginary component of refractive index is due to *loss* arising from (i) optical absorbance or (ii) scattering which is attributed to coating roughness i.e. irregularities in surface smoothness[8]. After the transition region, there is a restoration of the distribution of effective indices of the cladding modes.

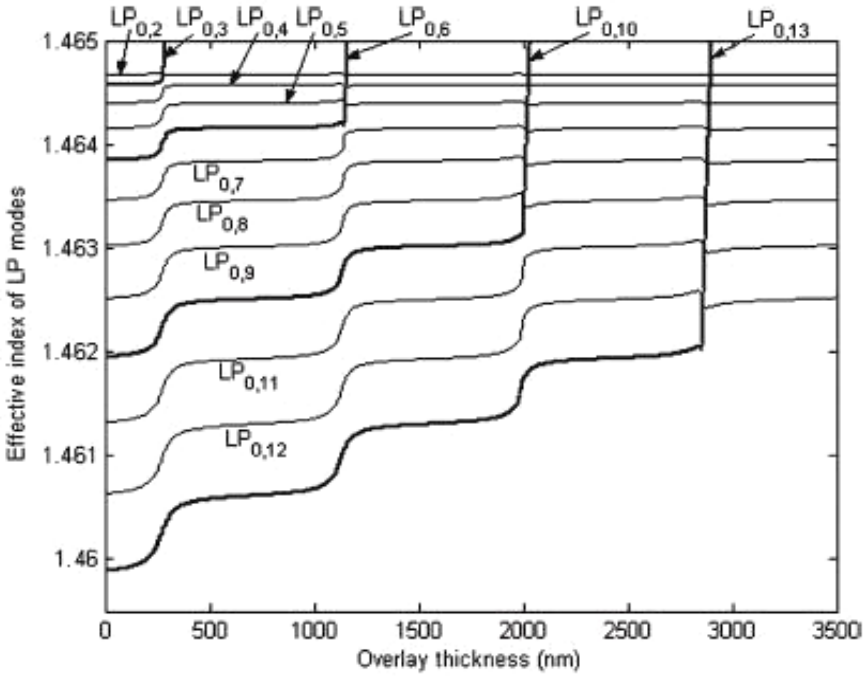

Figure 2.3 The dependence of the effective indices of the cladding modes upon coating thickness. Shown here are cladding modes LP_{02} to $LP_{0\,13}$.

Utilization of the transition region is important since the long period grating displays greater sensitivity to its external environment in this region. The LPG's sensitivity to the properties of the coating can be optimised by selecting a coating thickness that lies in the transition region.

2.3 DISPERSION AND PHASE MATCHING CURVES

The effective refractive indices of the core and cladding modes change with wavelength according to the dispersion curves, a typical set is shown in Figure 2.4[9].

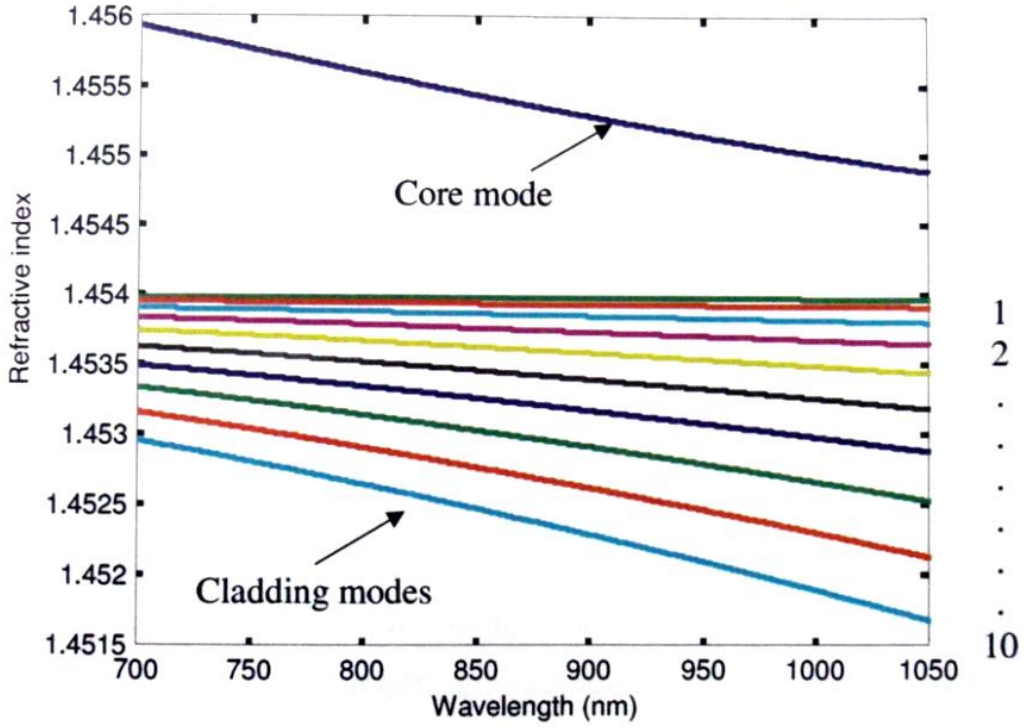

Figure 2.4 The dispersion curves for a long period grating with period 400μm, fabricated in SM750 single mode fibre, with a cut-off wavelength of 650nm. The core mode and the first ten cladding modes are indicated[9].

Knowing the effective indices of the core and cladding modes, the phase matching curves can be derived, according to Equation 2.1. These give a full set of the wavelength resonances that will occur in a long period grating. For long period gratings with periods of several hundred microns, the phase matching curves are illustrated in Figure 2.5[10].

The slope $d\lambda/d\Lambda$ from the phase matching curves is indicative of the sensitivity of the cladding mode to external measurands. The ninth order cladding mode with the largest $d\lambda/d\Lambda$ will exhibit the greatest sensitivity of those represented here. This

concurs with Figure 2.2, where the higher cladding mode shows a larger response to coating thickness.

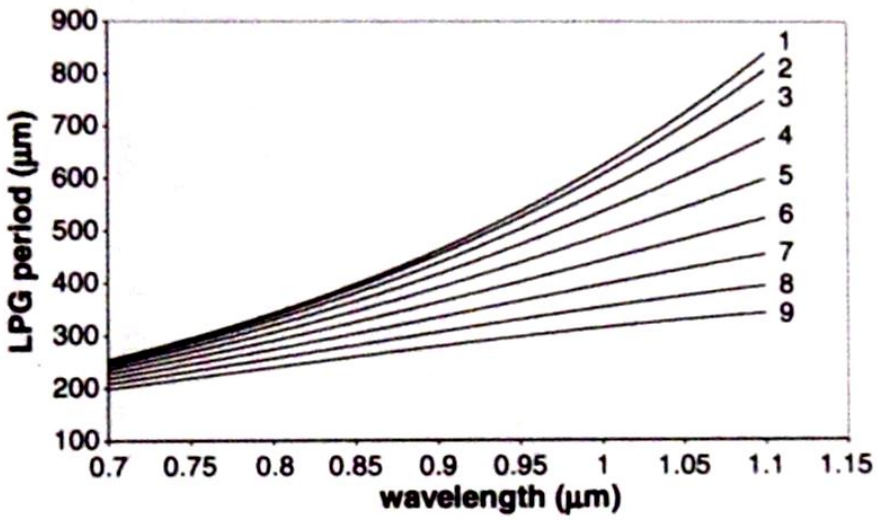

Figure 2.5 The phase matching curves for a long period grating, using single mode fibre with cut-off wavelength of 650nm[10]. The order of the cladding modes are labeled.

2.4 DUAL RESONANCE IN LONG PERIOD GRATINGS

The calculation of the phase matching curves for long period gratings with shorter grating periods show that a turning point occurs when coupling to the higher order cladding modes. This is referred to as the phase matching turning point[11]. Light can be coupled into the same cladding mode at two wavelengths with the formation of two attenuation bands and is known as dual resonance[12].

At the phase matching turning point, $d\lambda/d\Lambda$ becomes infinite meaning the LPG's sensitivity to external measurands is maximized[11]. Therefore, dual resonant cladding modes should be preferentially selected for sensing applications. Dual resonance has been used experimentally in sensing experiments for the measurement of temperature[11; 13], strain[11; 14; 15], surrounding refractive index[11; 16-18], and has been exploited in chemical and biochemical sensing applications for the detection of concentrations of ethanol[17], streptavidin[19] and hemoglobin[20].

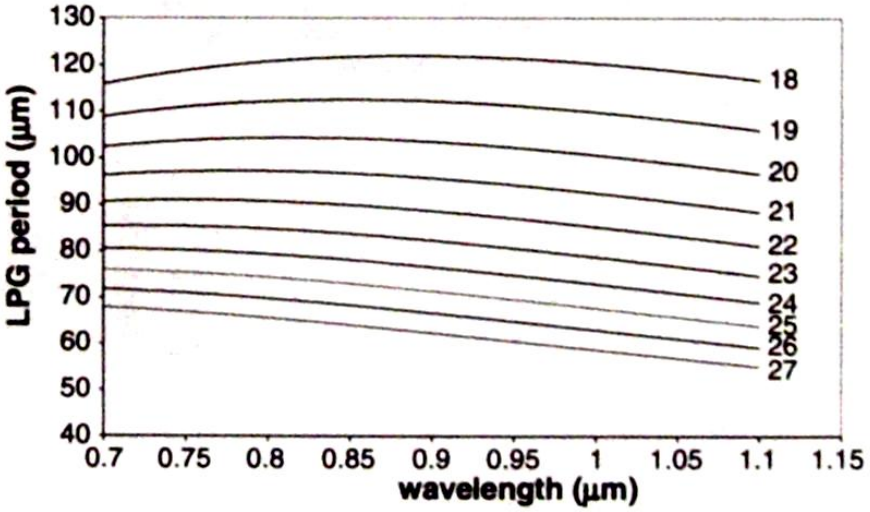

Figure 2.6 The phase matching curves showing the phase matching turning point. A dual resonance occurs in the long period grating, the 18th order cladding mode displays a turning point at a wavelength of ~900nm[10].

2.5 CONCLUSION

Long period gratings contain many attenuation bands in their transmission spectrum resulting from coupling of light from the core to the cladding modes. The extinction ratio of these attenuation bands depend upon the grating length and the cross coupling coefficient which is in turn dependent on the modulation index of the grating, Equation 2.2.

Coating a long period grating reveals that the attenuation bands in the spectrum show greatest sensitivity in the transition region. Figure 2.2 also reveals that the width of the transition region increases with mode order. For sensing applications, high sensitivity can be achieved with monitoring the attenuation band from a higher cladding mode.

The phase matching curves reveal that the sensitivity of a cladding mode to external measurands is dependent upon $d\lambda/d\Lambda$. Modelling the phase matching curves at shorter grating periods shows a turning point where $d\lambda/d\Lambda$ becomes infinite. This indicates that maximum sensitivity can be achieved by monitoring the attenuation bands from a dual resonant cladding mode.

2.6 REFERENCES

1. Fujita, K., Masuda, Y., Nakayama, K., Ando, M., Sakamoto, K., Mohri, J., Yamauchi, M., Kimura, M., Mizutani, Y., Kimura, S., Yokouchi, T., Suzaki, Y. and Ejima, S. (2005), "Dynamic evolution of the spectrum of long-period fiber Bragg gratings fabricated from hydrogen-loaded optical fiber by ultraviolet laser irradiation", *Applied Optics,* vol. 44, no. 33, pp. 7032-7038.

2. Mizunami, T. and Fukuda, T. (2005), "Hydrogen diffusion in fabrication processes of long-period fiber gratings: Measurement and finite-element-method analysis", *Proceedings of WFOPC2005 - 4th IEEE/LEOS Workshop on Fibres and Optical Passive Components* vol. 2005, Article number 1462128, pp. 198-203.

3. James, S. W., Cheung, C. S. and Tatam, R. P. (2007), "Experimental observations on the response of 1st and 2nd order fibre optic long period grating coupling bands to the deposition of nanostructured coatings", *Optics Express,* vol. 15, no. 20, pp. 13096-13107.

4. Kashyap, R. (1999), *Fiber Bragg Gratings* Academic Press.

5. Rees, N. D., James, S. W., Tatam, R. P. and Ashwell, G. J. (2002), "Optical fiber long-period gratings with Langmuir-Blodgett thin-film overlays", *Optics Letters,* vol. 27, no. 9, pp. 686-688.

6. Yang, J., Yang, L., Xu, C. and Li, Y. (2007), "Optimization of cladding-structure-modified long-period-grating refractive-index sensors", *Journal of Lightwave Technology,* vol. 25, no. 1, pp. 372-380.

7. Del Villar, I., Matias, I. R., Arregui, F. J. and Achaerandio, M. (2005), "Nanodeposition of materials with complex refractive index in long-period fiber gratings", *Journal of Lightwave Technology,* vol. 23, no. 12, pp. 4192-4199.

8. Corres, J. M., Matias, I. R., del Villar, I. and Arregui, F. J. (2007), "Design of pH sensors in long-period fiber gratings using polymeric nanocoatings", *IEEE Sensors Journal,* vol. 7, no. 3-4, pp. 455-463.

9. Buggy, S. J. (2008), *Composite material process monitoring using optical fibre grating sensors,* PhD Thesis, Cranfield University, Cranfield, UK.

10. James, S. W. and Tatam, R. P. (2003), "Optical fibre long-period grating sensors: Characteristics and application", *Measurement Science & Technology,* vol. 14, no. 5, pp. R49-R61.

11. Shu, X. W., Zhang, L. and Bennion, I. (2002), "Sensitivity characteristics of long-period fiber gratings", *Journal of Lightwave Technology,* vol. 20, no. 2, pp. 255-266.

12. Shu, X., Zhu, X., Wang, Q., Jiang, S., Shi, W., Huang, Z. and Huang, D. (1999), "Dual resonant peaks of LP015 cladding mode in long-period gratings", *Electronics Letters,* vol. 35, no. 8, pp. 649-651.

13. Shu, X., Zhang, L. and Bennion, I. (2001), "Sensitivity characteristics near the dispersion turning points of long-period fiber gratings in B/Ge codoped fiber", *Optics Letters,* vol. 26, no. 22, pp. 1755-1757.

14. Han, Y. G., Lee, B. H., Han, W. T., Paek, U. C. and Chung, Y. (2001), "Resonance peak shift and dual peak separation of long-period fiber gratings for sensing applications", *IEEE Photonics Technology Letters,* vol. 13, no. 7, pp. 699-701.

15. Grubsky, V. and Feinberg, J. (2000), "Long-period fiber gratings with variable coupling for real-time sensing applications", *Optics Letters,* vol. 25, no. 4, pp. 203-205.

16. Liu, Q., Chiang, K. S. and Liu, Y. (2007), "Characterization of single-mode fiber with fiber Bragg gratings for the design of long-period gratings", *Journal of Lightwave Technology,* vol. 25, no. 8, pp. 2129-2134.

17. Shu, X. W., Zhu, X. M., Jiang, S., Shi, W. and Huang, D. X. (1999), "High sensitivity of dual resonant peaks of long-period fibre grating to surrounding refractive index changes", *Electronics Letters,* vol. 35, no. 18, pp. 1580-1581.

18. Wang, Z. and Ramachandran, S. (2003), "Ultrasensitive long-period fiber gratings for broadband modulators and sensors", *Optics Letters,* vol. 28, no. 24, pp. 2458-2460.

19. Wang, Z., Heflin, J. R., Van Cott, K., Stolen, R. H., Ramachandran, S. and Ghalmi, S. (2009), "Biosensors employing ionic self-assembled multilayers adsorbed on long-period fiber gratings", *Sensors and Actuators, B: Chemical,* vol. 139, no. 2, pp. 618-623.

20. Chen, X. F., Zhou, K. M., Zhang, L. and Bennion, I. (2007), "Dual-peak long-period fiber gratings with enhanced refractive index sensitivity by finely tailored mode dispersion that uses the light cladding etching technique", *Applied Optics,* vol. 46, no. 4, pp. 451-455.

CHAPTER 3: REVIEW OF LPG COATING TECHNIQUES AND LPG BASED CHEMICAL SENSORS

3.1 INTRODUCTION

In Section 2.2, the deposition of a coating on the surface of the fibre cladding causes a change in the central wavelengths of the attenuation bands of an LPG device. This is the basis for creating a chemical sensor by the application of a coating that changes its thickness or density in response to an analyte chemical.

It is important to control of the thickness of the coating (see Section 2.2,) and a number of techniques that allow this have been presented in the following sections. Two chemically responsive coatings that have been widely reported are also reviewed, calixarenes and merocyanine dyes. Also, experimental results for coated LPG based organic chemical sensors have been formulated.

3.2 NANOSTRUCTURED COATING TECHNIQUES

For the deposition of coatings, an important method is the technique of spin coating. A solution of the material to be deposited is placed onto a flat substrate and the substrate is rotated. The centrifugal force causes the solution to become evenly spread over the substrate, and in conjunction with the evaporation of the solvent in the solution, the thickness of the deposited material can be controlled with great reproducibility[1].

Using the spin coating technique, materials have been deposited onto planar sensors, which utilise the Surface Plasmon Resonance (SPR) technique[2]. Using spin speeds of 1000-2000rpm for the deposition of a calixarene[3], and 1000-6000rpm for a poly methyl methacrylate[4], the material forms a thin film on the substrate when it is rotated at high speed.

This technique is normally applied to the coating of wafers. Optical fibres have a cylindrical geometry, so unfortunately this technique cannot be applied for coating the cladding of optical fibres. Apart from rudimentary dipping techniques, three of the most common coating techniques applied to long period fibre gratings are detailed in the next sections, Langmuir-Blodgett (LB), electrostatic self assembly (ESA), and solgel.

3.3 NANOSTRUCTURED COATING TECHNIQUES - LANGMUIR-BLODGETT

The Langmuir-Blodgett (LB) technique[5-10] is a vertical dipping method, which is facilitated by utilization of a Langmuir-Blodgett trough. A thin layer of a material is spread onto the fluid surface of a water subphase, and by compression of the surface

area with a moveable barrier forms a highly packed monomolecular film known as a Langmuir film. The monolayer film is transferred to the fibre surface by the vertical dipping method to create monolayer LB films. Repeated dipping allows a multilayer film to be built up one molecule thickness at a time. In this way, an optical film is deposited on the fibre with such uniformity that it is suitable as an optical wave guide with minimal light scattering properties. Further details of the LB process are given in Chapter four.

The Langmuir-Blodgett process has been used in the deposition of calixarenes onto substrates of ultrasonically cleaned microscopic glass slides coated with a 45nm thick layer of gold. This is to create a sensor which utilizes the Surface Plasmon Resonance (SPR) phenomenon. A toluene vapour sensor has been fabricated in this way[5]. The LB technique has also been used for deposition of calixarenes onto flat hydrophobic glass substrates, in order to perform spectroscopy on the film in the presence of amino acids of the form alanine, glutamic acid and lysine[6].

The LB technique can also be used to deposit a multilayer film with alternating layers of two different materials, by utilizing both compartments of the LB trough. It has been reported that two types of calixarenes, a carboxyl-substituted and an amino-substituted calixarene have been alternately deposited onto a glass microscope slide. The glass substrate has imprinted on it a layer of aluminum forming a bottom electrode. After the LB film is deposited on this electrode, aluminium is thermally evaporated onto the LB film to form a top electrode. The geometry of the resulting structure resembles a capacitor, and this structure has been created to make a temperature sensor which measures the change in current between the two electrodes[7].

It has been reported that stilbazolium merocyanine dye has been deposited onto quartz crystal slides using the LB technique[8]. Furthermore, polished fibre devices have been LB dipped with a bromine-substituted merocyanine dye to create a sensor that is pH sensitive. The sensor consists of a single mode optical fibre that has been side polished. Light from the core mode is evanescently coupled into the coating material, which is deposited as an LB film onto the polished region of the fibre. The dye is a pH sensitive organic material which undergoes a change in its absorption spectra in the presence of an acidic vapour, e.g. hydrochloric acid vapour[9].

The quartz substrate has been LB coated with a calixarene film to form a sensor that responds selectively to aliphatic alcohols e.g. methanol, ethanol, propanol, butanol and pentanol[10]. This is the Quartz Crystal Microbalance (QCM) technique where the variation of the resonance frequency of the quartz crystal oscillator is measured. The alcohol is absorbed into the calixarene, thereby changing the weight of the calixarene

film. Since the calixarene is deposited onto the oscillator there is a commensurate change in the resonance frequency.

3.4 NANOSTRUCTURED COATING TECHNIQUES - ELECTROSTATIC SELF ASSEMBLY

Another technique for depositing coatings is the method of Electrostatic Self Assembly[11-16] (ESA). This requires the dipping of the substrate alternatively into a cationic solution i.e. positively charged molecules, and an anionic solution, i.e. negatively charged molecules. Between each dip, the substrate is washed. Through self assembly, a multilayer structure is built up. It is possible to substitute different solutions to build up a coating comprising different layers of molecules. This technique has been widely applied to fibre substrates.

The first step is to clean the substrate and treat it so that the surface becomes charged, for example negatively. Then the substrate is dipped into a polycation solution, Figure 3.1. The use of poly allylamine hydrochloride (PAH) has been widely reported. This is a polymer with an amine moiety and a hydrochloride moiety. Then the substrate is dipped into a polyanion solution. The anionic solution, poly acrylic acid (PAA) solution has been widely reported. This is a polymer with a carboxylic acid moiety[11]. The ESA process creates a monolayer of a single molecule thickness each time the substrate is dipped. Between each dip, the substrate is rinsed in water or as reported a citrate pH 4.4 buffer solution[12]. This removes the excess molecules. The dipping time is about 4 minutes and the rinse time, 1 minute.

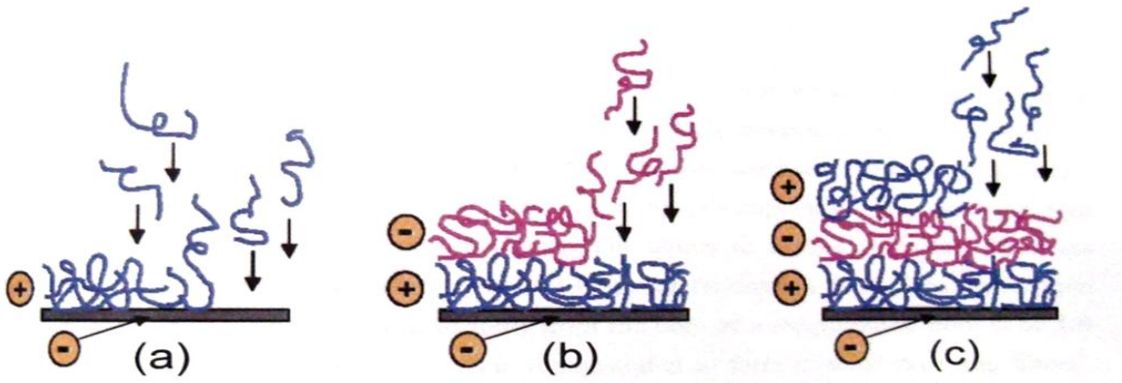

Figure 3.1 The Electrostatic Self Assembly (ESA) process. After the substrate is cleaned and treated so that the surface becomes negatively charged, (a) the substrate is dipped into a cationic solution i.e. positively charged, and (b) into an anionic solution i.e. negatively charged molecules, and (c) into a cationic solution. The molecules self assemble to form a multilayer coating[13].

A 25 layer poly allylamine hydrochloride/poly acrylic acid (PAH/PAA) coating has been used to create a long period grating based pH sensor. The refractive index of the composite PAH/PAA film is 1.55[14]. In the presence of a pH buffer solution, the charges of the PAA chains increase, which changes the electrostatic attraction between the layers. This in turn changes the thickness of the coating which has the effect of a commensurate change in wavelength of the attenuation bands that are characteristic of a long period grating that has been coated with a film of refractive index higher than that of the cladding[15].

The multilayer structure is often referred to as a polymeric matrix. Dopants can be introduced into this structure. In order to do this, the dopants must be added to one of the dipping solutions. The dopant Prussian Blue (PB), which is a dye has been found to improve permeability of the polymeric matrix. A long period grating has been coated with a PAA/PAH multilayer structure to form a pH sensor. A second sensor containing the addition of the dopant PB was found to improve the response time of the sensor, however the sensitivity to pH was diminished[16].

In another example, a tapered optical fibre has been tip coated with a PAA/PAH polymeric coating. Another dopant 1-hydroxypyrene-3,6,8-trisulphonate (HPTS) which is a pH sensitive dye has been added to the polymeric structure. The HPTS is a fluorophore thus enabling the sensor to utilize fluorescence to create a pH sensor on a tip coated tapered optical fibre[11].

Nanoparticles in the form of 20nm silica particles can also be used to build a hydrophilic block in an ESA multilayer structure. The nanoparticles are formed into a polyanion solution which in conjunction with the polycation solution PAH, can then create a multilayer structure through ESA. On top of the hydrophilic layers, a PAH/PAA with dopant HTPS structure was deposited through ESA. A tip coated tapered optical fibre was coated with this complex layer structure to form an optical florescence sensor that is responsive to pH. The hydrophilic block increases the OH- and H+ ion diffusion through the multilayer structure. An improvement in the sensor's response time was observed as compared to a sensor constructed without the hydrophilic block[12].

Other materials have also been deposited using the ESA technique to create a sensor that responds to humidity. It has been reported that a long period grating sensor has been coated using a cationic solution of alumina (Al_2O_3) and an anionic solution of poly sodium 4-styrenesulfonate (PSS). The adsorption of water molecules into this composite film causes the optical thickness to increase, thereby provoking a response in the transmission spectrum of the long period grating[14].

3.5 NANOSTRUCTURED COATING TECHNIQUES - SOL-GEL

A third way is the sol-gel approach, a term which comes from *sol*ution *gel*ation. In the context of fibre optics, it is used as a dip coating process that creates a nanoporous glassy coating on the fibre. The silica sol-gel glass is fabricated using hydrolysis and condensation polymerisation of silicon alkoxide solutions, followed by placing it inside an oven and following a temperature program[17]. A silicon alkoxy compound has for example, four oxygen-ethyl groups attached to the silicon atom. During hydrolysis, some of the oxygen-ethyl moieties are replaced by hydroxyl moieties. This facilitates polymerisation since (i) two silicon-hydroxyl moieties or (ii) a silicon-hydroxyl and a silicon-oxygen-ethyl moiety combines during the condensation reaction to form an amorphous 3D polymer structure of silicon-oxygen-silicon, i.e. the building block of silica glass. The by-product of the reaction (i) is water and is known as water condensation, in the reaction (ii) the by-product is alcohol and is known as alcohol condensation[18].

Dopants can also be introduced during these reactions, see Figure 3.2. The nanoporous glass acts as a support matrix for these dopants, typically analyte sensitive materials i.e. fluorescein. The dye molecules are *entrapped* in the nanoscale cages formed by the cross-linking silicon and oxygen units. With the introduction of an analyte i.e a pH solution, the smaller molecules of the analyte permeate the matrix and access the fluorescein molecules.

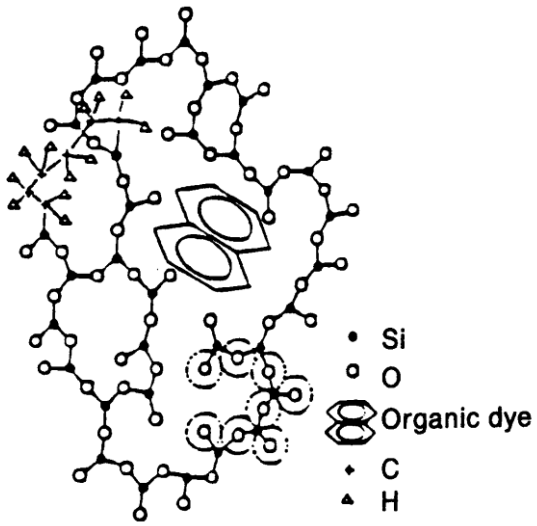

Figure 3.2 The amorphous silicate structure in glassy sol-gel matrices. Here, organic molecules introduced as dopants are trapped as individual entities in the pores of the gel[20].

An evanescent wave fibre optic sensor has been coated with a thin film of sol-gel entrapped fluorescein. A coating was applied to declad optical fibre to a thickness of 300nm. The sensor was placed in pH buffer solutions ranging from 3.5 to 6.5. The fluorescence intensity of the dopant responded to the pH and this was detected optically. A response time of 5s is largely associated with the transfer of the hydrogen ions through the sol-gel matrix to access the fluorescein molecules. The time response is determined to a large extent by the thickness of the coating, which can be accurately controlled by the rate of withdrawal during the dip coating process[19].

Sol-gel glass has some advantages over other techniques. By judicious choice of fabrication parameters e.g. dip velocity, sol viscosity, annealing temperature, the silica cages can be tailored in size appropriate to the size of the dopant molecule. Alternatively, the size of the dopant molecule can be selected that is appropriate for the silica cage. In this way, leaching of the dopants can be made negligible. The sol-gel coating has greater strength in the presence of organic solvents, strong acids and bases as compared to other polymeric sensor compounds[21]. The relatively low temperature of the process enables the use of a wide range of dopants with low thermal stability[22].

3.6 ORGANIC CHEMICAL SENSING – UNCOATED LPGS

Uncoated long period gratings can detect ambient refractive index changes, since some of the cladding mode field extends outside the diameter of the fibre which gives rise to a dependency of the cladding modes on the ambient refractive index. The cladding mode propagation is lossy as compared to core mode propagation, so this gives rise to attenuation bands appearing in the transmission spectrum. By monitoring these attenuation bands, the ambient refractive index can be sensed. The sensitivity of this arrangement is greatest when the ambient refractive index is close to that of the cladding refractive index[23].

A long period grating has been reported that can detect variations in the concentration of the organic compound xylene[24]. The LPG has a period of 111μm, and is immersed in a solution containing the solvent heptane, and xylene. Different concentrations of xylene in the solution are measured by monitoring the wavelength change of an attenuation band in the transmission spectrum. Detectable wavelength shifts were recorded for volumetric concentrations of 0.1% to 0.5% of xylene in the heptane solution. The response is from a change in the ambient refractive index surrounding the LPG due to changes in the refractive index of the solution. The minimum detectable change in refractive index with this detection system is $\Delta n = 6x10^{-5}$. This method is limited in chemical selectivity since the response is only determined by the

refractive index and concentration of the analyte solution. See Table 8.1 for refractive indices of some organic solvents.

3.7 ORGANIC CHEMICAL SENSING – COATED LPGS

For chemical sensing, instead of a direct measurement of the analyte chemical, a reagent mediated measurement can be performed by introducing a coating on the LPG. For coatings of refractive index less than the cladding, the principle above applies, the attenuation bands show a wavelength change due to the change in the surrounding refractive index which includes the coating. However, by introducing a coating of a higher refractive index than the cladding, the sensitivity of the LPG can be increased in the region of mode reorganization[25]. This requires the precise control of the thickness of the coating to access the transition region of the attenuation bands.

A number of LPG based chemical sensors have been reported, and are listed in Table 3.1. Here, some have a coating with a refractive index less than the cladding, ($n_{cladding}$=1.45) and have a coating thickness of tens of microns. The high refractive index (HRI) coatings however are applied to the fibre in a much thinner film, with thickness of several hundred nanometers in order to achieve a high sensitivity.

A zeolite thin film coated LPG has been fabricated and its response to toluene and isopropanol vapour has been measured[26; 27]. Zeolites contain nanoscale pores which are able to selectively absorb molecules. These shape selective cavities are able to separate para-xylene from the meta-xylene and iso-xylene isomers since para-xylene is able to diffuse through this material whilst the other more bulky isomers are far less mobile. This is important in the petroleum industry, since zeolite filters can separate out diffent organic species from petroleum raw materials[28]. Here, a silica zeolite coated LPG with a pore size of 0.6nm has been demonstrated to absorb toluene and iospropanol vapours. The refractive index of the coating was found to increase from $n_{coating}$ = 1.3361 to $n_{coating}$ = 1.402 in isopropanol vapour at a concentration of 5.4kppm. The increase in density and refractive index of the coating provokes a response in the transmission spectrum of the LPG. Wavelength shifts of several nm's have been measured[27].

Another LPG chemical sensor has been reported which responds to the vapours xylene and cyclohexane. A polymer coating, a phenyl-doped polydimethylsiloxane (PDMS), is applied to the fibre cladding, and the analyte molecules are adsorbed into the polymer coating. Here, the refractive index of the coating is $n_{coating}$ = 1.4237, and the presence of the analyte vapours moved the refractive index in opposite directions. For cyclohexane, $n_{cyclohexane}$ = 1.4141 so a reduction in the refractive index of the coating was measured. For xylene, n_{xylene} = 1.4802, so an increase in the refractive index of the

coating was found. These phenomena result in the spectral attenuation bands of the LPG with grating period of 236μm to move in wavelength in opposite directions, of the order of 40-60nm[29].

Table 3.1 Coated long period grating based chemical sensors

LPG Period	Coating	$n_{coating}$	Coating thickness	Analyte
520μm[27]	Silicalite (zeolite)	1.3361	10μm	Toluene and isopropanol vapour
236μm[29]	PDMS[g]	1.4237	20μm	Xylene and cyclohexane vapour
340μm[30]	SPS[h]	1.578	260nm	Chloroform in water solution
450μm[31]	SnO_2 (sol-gel)	1.75	200nm	Ethanol vapour
500μm[32]	Palladium	NK	70nm	Hydrogen Gas

A chloroform chemical sensor has been demonstrated using an LPG with grating period 340μm. A nanoporous material Syniotactic Polytyrene (SPS) has been coated at 260nm in thickness. The size and shape of the chloroform molecule is suited to absorption into the nanoscale cavities in SPS in the crystalline δ form. The δ form is characterized by a "*regularly spaced array of nanocavities of well defined shape and size, where penetrant molecues can be hosted with a certain selectivity based on both size exclusion and host-guest interactions*"[30]. Wavelength shifts in the LPG spectrum of 5-10nm have been measured[30; 33].

Some more LPG's are listed in Table 3.1. A sol-gel derived tin dioxide coated LPG has been reported that can sense ethanol vapour[31]. A palladium coated LPG has also been demonstrated to detect hydrogen gas[32].

[g] PDMS Polydimethylsiloxane

[h] SPS Syndiotactic polystyrene

3.8 ORGANIC CHEMICAL SENSING – MEROCYANINE DYES

An LPG based pH sensor coated with a dye compound, a quinolinium dye, has been described in Chapter 5, see Section 5.5 to 5.7. A related dye compound, a merocyanine dye is reviewed in this section.

Merocyanine dyes may be used as the active material of pH sensors. They are characterized by having a nitrogen atom in an aromatic ring, and a carbonyl group (C=O), of which the oxygen atom that can be reversibly protonated, Figure 3.3. This type of molecule can exist in two distinct formats depending on the pH of the solution into which it is immersed. In the presence of an acid, an H+ ion (proton) from the acidic solution becomes attached to the oxygen atom forming a hydroxyl ion. In a base solution, the merocyanine molecule takes on the unprotonated form, the nitrogen and oxygen atoms are in their oppositely polarised states. This is known as the zwitterionic form. This triggers a rearrangement of the energy states. An electronic reorganisation takes place that travels along the molecule to the nitrogen ion in the aromatic ring, and this changes the absorbance spectra[34]. The absorbance change is reflected in a change of refractive index of the bulk material since refractive index is related to absorbance through the Kramers-Kronig model[9].

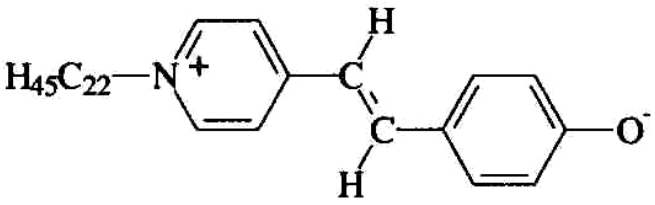

Figure 3.3 The zwitterionic form of a merocyanine dye, E-N-docosyl-4[2-(4-ox phenyl) ethenyl] pyridinium, is unprotonated. The nitrogen and oxygen atoms are in their oppositely polarised states[35].

If a merocyanine dye is applied to the cladding of a long period grating as a high refractive index coating, a change in the LPG resonance band wavelengths will be observed when the coating is exposed to different pH environments. Merocyanine dyes have been reported for pH sensing applications, with a stilbazolium merocyanine dye exhibiting its greatest sensitivity to pH, for pH values ranging from 3 to 5.8[8]. Lower sensitivity is then observed for pH values outside this range. The two forms of the molecule exist in a dynamic equilibrium, where the quantities of each are determined

by the relative H+ and OH- (proton donor & proton acceptor) concentrations. The differing absorbances of each form of the molecule result in an aggregate absorbance spectra for the chemical, indicating the relative proportions of each type of molecule. Outside the pH ranges of 3 and 5.8, the molecule is dominated by one state or the other, Figure 3.4.

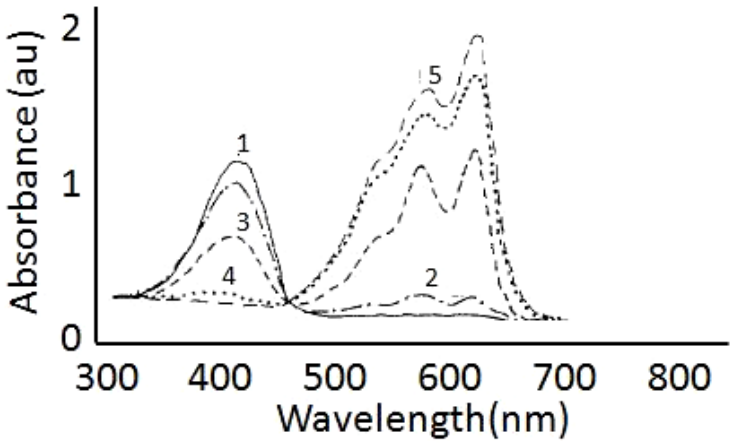

Figure 3.4 The absorption spectra of a merocyanine dye in chloroform solution mixed with buffers of various pH; KEY: (1) pH3, (2) pH4, (3) pH4.9, (4) pH5.8, (5) pH8. The two peaks represent the different absorbances of the protontated and unprotonated form of the molecule[8].

Merocyanine dyes can also be used to detect transition metal ions i.e. Cu2+, Co2+ and Fe3+. In the same way as the H+ protonates the oxygen atom, the presence of these metal ions in solutions changes the absorbance of the merocyanine molecule by protonation. Different absorbance bands have been observed for each metal ion[36].

3.9 ORGANIC CHEMICAL SENSING – CALIXARENES

Calixarenes have been used in this thesis (see Chapters 8 and 9) to create chemical sensors by coating an LPG with a calixarene to detect organic vapours.

Calixarenes have been reported with a number of detector types in order to sense organic compounds. The calixarene molecule contains a molecular cavity, Figure 3.5, and this can encapsulate small organic species through supramolecular binding[28]. The calixarene thus forms a nanoporous matrix structure, which with the adsorption of another chemical species, changes its density. This change in density can be utilized in various types of detectors.

Using Surface Plasmon Resonance (SPR) techniques, calixarene films have been investigated and their response to benzene[37], toluene[2] and chloroform[38]. Chemical sensors are susceptible to cross-sensitivity to other chemical species, whereby there is an interaction between the functional coating and other chemical species which are not the target analyte of the sensor. Chemical selectivity is a measure of the sensors' preference of the target chemical species compared to others[42 p571]. Comparative studies of BTEX compounds at concentrations of 400ppm[3]; benzene, toluene, ethylbenzene and xylene, have shown the chemical selectivity of calixarenes, with ethylbenzene giving the greatest response by a factor of three.

Table 3.2 Organic compound chemical sensing with calixarenes using Quartz Crystal Microbalance (QCM), Surface Plasmon Resonance (SPR) and Discontinuous Gold Film[i] (DGF) techniques. The analyte molecules, benzene, toluene, ethanol, chloroform and butylamine which have been investigated are highlighted.

Coating	Benzene	Toluene	C_2H_5OH	$CHCl_3$	$C_4H_9NH_2$	Detector
Calix[4]resorcarene						SPR[37]
Calix[4]resorcarene						SPR[2]
Calix[4]resorcarene						QCM[10]
Calix[4]resorcarene						SPR[3]
Calix[4]resorcarene & Calix[6]arene						DGF[41]
Calix[4]arene & Calix[6]arene						SPR[38]
Calix[4]arene acid & Calix[6]arene acid						QCM[39]
Calix[8]arene						QCM[40]

[i] The detector comprises gold electrodes coated with a calixarene layer, with the electrical conductivity between electrodes being measured.

The Quartz Crystal Microbalance (QCM) technique has also been used to investigate calixarenes with its response to alcohols from concentrations of 50ppm; methanol, ethanol, propanol, butanol and pentanol. The response was greatest for pentanol, decreasing for the smaller analyte molecules[10]. QCM has also been used for an investigation of the aliphatic amines; propylamine, three isomers of butylamine, diethylamine and triethylamine. The strongest response was with *n*-butylamine[39]. In another report, a comparative study of the solvents; benzene, toluene and chloroform was reported at 40ppm, showing toluene to give the greatest response[40]. See Table 3.2.

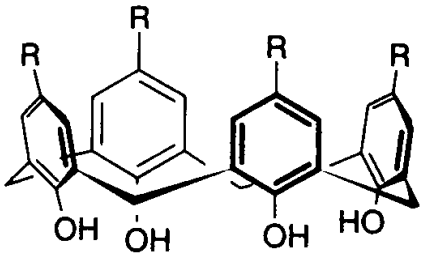

Figure 3.5 The molecular structure of a calixarene, comprising four phenol rings interlinked to form a larger ring. This is a molecular cavity that can encapsulate smaller organic molecules[28].

Another technique reported is where the calixarene is deposited between two electrodes and the electrical conductivity is monitored. Referred to as the Discontinuous Gold Film (DGF) technique, it has been used to investigate the alcohols; methanol and ethanol. Methanol gave the larger response[41].

3.10 SUMMARY

A review of the chemical sensors using the LPG device has been presented, with focus on organic chemicals. This can be achieved by using the LPG in an uncoated form, whereby ambient refractive index changes can be detected to sense the chemical concentration. The wider range of chemicals can be detected using a functional coating applied to the LPG cladding. Here, a porous coating applied selectively absorbs the analyte chemical.

Some widely reported coating materials, calixarenes and merocyanine dyes, have been presented, which have a sensitivity to organic compounds and pH respectively. The work presented in this thesis is based on derivatives from these compounds, to coat the LPG device.

A review of three coating techniques relevant to optical fibre has been presented. One of these, the Langmuir-Blodgett technique, has been used to fabricate optical fibre LPG based chemical sensors described in Chapters 5 to 9.

3.11 REFERENCES

1. Koehler, M. and Fritzsche, W. (2004), "Deposition by Spinning", in *Nanotechnology: An introduction to nanostructuring techniques,* Wiley-VCH Verlag GmbH & Co., pp. 50.

2. Hassan, A. K., Nabok, A. V., Ray, A. K., Lucke, A., Smith, K., Stirling, C. J. M. and Davis, F. (1999), "Thin films of calix-4-resorcinarene deposited by spin coating and Langmuir-Blodgett techniques: Determination of film parameters by surface plasmon resonance", *Materials Science and Engineering C,* vol. 8-9, pp. 251-255.

3. Hassan, A. K., Ray, A. K., Nabok, A. V. and Wilkop, T. (2001), "Kinetic studies of BTEX vapour adsorption onto surfaces of calix-4-resorcinarene films", *Applied Surface Science,* vol. 182, no. 1-2, pp. 49-54.

4. Capan, R., Ray, A. K., Hassan, A. K. and Tanrisever, T. (2003), "Poly(methyl methacrylate) films for organic vapour sensing", *Journal of Physics D: Applied Physics,* vol. 36, no. 9, pp. 1115-1119.

5. Nabok, A. V., Hassan, A. K., Ray, A. K., Omar, O. and Kalchenko, V. I. (1997), "Study of adsorption of some organic molecules in calix[4]resorcinolarene LB films by surface plasmon resonance", *Sensors and Actuators, B: Chemical,* vol. 45, no. 2, pp. 115-121.

6. Sugden, M. W., Richardson, T. H., Davis, F., Higson, S. P. J. and Faul, C. F. J. (2008), "Langmuir and LB properties of two calix[4]resorcinarenes: Interactions with various analytes", *Colloids and Surfaces A: Physicochemical and Engineering Aspects,* vol. 321, no. 1-3, pp. 43-46.

7. McCartney, C. M., Richardson, T., Pavier, M. A., Davis, F. and Stirling, C. J. M. (1998), "The temporal and thermal stability of pyrodectric calix[8]arene Langmuir-Blodgett films", *Thin Solid Films,* vol. 327-329, no. 1-2, pp. 431-434.

8. Martyński, T., Tateishi, T., Miyake, J., Ptak, A. and Frąckowiak, D. (1997), "Two forms of stilbazolium merocyanine on Langmuir-Blodgett monolayers", *Thin Solid Films,* vol. 306, no. 1, pp. 154-159.

9. Flannery, D., James, S. W., Tatam, R. P. and Ashwell, G. J. (1999), "Fiber-optic chemical sensing with Langmuir-Blodgett overlay waveguides", *Applied Optics,* vol. 38, no. 36, pp. 7370-7374.

10. Koshets, I. A., Kazantseva, Z. I., Belyaev, A. E. and Kalchenko, V. I. (2009), "Sensitivity of resorcinarene films towards aliphatic alcohols", *Sensors and Actuators, B: Chemical,* vol. 140, no. 1, pp. 104-108.

11. Goicoechea, J., Zamarreño, C. R., Matias, I. R. and Arregui, F. J. (2007), "Minimizing the photobleaching of self-assembled multilayers for sensor applications", *Sensors and Actuators, B: Chemical,* vol. 126, no. 1, pp. 41-47.

12. Zamarreño, C. R., Bravo, J., Goicoechea, J., Matias, I. R. and Arregui, F. J. (2007), "Response time enhancement of pH sensing films by means of hydrophilic nanostructured coatings", *Sensors and Actuators, B: Chemical,* vol. 128, no. 1, pp. 138-144.

13. Cooper, K. L. (1999), *Electrostatic self assembly of linear and non-linear optical thin films,* PhD thesis, Virginia Polytechnic and State University, Blacksburg, Virginia, USA.

14. Corres, J. M., Del Villar, I., Matias, I. R. and Arregui, F. J. (2008), "Two-layer nanocoatings in long-period fiber gratings for improved sensitivity of humidity sensors", *IEEE Transactions on Nanotechnology,* vol. 7, no. 4, pp. 394-400.

15. Corres, J. M., del Villar, I., Matias, I. R. and Arregui, F. J. (2007), "Fiber-optic pH-sensors in long-period fiber gratings using electrostatic self-assembly", *Optics Letters,* vol. 32, no. 1, pp. 29-31.

16. Corres, J. M., Matias, I. R., del Villar, I. and Arregui, F. J. (2007), "Design of pH sensors in long-period fiber gratings using polymeric nanocoatings", *IEEE Sensors Journal,* vol. 7, no. 3-4, pp. 455-463.

17. MacCraith, B. D. (1998), "Optical fiber chemical sensor systems and devices", in Grattan, K. T. V. and Meggitt, B. T. (eds.) *Optical Fiber Sensor Technology, Volume 4: Chemical and Environmental Sensing,* Kluwer Academic Publishers.

18. Grattan, K. T. V., Badini, G. E., Palmer, A. W. and Tseung, A. C. C. (1991), "Use of sol-gel techniques for fibre-optic sensor applications", *Sensors and Actuators, A: Physical,* vol. 26, no. 1-3, pp. 483-487.

19. MacCraith, B. D. (1993), "Enhanced evanescent wave sensors based on sol-gel derived porous glass coatings", *Sensors and Actuators, B: Chemical,* vol. B11, no. 1-3, pp. 29-34.

20. Shahriari, M. R. (1998), "Sol-gel fiber optical chemical sensors ", in Grattan, K. T. V. and Meggitt, B. T. (eds.) *Optical Fiber Sensor Technology, Volume 4: Chemical and Environmental Sensing,* Kluwer Academic Publishers.

21. Ding, J. Y., Shahriari, M. R. and Sigel Jun, G. H. (1991), "Fibre optic pH sensors prepared by sol-gel immobilisation technique", *Electronics Letters,* vol. 27, no. 17, pp. 1560-1562.

22. MacCraith, B. D., Ruddy, V., Potter, C., O'Kelly, B. and McGilp, J. F. (1991), "Optical waveguide sensor using evanescent wave excitation of fluorescent dye in sol-gel glass", *Electronics Letters,* vol. 27, no. 14, pp. 1247-1248.

23. Patrick, H. J., Kersey, A. D. and Bucholtz, F. (1998), "Analysis of the response of long period fiber gratings to external index of refraction", *Journal of Lightwave Technology,* vol. 16, no. 9, pp. 1606-1612.

24. Allsop, T., Zhang, L. and Bennion, I. (2001), "Detection of organic aromatic compounds in paraffin by a long-period fiber grating optical sensor with optimized sensitivity", *Optics Communications,* vol. 191, no. 3-6, pp. 181-190.

25. Rees, N. D., James, S. W., Tatam, R. P. and Ashwell, G. J. (2002), "Optical fiber long-period gratings with Langmuir-Blodgett thin-film overlays", *Optics Letters,* vol. 27, no. 9, pp. 686-688.

26. Zhang, J., Tang, X., Dong, J., Wei, T. and Xiao, H. (2008), "Zeolite thin film-coated long period fiber grating sensor for measuring trace organic vapors", *Sensors and Actuators, B: Chemical,* vol. 135, no. 2, pp. 420-425.

27. Zhang, J., Tang, X., Dong, J., Wei, T. and Xiao, H. (2008), "Zeolite thin film-coated long period fiber grating sensor for measuring trace chemical", *Optics Express,* vol. 16, no. 11, pp. 8317-8323.

28. Steed, J. W. and Atwood, J. L. (2009), *Supramolecular Chemistry,* Second Edition, John Wiley & Sons, Ltd.

29. Barnes, J., Dreher, M., Plett, K., Brown, R. S., Crudden, C. M. and Loock, H. (2008), "Chemical sensor based on a long-period fibre grating modified by a functionalized polydimethylsiloxane coating", *Analyst,* vol. 133, no. 11, pp. 1541-1549.

30. Cusano, A., Iadicicco, A., Pilla, P., Contessa, L., Campopiano, S., Cutolo, A., Giordano, M. and Guerra, G. (2006), "Coated long-period fiber gratings as high-sensitivity optochemical sensors", *Journal of Lightwave Technology,* vol. 24, no. 4, pp. 1776-1786.

31. Gu, Z. and Xu, Y. (2007), "Design optimization of a long-period fiber grating with sol-gel coating for a gas sensor", *Measurement Science and Technology,* vol. 18, no. 11, pp. 3530-3536.

32. Wei, X., Wei, T., Xiao, H. and Lin, Y. S. (2008), "Nano-structured Pd-long period fiber gratings integrated optical sensor for hydrogen detection", *Sensors and Actuators, B: Chemical,* vol. 134, no. 2, pp. 687-693.

33. Cusano, A., Pilla, P., Contessa, L., Iadicicco, A., Campopiano, S., Cutolo, A., Giordano, M. and Guerra, G. (2005), "High-sensitivity optical chemosensor based on coated long-period gratings for sub-ppm chemical detection in water", *Applied Physics Letters,* vol. 87, no. 23, pp. 234105.

34. Tsuboi, K., Seki, K., Ouchi, Y., Fujita, K. and Kajikawa, K. (2003), "Formation of merocyanine self-assembled monolayer and its nonlinear optical properties probed by second-harmonic generation and surface plasmon resonance", *Japanese Journal of Applied Physics, Part 1: Regular Papers and Short Notes and Review Papers,* vol. 42, no. 2 A, pp. 607-613.

35. Flannery, D., James, S. W., Tatam, R. P. and Ashwell, G. J. (1997), "pH sensor using Langmuir-Blodgett overlays on polished optical fibers", *Optics Letters,* vol. 22, no. 8, pp. 567-569.

36. Cegielski, R., Niedbalska, M. and Manikowski, H. (2001), "Interactions of stilbazolium merocyanine with transition metal ions", *Dyes and Pigments,* vol. 50, no. 1, pp. 35-39.

37. Nabok, A. V., Lavrik, N. V., Kazantseva, Z. I., Nesterenko, B. A., Markovskiy, L. N., Kalchenko, V. I. and Shivaniuk, A. N. (1995), "Complexing properties of calix[4]resorcinolarene LB films", *Thin Solid Films,* vol. 259, no. 2, pp. 244-247.

38. Shirshov, Y. M., Zynio, S. A., Matsas, E. P., Beketov, G. V., Prokhorovich, A. V., Venger, E. F., Markovskiy, L. N., Kalchenko, V. I., Soloviov, A. V. and Merker, R. (1997), "Optical parameters of thin calixarene films and their response to benzene, toluene and chloroform adsorption", *Supramolecular Science,* vol. 4, no. 3-4, pp. 491-494.

39. Liu, Y., You, C., Kang, S., Wang, C., Chen, F. and He, X. (2002), "Synthesis of novel β-cyclodextrin and calixarene derivatives and their use in gas sensing on the basis of molecular recognition", *European Journal of Organic Chemistry,* , no. 4, pp. 607-613.

40. Roesler, S., Lucklum, R., Borngraeber, R., Hartmann, J. and Hauptmann, P. (1998), "Sensor system for the detection of organic pollutants in water by thickness shear mode resonators", *Sensors and Actuators, B: Chemical,* vol. B48, no. 1 -3 pt 4, pp. 415-424.

41. Filenko, D., Gotszalk, T., Kazantseva, Z., Rabinovych, O., Koshets, I., Shirshov, Y., Kalchenko, V. and Rangelow, I. W. (2005), "Chemical gas sensors based on calixarene-coated discontinuous gold films", *Sensors and Actuators, B: Chemical,* vol. 111-112, no. SUPPL., pp. 264-270.

42. Fraden, J. (2010) *Handbook of Modern Sensors : Physics, Designs and Applications,* Fourth Edition, Springer.

CHAPTER 4: EXPERIMENTAL METHODS.

4.1 INTRODUCTION

The processes used in the fabrication of thin film coated optical fibre long period gratings investigated in this thesis are

- hydrogen loading of the optical fibre, to increase its photosensitivity
- writing the long period grating
- depositing the coating

4.2 PHOTOSENSITIZATION OF THE FIBRE

Standard telecoms fibre i.e. low loss germanosilica fibre, has a germanium doped core, with a doping level of ~5% mol. By the incorporation of extra germanium doping to a level between 15% and 20% mol raises the fibres photosensitivity[1]. This type of fibre is referred to as photosensitive fibre. This specialist fibre can easily be used for the fabrication of long period gratings by the direct exposure of the fibre to UV light, see Section 4.3.

Table 4.1 Specification of single mode optical fibre, type SM750. This batch of fibre has been used throughout this thesis for grating fabrication and sensing.

Manufacturer	Fibercore Ltd.
Fibre Type	SM750
Attenuation at 780nm	3.3dB/km
Coating Diameter	239μm
Core Concentricity	0.21μm
Cut-off Wavelength	619nm
Fibre Diameter	124.9μm
Mode Field Diameter	5.2μm
Numerical Aperture	0.12
Operating Wavelength	780nm

For high volume production, it may be cost effective to use standard off-the-shelf fibre of lower cost. In this case, an extra process is required to fabricate an LPG. It is necessary to hydrogen load this fibre to increase its inherent photosensitivity. Taking standard germainium doped fibre and performing hydrogenation increases its photosensitivity by a factor of 2.5[1].

The hydrogen treatment process requires placing the fibre in a sealed chamber for the duration of 14 days at 150 bar pressure at room temperature. The other types of photosensitive fibre i.e. high germanium doped and boron/germanium codoped, give higher photosenstivities upon hydrogenation. Unless otherwise stated, the fibre type throughout this thesis is Fibercore SM750 with a cut-off wavelength of 619nm. The fibre specification is recorded in Table 4.1.

The hydrogen chamber is shown in Figure 4.1. Reeled sections of fibre ~2m in length are inserted into the chamber. Eight retaining bolts and a rubber gasket seal the chamber. The chamber is pressurized with hydrogen from the cylinder, and a tap (not shown) isolates the chamber from the gas cylinder. To remove the fibre, the hydrogen in the pressurized chamber must be slowly released via the outlet shown.

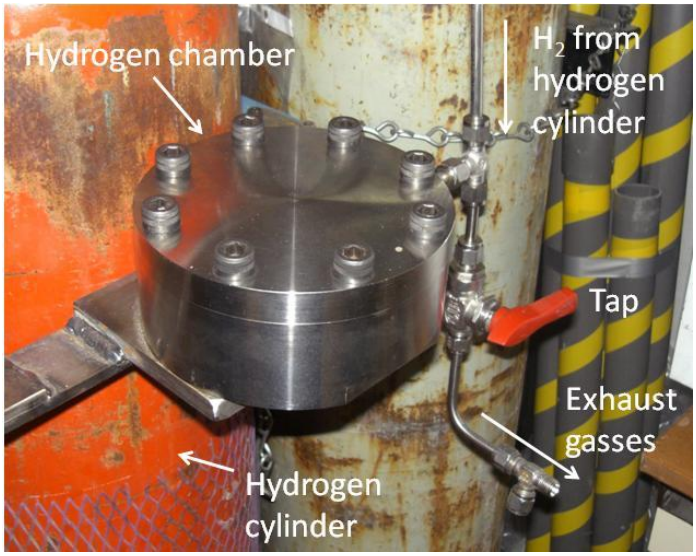

Figure 4.1 The hydrogen chamber. The high pressure sealed hydrogen chamber contains the fibre that is to be hydrogen loaded.

4.3 UV INSCRIPTION

UV inscription of the LPG should take place shortly after the removal of the fibre from the chamber. After a period of ~40 hours, the hydrogen out-diffuses and the enhancement in photosensitivity is lost[15]. To prepare the hydrogen loaded optical fibre for the inscription of the LPG, the polymer buffer coating is removed from the section of the fibre where the grating is to be located. Since the LPG is fabricated in the middle of the fibre, the coating can be removed using Nitromors paint stripper (a substance containing dichloromethane and methanol), as this process is less likely to reduce the strength of the fibre by damaging the surface of the cladding. After three minutes, the polymer coating can be removed with friction using a coarse tissue. Then the target

grating region of the fibre is then cleaned with acetone and optical tissue to remove any residue of the buffer coating. The buffer coating is opaque to UV light, and its presence would prevent the inscription process.

Point by point fabrication of long period gratings is a flexible technique that allows the user to create bespoke designs by selecting the grating pitch, grating length and even the implementation of phase shifts and chirp. The laser used is an injection-seeded frequency quadrupled Spectra Physics Quanta-Ray, Neodynium doped Yttrium Aluminium Garnet (Nd:YAG) which produces ultraviolet (UV) radiation at a wavelength of 266nm and a pulse width of 5ns. The laser is allowed to warm up at low power prior to writing, for a period of 30 minutes. Then the incident optical power is set close to 40mW with the seed on, using a wide area optical power meter located at the cylindrical lens. A further time is allowed for the power to stabilize.

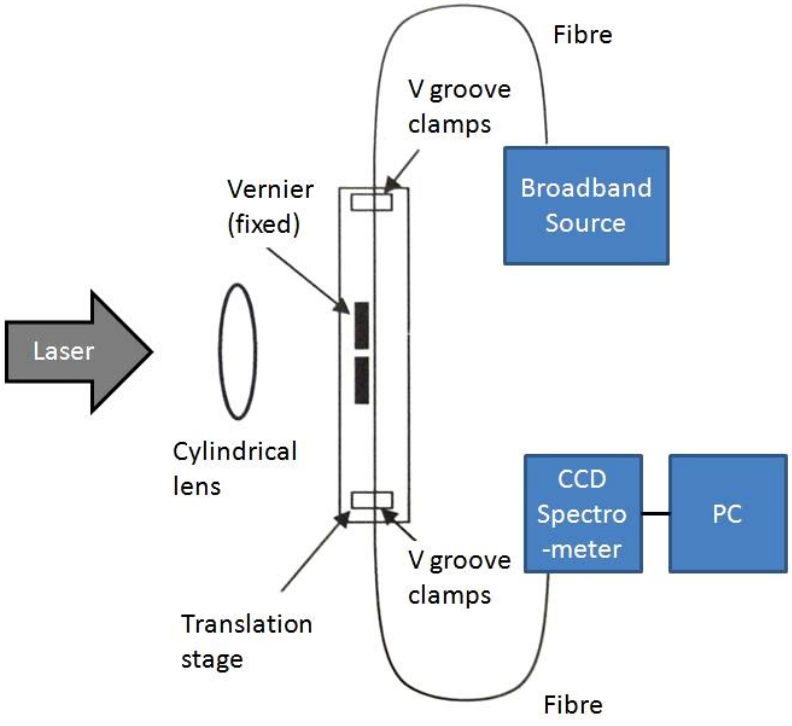

Figure 4.2 Apparatus for UV inscription, with the monitoring of the transmission spectrum of the fibre grating using an Ocean Optics lamp and spectrometer[3].

During writing, the laser irradiates the stripped region of the fibre through the aperture to produce a local change in the refractive index of the core. The fibre is typically exposed for a period of 30 seconds before the fibre is translated along its axis by a distance equal to the desired period, and the next section is exposed. The apparatus is illustrated in Figures 4.2 and 4.3. Here, a cylindrical lens with focal length

100mm focuses the beam into a horizontal stripe. The focus is located a distance approximately 5mm beyond the fibre. Specially adapted vernier calipers with a resolution of 10μm[j], which are fixed to the optical table, act as an adjustable slit. The vernier is used to generate a beam that is a vertical stripe, of width a half of the grating pitch. The fibre is mounted to a computer controlled translation stage which traverses the optical fibre across the slit in a series of steps with the step size equal to the desired grating pitch[2].

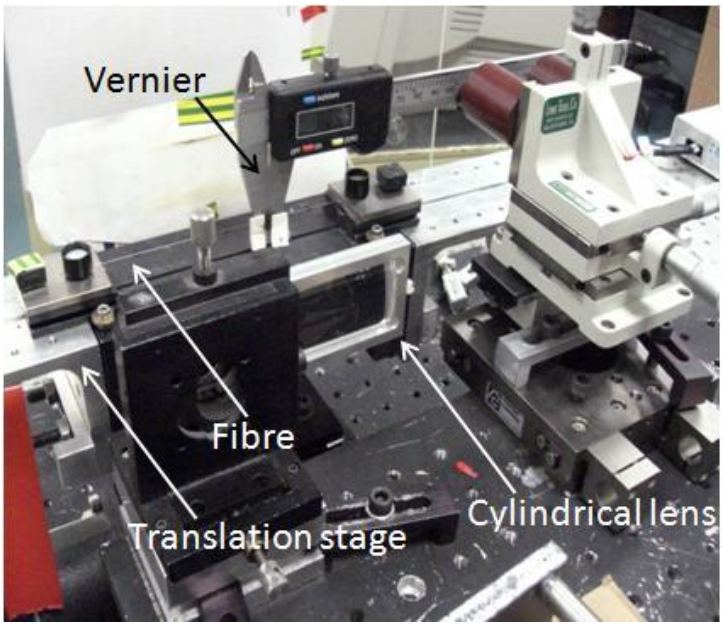

Figure 4.3 Writing of a grating using point by point UV inscription. The vernier caliper is mounted to the bench, with the fibre mounted to the translation stage.

The fibre is mounted horizontally in V grooves, using two magnets at each end of the stripped fibre section to keep the fibre in tension. The fibre is manipulated to be less than 1mm behind the aperture. The translation stage is controlled by a NEAT 3000 programmable controller which can be programmed to move the fibre with a resolution of 2μm. By moving the fibre a distance equal to the grating pitch, a regular induced refractive index change in the core is achieved. The fibre is traversed over a length of between 16mm and 35mm, equal to the final grating length. This process takes several hours, depending upon the grating pitch. It is typically repeated twice to ensure the level of extinction of the LPGs attenuation bands exceeds 4dB.

---

[j] Since the resolution of the vernier caliper is 10μm, and the required mark space ratio of the grating is 50%, this allows only for grating pitches that are divisible by 20μm. The accuracy of the mark space ratio is poor for gratings of these pitches given that the calipers adjustment accuracy is ±5μm.

During the writing process, the transmission spectrum of the optical fibre is monitored using the configuration shown in Figure 4.2. The output from a broadband optical source, in this case a Tungsten Halogen lamp, Ocean Optics HL2000, is coupled to the optical fibre containing the LPG. The transmitted light is detected at the distal end of the fibre using an Ocean Optics S2000 CCD spectrometer interfaced to a computer running propriety software. This spectrometer comprises a fixed grating across a linear Charge Coupled Device (CCD) array. With this arrangement, the light is dispersed across the array with each element of the CCD array assigned a pixel. Each pixel is separated in wavelength by 0.3nm. In this way, the transmission spectrum of the fibre grating in the range 520nm to 1160nm has been captured, with a resolution of 0.3nm.

The attenuation bands in the transmission spectrum of the LPG are monitored during the writing process. The spectrum from the broadband source is first normalized. This can be achieved using a procedure in the Ocean Optics spectrometer application. This allows the extinction of the attenuation bands to be monitored, in order to ensure that coupling has occurred between light in the core mode and the cladding modes.

Table 4.2 Attenuation band extinction ratios after first and second exposure cycles recorded for the fabrication of five 100μm long period gratings

Grating No.	1	2	3	4	5
Grating period	100μm	100μm	100μm	100μm	100μm
1st exposure time	30s	30s	30s	30s	30s
Mean laser power	39mW	40mW	40mW	43mW	42mW
Resulting extinction ratio	2.76dB	2.29dB	1.61dB	2.01dB	1.67dB
2nd exposure time	30s	30s	30s	30s	30s
Mean laser power	43mW	46mW	43mW	43mW	43mW
Final extinction ratio	5.85dB	4.44dB	4.69dB	4.20dB	3.57dB
Grating length	26mm	25mm	23mm	23mm	23mm

It has been noted that an exposure time of 30 seconds on the first pass will result in an extinction ratio of ~2dB, and this is repeated with a further 30 second exposure to obtain an extinction ratio of at least 4dB for the attenuation bands in the central region of the spectrum[k]. A further repeat of the exposure process is sometimes required to achieve this level of extinction. The attenuation band depths of a number

[k] This could also be achieved by a single exposure of 60s. The 30/30 method was used for practicality. Power fluctuations of the UV laser would be more damaging to the fibre with a 60s exposure than a 30s exposure. The risk of fibre breakage is therefore reduced.

of LPGs of period 100μm following the first and second exposure cycles are recorded in Table 4.2.

An alternative to the point by point technique for fabricating LPGs is the amplitude mask method. An amplitude mask is a copper foil that has been machined with a 50/50 mark space ratio. This is mounted to a right angle bracket and both are fixed to the translation stage. The amplitude mask is located less than 1mm in front of the fibre. The mask is irradiated with UV light in a broad area and the fibre is exposed. The fibre and mask assembly is traversed across the beam creating a grating of the required length. The technique lacks the flexibility of the point by point approach, as the period is determined by the mask. However, it is possible to fabricate LPGs more rapidly using this approach. The long period grating of period 400μm reported in Chapter 2 was fabricated in this way.

4.4 LANGMUIR-BLODGETT COATING

The last stage is the process of coating the optical fibre with a thin optical film. The optical coating must be deposited in a uniform manner to minimise optical scattering, and with a high degree of control of the final coating thickness. Various techniques are at our disposal, one of them, the Langmuir-Blodgett (LB) technique, has been adapted here for use on an optical fibre. This technique deposits one molecular layer at a time and forms a multilayer coating which is sometimes described as a nanostructured coating[4].

The equipment used for Langmuir-Blodgett deposition is the Nima Technology LB trough, model 2410A. The basic configuration of the apparatus is shown in Figure 4.4. The Langmuir-Blodgett trough is filled with a liquid of high surface tension, known as the subphase. Here purified water[l] with a resistivity of 0.18MΩm is used.

The apparatus is operated in the dust free environment of a clean room, and the surface of the equipment is cleaned with acetone[m] to remove dust and chemical deposits. The area between the steel barrier and the PTFE barrier is particularly important to clean, Figure 4.5, since deposition takes place in this part of the trough.

[l] Mercury and glycol are examples of other subphase materials[6]

[m] The Perspex parts of the apparatus must be cleaned with isopropanol only

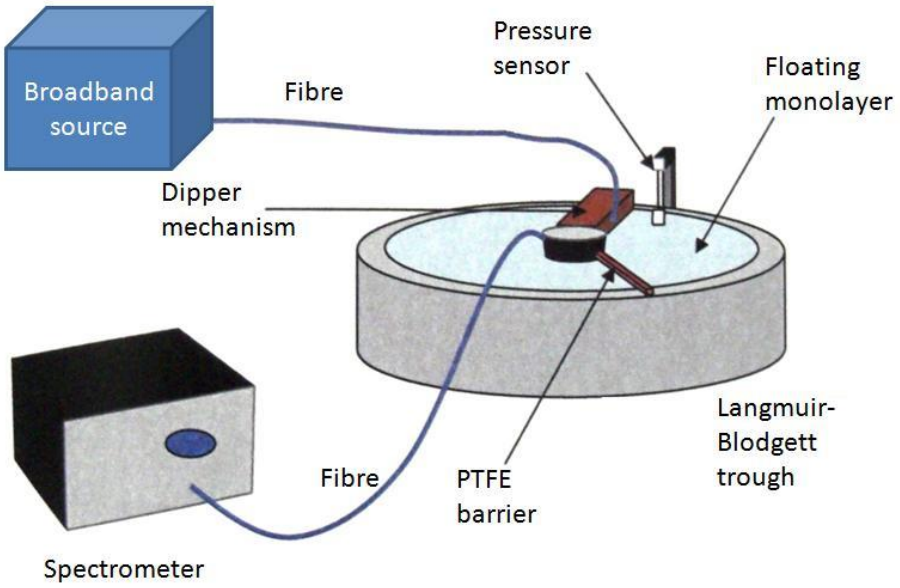

Figure 4.4 The apparatus used for Langmuir-Blodgett deposition. The round trough is shown with a pressure sensor and PTFE barrier. Monitoring optics record the progress of the coating process[5].

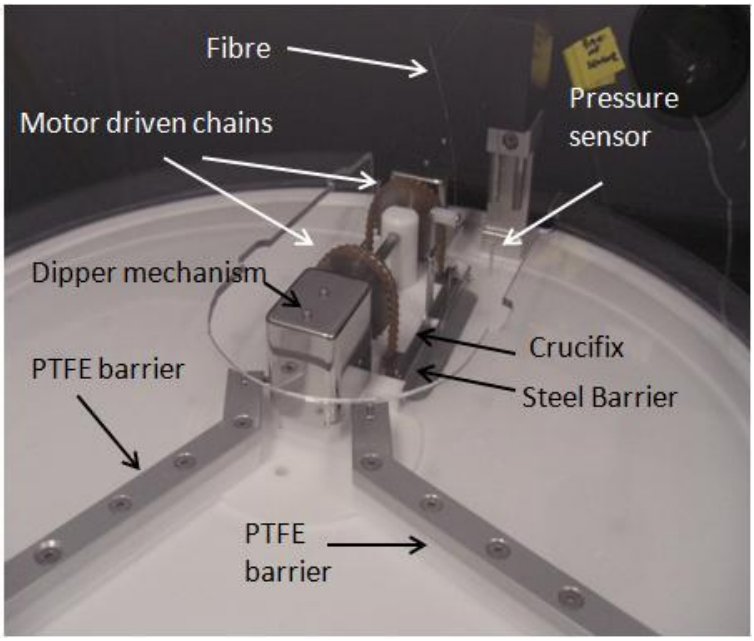

Figure 4.5 Langmuir-Blodgett trough used for depositing optical coatings onto optical fibres. The dipper mechanism shown in the centre raises and lowers the fibre alternately through the subphase. The PTFE barrier controls the surface pressure of the film so that it remains in the 'solid' phase.

A requirement of materials that are to be deposited via this technique is that their molecular structure must be amphiphilic. An amphiphilic molecule consists of a hydrophilic and hydrophobic group in the same molecule. Examples of hydrophilic groups are carboxylic acids, sulphates, amines and alcohols[6]. The hydrocarbon chain found in organic molecules is a hydrophobic group.

The coating material must first be dissolved in a suitable solvent. Here, it was dissolved in the solvent chloroform at a concentration of between 0.1 - 0.2g/l, as detailed in the following chapters. The coating material was then spread onto a pure water subphase of one compartment of the trough. The consequent evaporation of the solvent leaves the amphiphilic molecule as a film on the surface.

With the introduction of the molecule on the surface of the water, the surface tension of the water is reduced. This is monitored by means of a pressure sensor of the form of a Wilhelmy plate pressure sensor. This is a thin plate oriented perpendicular to the surface of the water. The force exerted on it at the air-liquid interface is measured. This sensor is incorporated in a control loop with the PTFE barrier.

Amphiphilic molecules that are deposited onto the surface of the subphase become trapped on the surface. A material with less hydrophobicity would dissolve into the water, a material less hydrophilic may form a thick multilayer film unsuitable for coating.

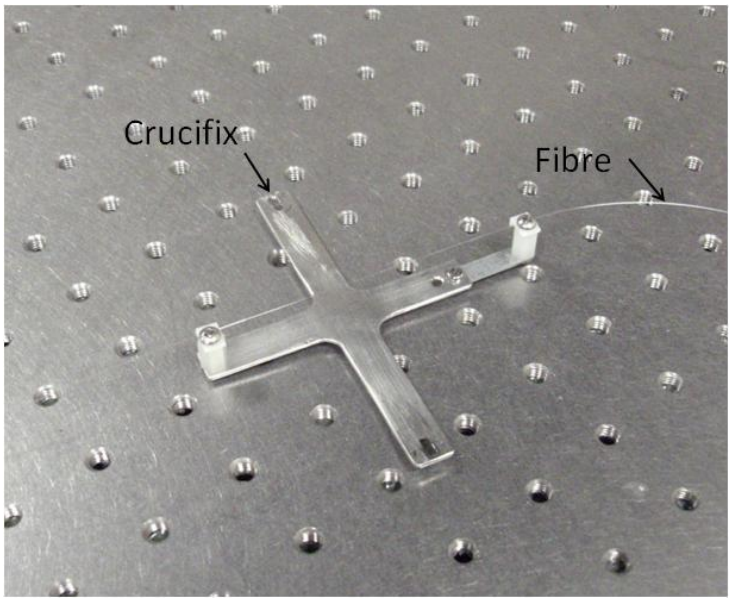

Figure 4.6 The crucifix is a special jig to hold the long period fibre grating and is attached to the dipper mechanism.

Sweeping a PTFE barrier over the surface of the water compresses the molecules into a monolayer. The surface pressure is set to 26-30mN/m, as determined by performing an isotherm on each coating material. An isotherm is a characterization of the molecule by its response to pressure changes while the temperature is constant. The surface pressure set point is established during the isotherm, this process increases the surface pressure of the film to beyond the *solid* phase whereupon the monolayer structure breaks down. Once this has been established, the surface pressure can be set with a margin e.g. 5mN/m, to ensure breakdown will not occur. During deposition, the surface pressure of the film is controlled using a Wilhemy plate operating in a control loop to ensure that it remains in the *solid* phase during the process[7].

The Langmuir-Blodgett technique requires the fibre to be passed vertically through a film of the material to be deposited. The fibre was mounted on the jig shown in Figure 4.6. The fibre is tensioned between the two clamps of the jig to ensure the fibre is straight. By concurrently observing the attenuation band extinction ratio of the transmission spectrum of the LPG, whilst manually tensioning the fibre, the fibre can be correctly tensioned in the jig and clamped.

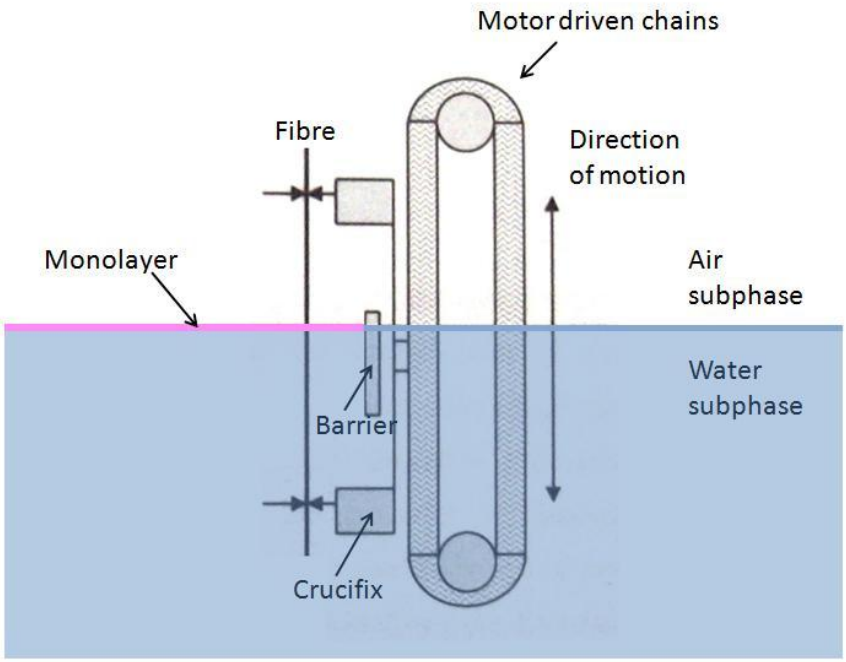

Figure 4.7 The dipper mechanism and the crucifix attachment. The fibre passes through the monolayer which is confined by a steel barrier[5].

The jig is attached to the dipper mechanism behind the steel barrier, and is designed to hold the fibre forward of the barrier, whilst being attached to the dipper mechanism, Figure 4.7. The dipper mechanism is a motor driven chain which lowers and raises the fibre. This operates with the aid of a NIMA controller via a computer running Labview software.

For the correct deposition of a monolayer film onto the fibre, a knowledge of the interaction of the substrate material with water is required. Glass is a hydrophilic material. This means that deposition of the first layer occurs on the upstoke from the water subphase since the shape of the meniscus is not suitable for depositing the molecule on the first downstroke. To avoid problems with unwanted deposits during the first downstroke, the substrate should be immersed in the subphase as the starting position.

After the first upstoke, the substrate is coated with the hydrophilic group of the molecule, which is attached as a molecular film over the substrate. On the next down stroke, the coated substrate now behaves in a hydrophobic way since the hydrophobic part of the chemical forms the surface of the substrate. The meniscus now is suitable for coating on the downstroke and another layer is deposited, the hydrophobic group attaches to the previous layer's hydrophobic group. The layers build up after multiple strokes, resulting in a Y type structure, where the orientation of the molecule on each adjacent layer is opposite, Figure 4.8.

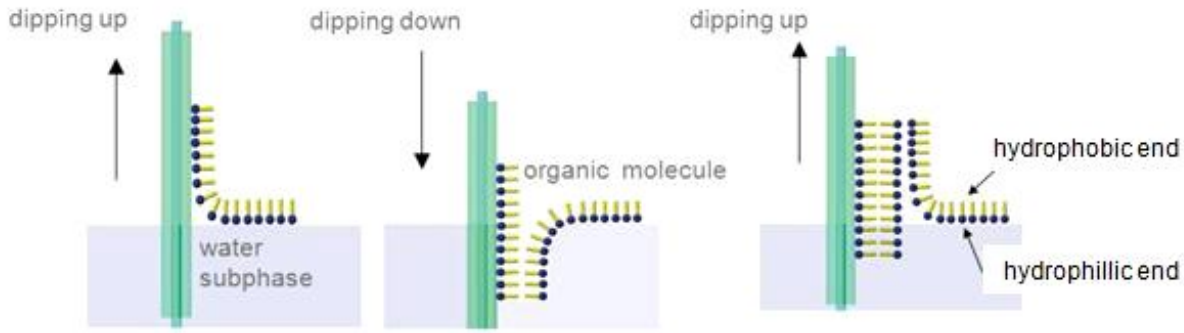

Figure 4.8 The molecular deposition process. The build-up of multiple layers on the substrate forms a Y-type film.

The coating process is stopped when the required coating thickness is achieved. Further details of the optimum coating thickness are given in the following chapters, and are of the order of hundreds of nanometres. The coating process is monitored

using a broadband source, the Ocean Optics HL2000 tungsten halogen lamp, and a spectrometer, the Ocean Optics S2000 CCD analyser as is shown in Figure 4.4. The transmission spectrum of the LPG is recorded at the end of each transit of the dipper. In this way, the evolution of the LPG spectrum is built up after each layer. This process is fully automated[n].

4.5 VAPOUR SENSING

Vapour sensing is performed in a gas chamber to allow the controlled build up of known concentrations of the vapour. The fibre is held in a specially designed jig shown in Figure 4.9, and the fibre must be tensioned in the jig. This is achieved by concurrently observing the LPG transmission spectrum and manually tensioning the fibre so that attenuation bands in the spectrum reach their maximum extinction ratio. The optical source and detector are as stated in Section 4.4. A 1.5 litre jar is used to form a gas chamber. The fibre and jig assembly are inserted into the gas chamber with a steel block at the base of the gas chamber for supporting the jig, see Figure 4.10.

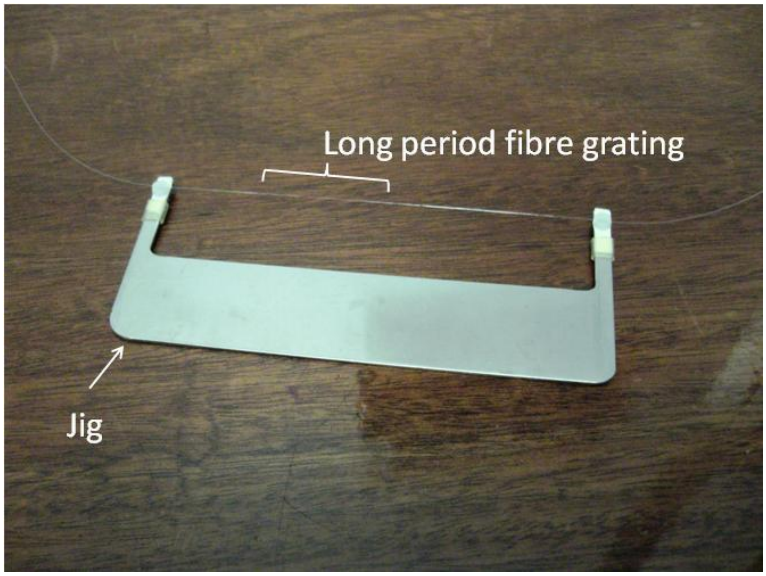

Figure 4.9 A jig used to tension the fibre inside the gas chamber. The long period grating is indicated on fibre, the LPG is about 1 inch in length.

The fibre is fed in and out of the gas chamber between the bung and the lid, ensuring that the fibre is not unduly stressed. Monitoring of the LPG transmission spectrum is necessary since bend losses can cause attenuation in the spectrum at longer

[n] Labview software controls the dipper. This is integrated with Ocean Optics proprietary software capturing the optical response of the spectrometer

wavelengths e.g. above 800nm, owing to the positioning of the fibre between the jig and the lid[o].

The gas chamber is sealed by wrapping a sealing tape around the space between the bung and the lid to prevent leaks. Since the fibre is trapped between the sealing tape and the bung, the transmission spectrum must be monitored to ensure that bending losses are not introduced. If this is the case, the sealing tape is removed, the fibre repositioned, and the bung is resealed with tape.

The Ocean Optics propriety software is used to capture the transmission spectrum at regular intervals. The time interval is normally set to 15s[p]. The signal amplitude detected at a particular wavelength is also recorded, and this is set around the centre wavelength of the dual resonant attenuation band of the long period grating, e.g. 800nm for the 100μm period LPG, and 900nm for the 180μm LPG.

Figure 4.10 The gas chamber is a 1.5 litre jar with an entry point for solvents. The fibre entry and exit point between the lid and bung is indicated.

The solvent under study is introduced into the gas chamber via the aperture in the bung, indicated in Figure 4.10. A pipette or syringe is used to insert the liquid into this tube. The opening of the tube is sealed immediately afterwards to prevent the egress

[o] It may be possible to use an alternative arrangement for fibre entry. A small section of fibre with connectors at each end can be mounted into the lid of the gas chamber and fixed with glue. The gas chamber must be of sufficient size to ensure this arrangement does not introduce fibre bend losses.

[p] The completion time of the sensing experiment is 2-3 hours.

of the solvent vapour. Fixed quantities of the solvents were introduced in steps, Table 4.3, to allow the progressive increase of vapour concentration.

The solvent was allowed to evaporate inside the chamber, and the progress was monitored by observing the change in the long period grating's transmission spectrum. It is reported in Chapter 8 that the optical intensity detected at the centre wavelength of dual resonance is seen to increase, Figure 8.6, and the transient is indicative of the evaporation taking place, Figure 8.9. Once a steady state or a maximum has been reached, then the data was recorded. In the following chapters, the quantities in Table 4.3 have been related to vapour concentrations in ppm by volume, and density in g/m^3, for the complete evaporation of the solvent.

The technique has been developed to allow the chemical selectivity of the sensor to be assessed, by repeating the tests with four organic solvents, toluene, benzene, hexane, and cyclohexane. The relative sensitivities of four sensors to these vapours have been reported in Chapters 8 and 9.

Table 4.3 Quantities of liquid solvent inside the gas chamber.

	Solvent inserted	Total solvent in chamber
Step 1	20µl	20µl
Step 2	30µl	50µl
Step 3	50µl	100µl
Step 4	100µl	200µl
Step 5	100µl	300µl
Step 6	100µl	400µl

Once the maximum concentration has been achieved, the lid is opened and the vapour is allowed to escape inside a fume cupboard. As the vapour concentration returns to zero, the transient response is observed, and some data has been presented on the kinetic response of the sensor in Chapter 9. However, this technique is not the best suited for this purpose, since the action of opening the lid releases the fibre and any bend losses that have been incorporated into the results are removed. A continuous gas flow arrangement[8] would best suit a more in depth analysis of the sensor's kinetics, to observe the effects of drifts and hysteresis. This technique has been reported for the detection of hydrogen[9], nitrogen dioxide[10], ethanol vapour[11], toluene vapour and isopropanol vapour[12].

Vapour sensing has been used for the detection of organic solvents since it has certain advantages over liquid sensing. The first is the results are free from solvent effects[13].

For liquid sensing, small quantities of the analyte to be detected must be dissolved in water or an organic solvent and this can alter the response. When sensing with calixarenes which contain a hydrophobic cavity, the analytes readiness to leave a hydrophilic environment to enter a hydrophobic one can affect the results. Also, the solvent molecule may itself form a complex with the host molecule. It is possible that some solvent molecules form inclusion complexes with the calixarene molecule, e.g. chloroform[14].

4.6 SUMMARY

The practical methodology for the fabrication of a sensor has been presented, a process that requires the inscription of an LPG in the fibre and the deposition of a coating of thickness of several hundred nanometers onto the fibre in the region of the LPG. Since a high level of control in the final coating thickness is required, the Langmuir-Blodgett technique has been adopted, which gives molecular scale control over this parameter.

The method of injection of a volatile solvent into a closed chamber has been adopted for initial investigations into the vapour sensor characteristics of the sensors fabricated in this thesis. This allows for a chemical selectivity of the sensor to be assessed. Some preliminary tests on kinetic response have also been performed. However, a continuous vapour flow set up would be more suitable for this characterization.

4.7 REFERENCES

1. Konstantaki, M., Tamiolakis, Q., Argyris, A., Othonos, A. and Ikiades, A. (2005), "Effects of Ge concentration, boron co-doping, and hydrogenation on fiber bragg grating characteristics", *Microwave and Optical Technology Letters,* vol. 44, no. 2, pp. 148-152.

2. Othonos, A. and Kalli, K. (1999), *Fiber Bragg Gratings: Fundamentals and Applications in Telecommunications and Sensing,* Artech House.

3. Buggy, S. J. (2008), *Composite material process monitoring using optical fibre grating sensors*. PhD thesis. Cranfield University, Cranfield, UK.

4. James, S. W. and Tatam, R. P. (2006), "Fibre optic sensors with nano-structured coatings", *Journal of Optics A-Pure and Applied Optics,* vol. 8, no. 7, pp. S430-S444.

5. Ishaq, I. M. (2006), *Fibre optic long period gratings with nanostructured coatings*. PhD thesis. Cranfield University, Cranfield, UK.

6. Martin, P. S. and Szablewski, M. (1999), *Tensionometers and Langmuir-Blodgett Troughs: Operating Manual,* Nima Technology Ltd.

7. Petty, M. C. (2008), *Molecular Electronics: From Principles to Practice,* John Wiley & Sons Ltd.

8. Nabok, A. V., Hassan, A. K. and Ray, A. K. (2000), "Condensation of organic vapours within nanoporous calixarene thin films", *Journal of Materials Chemistry,* vol. 10, no. 1, pp. 189-194.

9. Wei, X., Wei, T., Xiao, H. and Lin, Y. S. (2008), "Nano-structured Pd-long period fiber gratings integrated optical sensor for hydrogen detection", *Sensors and Actuators, B: Chemical,* vol. 134, no. 2, pp. 687-693.

10. Richardson, T. H., Brook, R. A., Davis, F. and Hunter, C. A. (2006), "The NO2 gas sensing properties of calixarene/porphyrin mixed LB films", *Colloids and Surfaces A: Physicochemical and Engineering Aspects,* vol. 284-285, pp. 320-325.

11. Gu, Z. and Xu, Y. (2007), "Design optimization of a long-period fiber grating with sol-gel coating for a gas sensor", *Measurement Science and Technology,* vol. 18, no. 11, pp. 3530-3536.

12. Zhang, J., Tang, X., Dong, J., Wei, T. and Xiao, H. (2008), "Zeolite thin film-coated long period fiber grating sensor for measuring trace chemical", *Optics Express,* vol. 16, no. 11, pp. 8317-8323.

13. Notestein, J. M., Katz, A. and Iglesia, E. (2006), "Energetics of small molecule and water complexation in hydrophobic calixarene cavities", *Langmuir,* vol. 22, no. 9, pp. 4004-4014.

14. Roesler, S., Lucklum, R., Borngraeber, R., Hartmann, J. and Hauptmann, P. (1998), "Sensor system for the detection of organic pollutants in water by thickness shear mode resonators", *Sensors and Actuators, B: Chemical,* vol. B48, no. 1 -3 pt 4, pp. 415-424.

15. Fujita, K., Masuda, Y., Nakayama, K., Ando, M., Sakamoto, K., Mohri, J., Yamauchi, M., Kimura, M., Mizutani, Y., Kimura, S., Yokouchi, T., Suzaki, Y. and Ejima, S. (2005), "Dynamic evolution of the spectrum of long-period fiber Bragg gratings fabricated from hydrogen-loaded optical fiber by ultraviolet laser irradiation", *Applied Optics,* vol. 44, no. 33, pp. 7032-7038.

CHAPTER 5: LONG PERIOD GRATINGS OPERATING NEAR THE PHASE MATCHING TURNING POINT

5.1 INTRODUCTION

Fibre optic long period gratings (LPGs) have been extensively investigated for sensing applications as a result of their sensitivities to measurands such as temperature[1], strain[1], refractive index[2] and curvature[3], and because of the ability to tune their sensitivity by virtue of the grating period, fibre composition and geometry[4,5]. It has been shown that, for highest sensitivity, the LPG should be designed to couple light from the propagating core mode to a cladding mode at a wavelength near the phase matching turning point[6], which is characterised by the generation of dual resonant bands that show sensitivities of opposite sign. This has been exploited to measure temperature and refractive index with high sensitivity[6].

The transmission spectrum of an LPG exhibits a high sensitivity to the optical properties of coatings of materials of refractive index higher than that of the cladding when the coating is of thickness of order 200 nm[7,8,9]. This sensitivity has been exploited to demonstrate a range of chemical sensors, for example, pH[10], copper[11] and DNA damaging agents[12]. To date, the studies of the response of LPG transmission spectra to the deposition of nanostructured coatings has focused on resonance bands corresponding to coupling to the lower order cladding modes, operating at wavelengths below their phase matching turning point. In this chapter, the response of resonance features designed to appear near the cladding modes' phase matching turning points to the deposition of nanostructured coatings is investigated. These resonance features have been utilized in a pH sensing experiment.

5.2 THEORY

A long period grating is a core-cladding mode coupling device, consisting of a periodic modulation of the refractive index of the core of a fibre. The modulation typically has a period in the range 100μm - 1000μm and may be induced using a variety of techniques, including UV laser irradiation[1], CO_2 laser irradiation[13] and exposure to an electric arc[14]. Efficient coupling between the core and cladding modes occurs only where there is significant overlap between the electric field profiles of the modes. Resonant bands corresponding to coupling from the guided core mode to a discrete set of symmetrical cladding modes appear in the transmission spectrum of the fibre, centred at discrete wavelengths that are governed by the phase matching expression[1].

$$\lambda_{(x)} = \frac{\left(n_{core} - n_{clad(x)}\right)\Lambda}{N} \qquad (5.1)$$

where $\lambda_{(x)}$ represents the wavelength at which coupling occurs to the LP_{0x} mode, n_{core} is the effective refractive index of the mode propagating in the core of the fibre, $n_{clad(x)}$ is the effective index of the LP_{0x} cladding mode, Λ is the period of the LPG and *N* is an integer representing the order of diffraction. The efficiency of coupling to the asymmetric modes is small, and thus in general no attenuation bands corresponding to this coupling are visible in the transmission spectrum.

Calculation of the core and cladding modes' dispersions allows the prediction of the coupling wavelength as a function of the period of the grating. Figure 5.1a shows the phase matching curves for LPGs fabricated in an optical fibre with cut-off wavelength 670nm with periods in the range 350μm to 450μm and over a wavelength range 750nm to 1150 nm. These parameters were selected to match the experimental constraints imposed by the use of a CCD spectrometer to monitor the transmission spectrum of an LPG fabricated in a fibre with cut-off wavelength in the visible region of the spectrum. The data plotted in Figure 5.1 has been calculated using the LP approximation to calculate the dispersion of the core and cladding modes[23].

In the regime depicted in Figure 5.1a, the coupling is to the lower order cladding modes LP_{01} – LP_{08}, with the graphs showing a positive gradient across the wavelength range. For shorter periods, as shown in Figure 5.1b, coupling takes place to higher order cladding modes. The behaviour in this regime is markedly different, with the phase matching condition showing a turning point in the wavelength range of interest. It should be noted that all cladding modes will exhibit a turning point, however for the lower order modes this lies at longer wavelengths, outside the range of interest here.

It is possible to select a period where the coupling to a single cladding mode occurs at two wavelengths. As the period changes, or the difference in the core and cladding mode effective indices change in response, for example, to a change in temperature or in the surrounding refractive index, the central wavelengths of the dual resonance bands move in opposite directions. It has been demonstrated theoretically and experimentally that the LPG resonance bands may exhibit their highest sensitivity to external perturbations at their phase matching turning point[6]. To design a device to operate at a specified wavelength with high sensitivity to external perturbation, a cladding mode and grating period that produce a turning point at that wavelength should be selected.

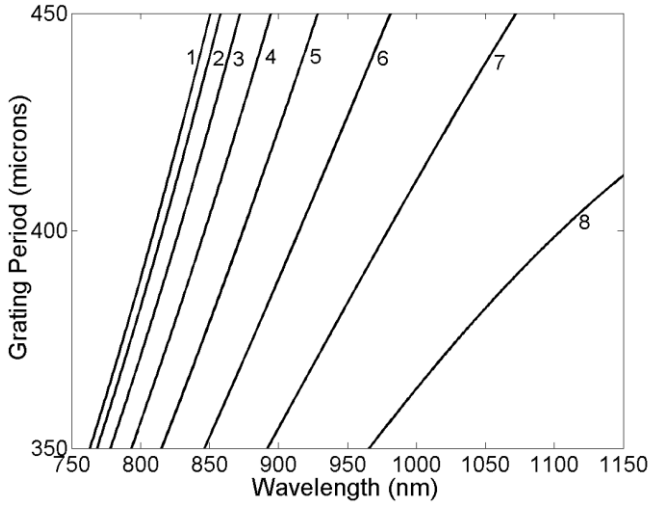

(a)

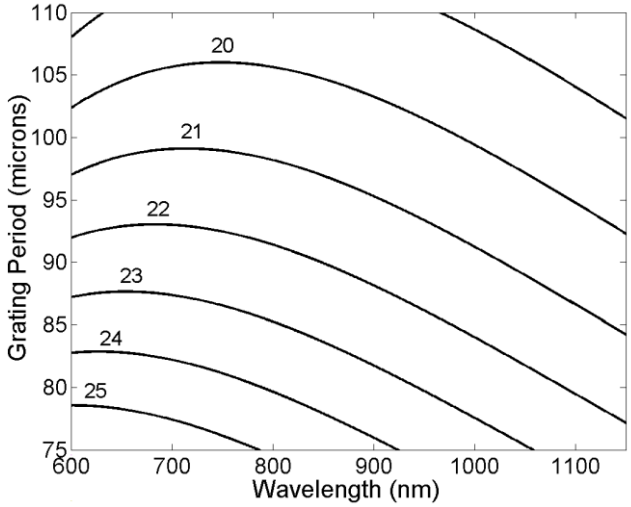

(b)

Figure 5.1 The relationship between the grating period and the wavelength at which coupling occurs to a set of symmetric cladding modes[23] (a) for the first eight modes (b) for the modes 20 – 25. The numbers refer to the order of the cladding mode, LP_{0x}.

5.3 EXPERIMENT

LPGs of length 30mm and of period 80µm and 100µm were fabricated in Fibrecore SM750, a single mode optical fibre with cut-off wavelength 619nm. The photosensitivity of the fibre was enhanced by pressurizing it in hydrogen for a period of 2 weeks at 150 bar at room temperature. The LPGs were fabricated in a point-by-point fashion, illuminating the fibre by the output from a frequency-quadrupled Nd:YAG laser, operating at 266nm. The transmission spectrum of the optical fibre was recorded by coupling the output from a tungsten-halogen lamp into the fibre, and

analysing the transmitted light using a fibre coupled CCD spectrometer. A typical transmission spectrum, illustrating the dual resonance bands, is shown in Figure 5.2a.

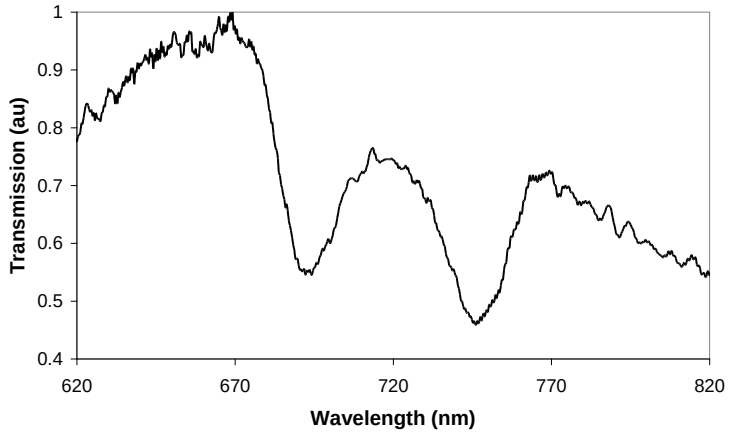

(a)

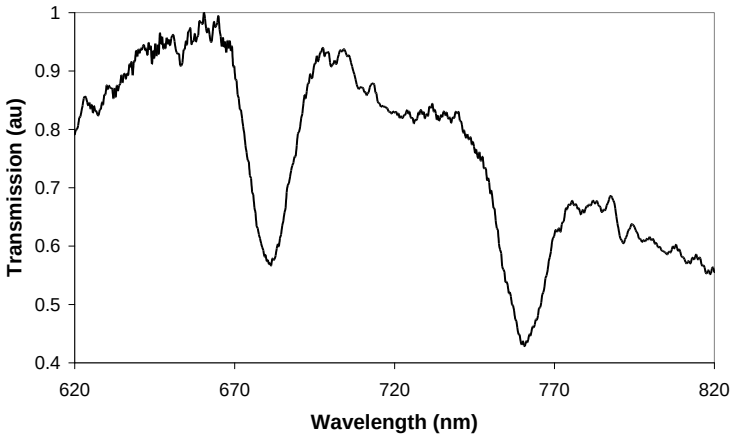

(b)

Figure 5.2 The transmission spectrum of the LPG of period 80µm with (a) no coating and (b) a coating of ω-tricosenoic acid of thickness 110nm.

The evolution of the resonance bands in response to increasing coating thickness was investigated by depositing a film of ω-tricosenoic acid, which has a refractive index of 1.57[15] and a molecular length of 2.6nm[15], onto the section of optical fibre containing the LPG using the Langmuir-Blodgett (LB) technique[7]. The LB technique facilitates deposition of the material one molecular layer at a time onto a substrate. The ω-tricosenoic acid was spread from dilute chloroform solutions (0.1g/l) onto the pure water sub-phase (resistivity 0.18MΩm) of one compartment of a Nima Technology Model 2410A LB trough, left for 20 min at 20°C, and compressed at 0.5 $cm^2\ s^{-1}$ (0.1% s^{-1} of total surface area). Deposition was achieved at a surface pressure of 26mN m^{-1} and a transfer rate of 8 mm min^{-1}. The fibre containing the LPG was positioned vertically so that its long axis was aligned with the dipping direction and was

alternately raised and lowered through the floating monolayer at the air–water interface to deposit the coating. The fibre was placed under tension, to ensure no bend-induced changes to the transmission spectrum[16,17]. Transmission spectra were recorded after the deposition of each monolayer, with the LPG below and above the water sub-phase for alternate layers. The effect of the presence of the coating material on the split resonance bands is shown in Figure 5.2b.

5.4 RESULTS AND DISCUSSION

The response of the central wavelengths of the resonance bands to layer by layer increases in the thickness of the coating deposited onto the LPG of period 80µm is illustrated in the grey scale plot shown, Figures 5.3a and 5.3b. Here, a transmission of 100% is represented by white and 0% by black. The dark line originating at a wavelength of 575nm in the uncoated LPG represents the resonance band corresponding to first order coupling to the $LP_{0\,23}$ cladding mode. The features visible in the range 850nm to 950nm in Figure 5.3b which do no change in wavelength with increasing coating thickness are a result of a cavity formed at a mechanical splice in the system.

This resonance band exhibits the typical behaviour reported previously for nanoscale coating deposition onto LPGs, in that the resonance band undergoes a blue shift, showing a region of high sensitivity that characterises the “mode transition region”, in which one of the lower order cladding modes becomes phase matched to a mode of the waveguide formed by the coating material. In this region the effective indices of the cladding modes change rapidly with increasing coating thickness[18,19], which, from Equation 5.1, causes a corresponding change in the central wavelength of the resonance bands.

The LPG was designed to access the phase matching turning point of the $LP_{0\,24}$ mode, generating two closely spaced resonance bands, centred at 700nm and 750nm, in the transmission spectrum of the uncoated 80µm period LPG surrounded by air. As the film thickness increases, the central wavelengths of the two bands shift in opposite directions, as plotted in Figure 5.4. As the thickness increases beyond the cladding mode transition region, the sensitivity to coating thickness reduces. The effect repeats as the coating thickness is increased further.

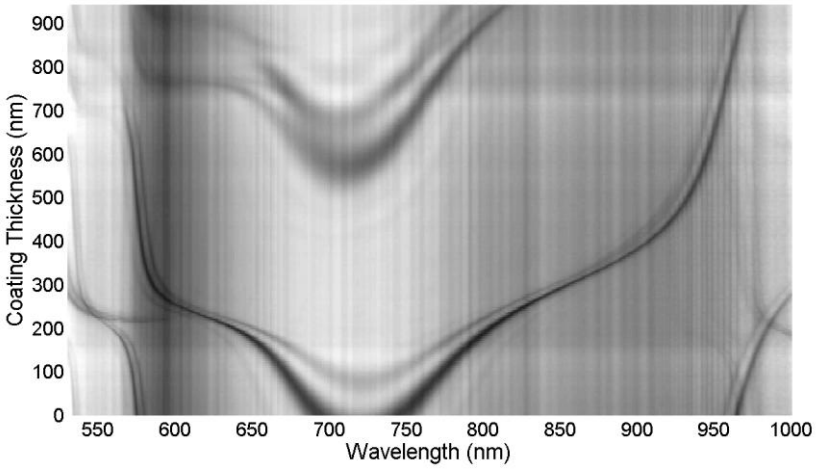

(a)

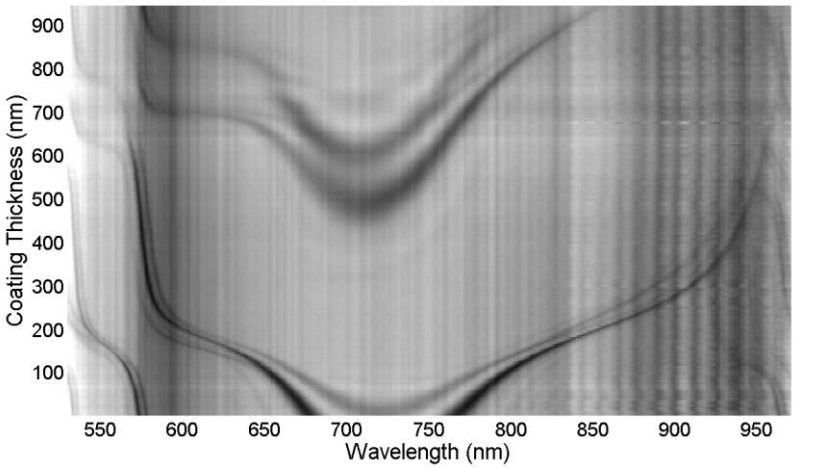

(b)

Figure 5.3 Evolution of the transmission spectrum of an LPG of period 80μm in response to the deposition of a coating of ω - tricosenoic acid using the Langmuir-Blodgett Technique (a) with the LPG above the water sub-phase and (b) with the LPG below the water sub-phase. The grey scale represents the measured transmission, with white corresponding to 100%, and black to 0%.

Comparison of Figures 5.3a and 5.3b shows the effect of monitoring the transmission spectrum with the LPG above and below the water subphase, as result of the refractive index sensitivity of the LPG. This indicates the need to consider the medium in which the LPG is immersed for sensing applications. It is interesting to note that, leading the response of each of the dominant resonance bands, there is a resonance band of considerably reduced extinction. It is suggested that these may correspond to coupling to an asymmetric cladding mode.

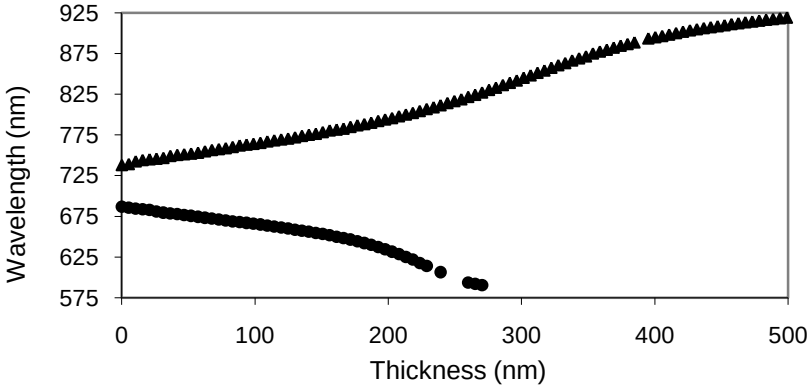

Figure 5.4 A plot of the wavelengths of the dual resonance bands as a function of the thickness of a coating of ω-tricosenoic acid deposited using the Langmuir-Blodgett technique onto an LPG of period 80μm.

The central wavelength of the resonance band has been measured using polynomial curve fitting. It can be seen from Figure 5.4 that the sensitivity of the resonant wavelengths to the coating thickness exhibits two gradients. The initial response shows a sensitivity to coating thickness of 0.27nm per nm thickness for the red shifted band, and - 0.25nm per nm thickness for the blue shifted band, over a thickness range from 0nm to 180nm. The region of highest sensitivity lies within the transition region, from 180nm to 300nm thickness, where the peak sensitivity is 0.47nm per nm thickness for the red shifted band, and - 0.62nm per nm thickness for the blue shifted band[23].

To investigate the influence of the period of the LPG on the sensitivity of the coated LPG to the thickness of the coating, the response of the transmission spectrum of the LPG of period 100μm was investigated. The results are shown in the grey scale images in Figure 5.5. In this case, the phase matching turning point of mode $LP_{0\,24}$ is accessed at 800nm for a coating thickness of order 200nm, which is coincident with the onset of the first mode transition region. Initially, there is no band in the 800nm wavelength range. As the film thickness increases, a broad attenuation band develops and splits in two, with the central wavelengths of the two bands shifting in opposite directions, as plotted in Figure 5.6. The peak sensitivity to coating thickness is 0.98nm per nm thickness for the red shifted band, and -1.45nm per nm thickness for the blue shifted band, over a thickness range from 220nm to 300nm[23]. The central wavelengths have been acquired by fitting a polynomial to the attenuation band profile and recording the minima of the polynomial. Clearly, the measurement of the wavelength separation of the bands will allow further increased sensitivity.

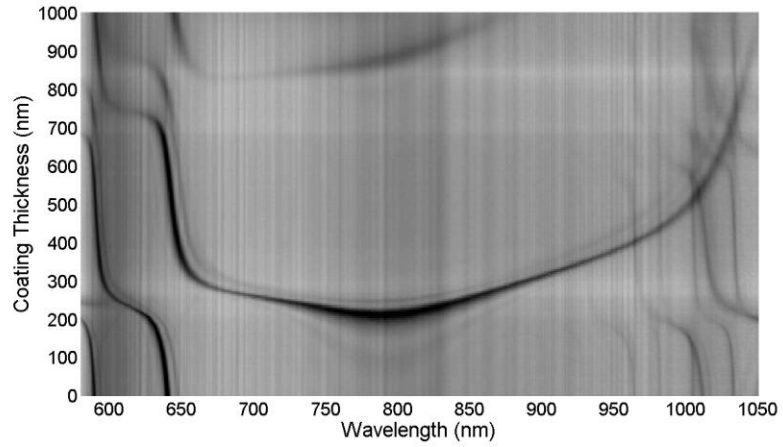

(a)

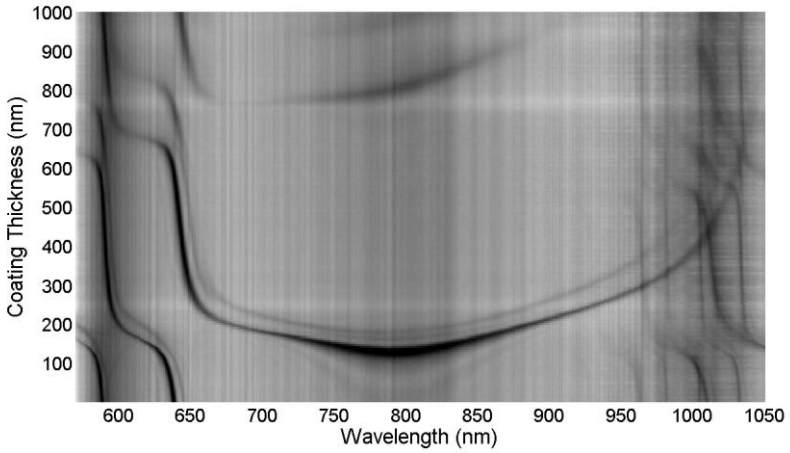

(b)

Figure 5.5 Evolution of the transmission spectrum of an LPG of period 100μm in response to the deposition of a coating of ω - tricosenoic acid using the Langmuir-Blodgett technique; (a) with the LPG above the water sub-phase and (b) with the LPG below the water sub-phase. The grey scale represents the measured transmission, with white corresponding to 100%, and black to 0%.

To illustrate the improvement in sensitivity, the highest sensitivity exhibited by a 1st order coupling resonance band of a 400μm period LPG, fabricated in the same type of fibre, is 0.5nm per nm thickness[20]. It is interesting to note that the 2nd order coupling dual resonance bands reported[20] to originate at a wavelength of approximately 800nm, also exhibit sensitivities of order 1nm per nm thickness.

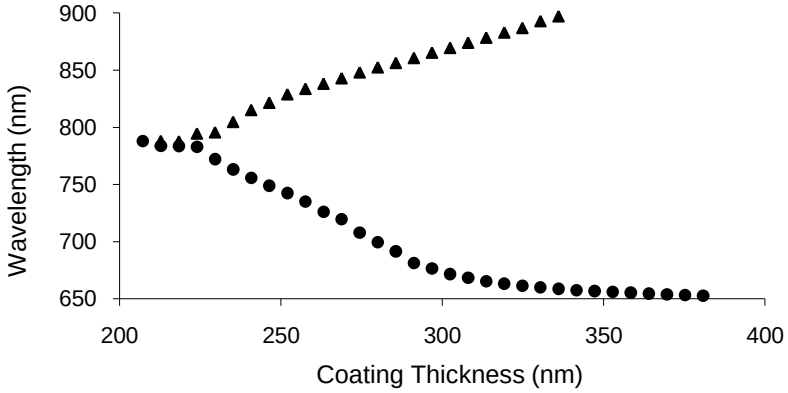

Figure 5.6 A plot of the wavelengths of the dual resonance bands as a function of the thickness of a coating of ω-tricosenoic acid deposited using the Langmuir-Blodgett technique onto an LPG of period 100μm.

The dual resonant bands show their highest sensitivity to external perturbation when the band is at the phase matching turning point. Thus the coincidence of the generation of the dual resonance band with the onset of the 1st transition region, where the cladding mode indices are most sensitive to the coating's optical properties[18], ensures that maximum sensitivity is obtained. Careful choice of the grating period, taking into account the fibre properties and the refractive index of the coating material, is needed to ensure optimum sensitivity. While, in principle, the LPG sensor exhibits its highest sensitivity to all external perturbations at the phase matching turning point, it should be noted that, appropriate choice of core and cladding materials can allow the phase matching condition to specific cladding modes to be insensitive to, for example temperature, eliminating cross-sensitivity issues[6]. In addition, cross-sensitivity effects can be minimized by appropriate packaging or by exploiting the different sensitivities of each resonance band to different measurands[1].

5.5 SENSING APPLICATION

To demonstrate the use of the dual resonant bands for a sensing application, a pH sensitive coating was deposited onto the fibre cladding in the region of the long period grating. A quinolinium dye was selected due to its pH sensitivity; this has a molecular structure as shown in Figure 5.7. These long chain molecules and aromatic rings with alternating single and double covalent bonds are called conjugated systems[21]. This property gives rise to strong colours, since they have absorption bands in the visible region of the spectra.

The 100μm period grating was selected to perform the sensing experiments, in order to benefit from the optimised sensitivity that occurs with coincidence of the phase matching turning point and the transition region.

5.6 PH SENSING EXPERIMENT

The 1-octadecyl-4-[2-(4-dimethylamino-naphthalene-1-yl)-vinyl]-quinolinium iodide dye[q] was dissolved in chloroform at 0.1g/l, and spread onto a pure water subphase of one compartment of a Nima Technology Model 2410A Langmuir-Blodgett trough. The dye was compressed to a surface pressure of 26mN/m. The dipping speed for the fibre substrate was set to 15mm/min. Ninety layers of the quinolinium dye were deposited giving an estimated coating thickness of ~200nm to obtain two resonant bands in the transmission spectrum of the LPG.

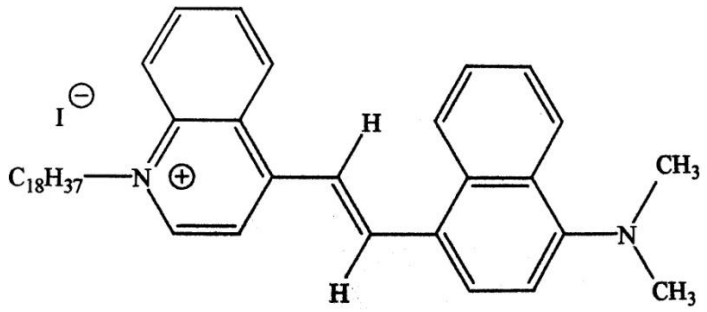

Figure 5.7 The deprotonated form of 1-octadecyl-4-[2-(4-dimethylamino-naphthalene-1-yl)-vinyl]-quinolinium iodide dye. In acidic conditions, a proton is gained by the dimethyl amino moiety.

Sigma-Aldrich, Hydrion™ buffer solutions in the range pH2-11 were prepared by dissolving the buffer powders in distilled water and adding a colour key buffer preservative. The coated long period grating was removed from the trough, and mounted in a liquid vessel containing the buffer solution. The response was allowed to stabilise for 2 minutes, and the transmission spectrum was recorded. Between each application of the buffer solution, the sensor was washed in distilled water. To determine the stability of the coating over time, the sensor was left for four days and the tests repeated.

[q] Cranfield reference APD172

5.7 PH SENSING RESULTS

The response of the quinolinium dye coating to the buffer solution is demonstrated by the movement of the LPG sensor's attenuation bands, Figure 5.8 and Figure 5.9.

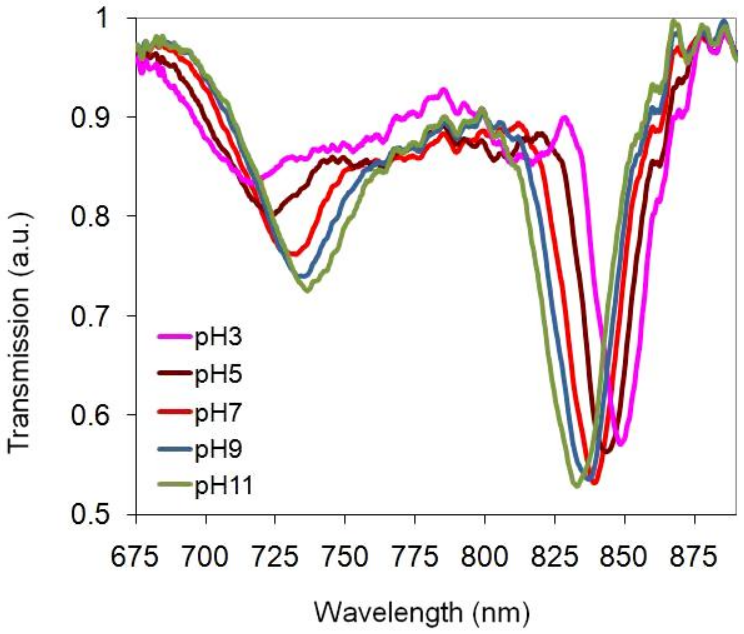

(a)

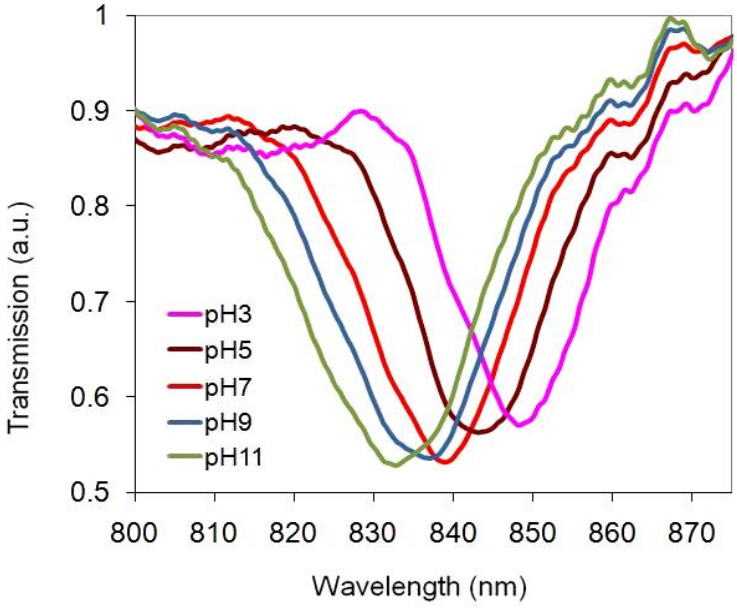

(b)

Figure 5.8 A long period grating with period 100μm, coated with a quinolinium dye coating which is pH sensitive. (a) The resonant bands to diverge in wavelength, with increasing acidity. (b) The spectrum magnified between 800nm and 875nm around the longer wavelength attenuation band.

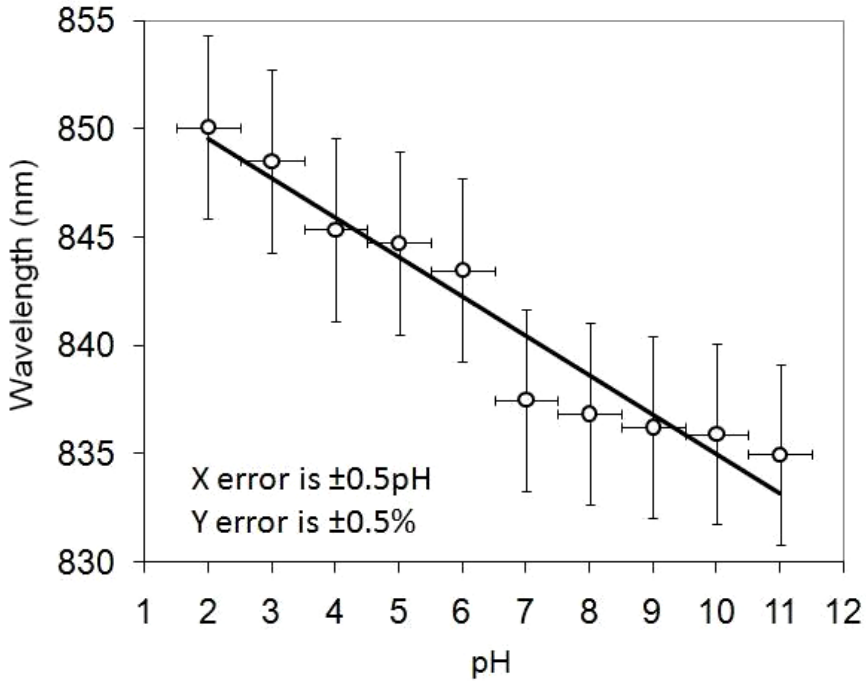

Figure 5.9 The wavelength sensitivity of the attenuation band between 800nm and 875nm for a long period grating with period 100μm, coated with pH sensitive quinolinium dye coating . The sensitivity of this feature is -0.55pH/nm.

The acidic strength of the solution causes protonation of the dimethyl amino group of the dye molecule[24], which in turn causes a change in the dye molecule's resonant structure of single and double covalent bonds. This changes the molecule's optical absorption in the visible spectrum, which changes the bulk refractive index of the coating at these wavelengths[21]. The long period grating is responsive to changes in the refractive index of a material coated on the cladding. The twin attenuations bands diverge in wavelength with increasing acidity of the analyte solution, Figure 5.8a. The longer wavelength attenuation band is displayed in greater detail in Figure 5.8b, and its wavelength sensitivity is measured in Figure 5.9. The central wavelength of the attenuation bands have been recorded by capturing the minimum value directly from the data in Figure 5.8. The asymmetry in the shape of the attenuation band and intensity noise gives an error, which is less than ±0.5%. By linear curve fitting, this yields an average value of pH sensitivity of -1.83nm/pH unit[r], for the longer

[r] Or -0.55pH/nm

wavelength attenuation band. This compares with ~-5nm/pH[s] unit for a 37.4μm diameter tapered optical fibre with the same coating with a thickness of 402nm[22].

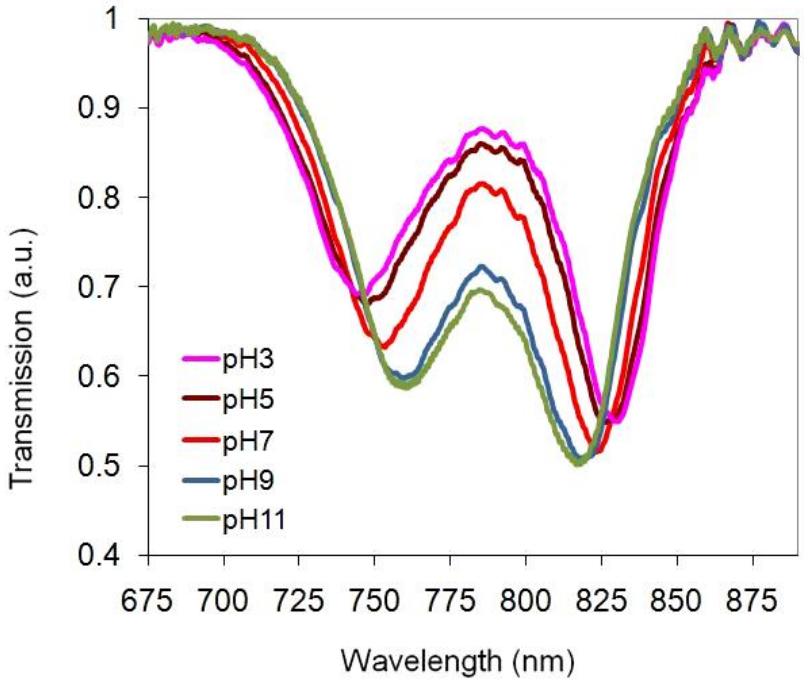

Figure 5.10 The dual resonant response of the quinolinium dye coated long period grating sensor with period 100μm, to changes in the analyte's pH.

The pH sensing tests were repeated after a period of four days[t]. The spectrum had changed corresponding to a decrease in thickness or density of the coating. The spectrum now showed two attenuation bands with their minima close together in wavelength, Figure 5.10. Repeating the pH sensing tests, the separations of the bands increased with acidity of the analyte.

This spectrum is interesting since there are wavelength dependent and amplitude dependent elements. The wavelength dependent parts are the two minima that diverge in wavelength. The amplitude dependent part is the central maximum located between the two minima. This maximum increases in amplitude as the two minima diverge. This maximum could be utilised in a system using a detector with a response

[s] Or ~-0.2pH/nm

[t] This indicates that the quinolinium coating requires further investigation to determine the long term stability and repeatability of these measurements.

to optical intensity. Here, a light source at a wavelength around that of the central maximum would be modulated as a result of changes in the transmission spectrum of the LPG in response to an analyte. This configuration could usefully be employed to build a simple sensor system. This interesting region of operation has been used in Chapters 8 and 9 for a chemical sensing application. In this case, Figure 5.10 serves as a useful comparison to Figures 8.6 and 9.10.

5.8 CONCLUSION

An investigation of the response of LPG dual resonance bands near the phase matching turning point to the deposition of a nanostructured coating has been presented[23]. Appropriate design of the device, taking into account the properties of the optical fibre, the period of the LPG and the refractive index of the coating material can ensure that the phase matching turning point of the LPG coincides with the mode transition region that characterises LPGs with nanostructured coatings. This is further analysed in the next chapter. Achieving this ensures optimum sensitivity to the coating's optical properties.

The ability to deposit, in a layer by layer fashion, materials onto an LPG that change their optical properties in response to a chemical analyte[10,11,12], offers the prospect for the development of optical chemical sensing. This has been demonstrated with a LPG sensor coated with 90 layers of a quinolinium dye. This material can be reversibly protonated, thus forming an optical pH sensor, and has been measured with a sensitivity of -0.55pH/nm.

5.9 REFERENCES

1. V. Bhatia, “Applications of long-period gratings to single and multi-parameter sensing”, Opt. Express **4**, 457–466 (1999).

2. H. J. Patrick, A. D. Kersey and F. Bucholtz, “Analysis of the response of long period fibre gratings to external index of refraction” J. Lightwave Technol. **16** 1606–42, (1998).

3. H. J. Patrick, C. C. Chang and S. T. Vohra, “Long period fibre gratings for structural bend sensing” Electron. Lett. **18** 1773–4, (1998)

4. T. Mizunami, T. Fukuda and A. Hayashi, “Fabrication and characterization of long-period-grating temperature sensors using Ge–B-co-doped photosensitive fibre and single-mode fibre”, Meas. Sci. Technol. **15,** 1467–1473 (2004).

5. S.W. James and R. P. Tatam “Optical Fibre Long Period Grating Sensors: Characteristics and Application” Meas. Sci. Technol. **14** , R49-R61, (2003)

6. X. Shu, L. Zhang, and I. Bennion, “Sensitivity Characteristics of Long-Period Fibre Gratings” J.Lightwave Technol. **20**, 255 – 266, (2002).

7. N. D. Rees, S. W. James, R. P. Tatam, and G. J. Ashwell, Optical Fibre Long Period Gratings With Langmuir-Blodgett Thin Film Overlays, Opt. Lett. **9**, 686-688, (2002).

8. I. Del Villar, M. Achaerandio, I. R. Matias and F. J. Arregui, “Deposition of overlays by electrostatic self-assembly in long-period fibre gratings,” Opt. Lett. **30**, 720-722, (2005).

9. A. Cusano, P. Pilla, L. Contessa, A. Iadicicco, S. Campopiano, A. Cutolo, M. Giordano and G. Guerra, “High-sensitivity optical chemosensor based on coated long-period gratings for sub-ppm chemical detection in water.” Appl. Phys. Lett. **87**, Art. No. 234105, (2005).

10. J. M. Corres, I. R. Matias, I. del Villar I and F. J. Arregui, “Design of pH sensors in long-period fiber gratings using polymeric nanocoatings” IEEE Sens. J. **7**, 455-463, (2007).

11. J. Keith, L. C. Hess, W. U. Spendel, J. A. Cox and G. E. Pacey, “The investigation of the behavior of a long period grating sensor with a copper sensitive coating fabricated by layer-by-layer electrostatic adsorption.” Tatanta **70**, 818-822, (2006).

12. G. E. Pacey, S. D. Puckett , L. Cheng, S. Khatib-Shahidi and J. A. Cox, “Detection of DNA damaging agents using layer-by-layer assembly.” Anal. Chem. ACTA **533**, 135-139, 2005.

13. D. D. Davis, T. K. Gaylord, E. N. Glytsis, S. G. Kosinski, S. C. Mettler and A. M. Vengsarkar, “Long-period fibre grating fabrication with focused CO2 laser beams.” Electron. Lett. **34,** 302–3 (1998).

14. G. Rego, O. Okhotnikov, E. Dianov and V. Sulimov, “High-temperature stability of long-period fibre gratings using an electric arc.” J. Lightwave Technol. **19,** 1574–9 (2001).

15. K. Skjonnemand, “The Optical and Structural Characterization of Ultra-Thin Films”, PhD Thesis, Cranfield University, Cranfield, UK (2000).

16. C. C. Ye, S. W. James and R. P. Tatam, “Simultaneous temperature and bend sensing using long period fibre gratings” Optics Letters, **25** , pp 1007-1009, (2000).

17. U. L. Block, V. Dangui, M. J. F. Digonnet, and M. M. Fejer, “Origin of Apparent Resonance Mode Splitting in Bent Long-Period Fibre Gratings.” J. Lightwave Technol., **24**, 1027-1034 (2006)

18. I. Del Villar, I. R. Matias and F. J. Arregui, “Influence on cladding mode distribution of overlay deposition on long period fibre gratings.” J. Opt. Soc. Am A **23**, 651-658, (2006).

19. A. Cusano, A. Iadicicco, P. Pilla, L. Contessa, S. Campopiano, A. Cutolo, and M. Giordano, "Mode transition in high refractive index coated long period gratings," Opt. Express **14**, 19-34 (2006).

20. S. W. James, C. S. Cheung, and R. P. Tatam, “Experimental observations on the response of 1st and 2nd order fibre optic long period grating coupling bands to the deposition of nanostructured coatings.” Opt. Express, **15**, 13096-13107, (2007).

21. E. Hecht, “Optics”, Third Edition, Addison Wesley Longman Inc., (1998)

22. R. Jarzebinska, C. S. Cheung, S. W. James, and R. P. Tatam, "Response of transmission spectrum of tapered optical fibres to the deposition of nanostructured coatings", Meas. Sci. Technol. **20,** Art. No. 034001 (2009).

23. C. S. Cheung, S. M. Topliss, S. W. James, and R. P. Tatam, "Response of fiber-optic long-period gratings operating near the phase-matching turning point to the deposition of nanostructured coatings", J. Opt. Soc. Am B **25**, 897-902, (2008).

24. S. A. Bourne, K. De Villiers, and T. J. Egan, "Three 4-aminoquinolines of antimalarial interest", Acta Crystallographica Section C: Crystal Structure Communications, **62**, 53-57, (2006).

CHAPTER 6: SYSTEMATIC EXPERIMENTAL INVESTIGATION OF THE DUAL RESONANCE PHENOMENON

6.1 INTRODUCTION

Long Period Gratings (LPGs) are devices that couple energy from the guided core mode to a discrete set of co-propagating symmetric fibre cladding modes[1]. A finite number of symmetric cladding modes are supported, denoted by LP_{0x}, which form concentric rings, where x denotes the number of rings[2]. For example, the modes LP_{03}, LP_{06}, LP_{08} and $LP_{0\,16}$, are shown in Figure 6.1. These images are created by coupling light from a tunable laser operating at the core-cladding mode resonance wavelength into the fibre, and capturing the near field pattern from the distal end of the fibre with an infrared camera[2].

The LPG induces resonance wavelengths which are given by

$$\lambda_{(x)} = \frac{(n_{core} - n_{clad(x)})\Lambda}{N} \tag{6.1}$$

where $\lambda_{(x)}$ represents the wavelength at which coupling occurs to the LP_{0x} mode, n_{core} is the effective refractive index of the mode propagating in the core of the fibre, $n_{clad(x)}$ is the effective index of the LP_{0x} cladding mode, N is an integer representing the order of diffraction and Λ is the period of the long period grating[3].

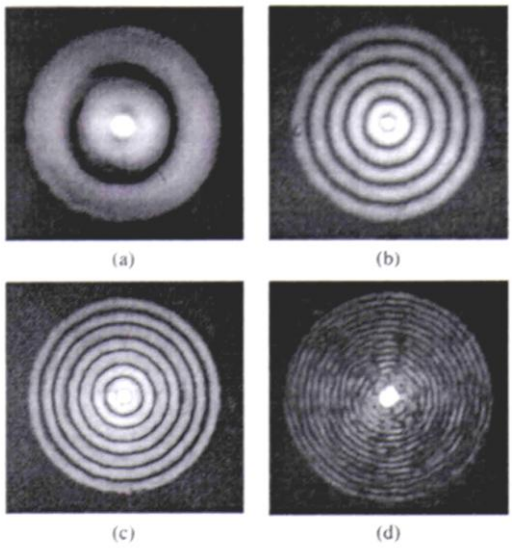

Figure 6.1 The near field images of four cladding modes of the fibre; (a) LP_{03}, (b) LP_{06}, (c) LP_{08} and (d) $LP_{0\,16}$, coupled into selectively by the LPG. The grating pitches are; (a) 590μm, (b) 410μm, (c) 295μm, (d) 100μm[2].

Equation 6.1 indicates that resonant coupling of energy between the modes occurs at wavelengths substantially less than the grating period, in contrast to the action of a Fibre Bragg Grating, which interacts with light of wavelength twice the period. The closeness of the effective refractive indices of the core mode and the modes of the cladding, around the actual refractive indices of the core and cladding, typically a difference of ~1%[4], gives rise to the large difference in grating period and resonance wavelength.

For long period gratings, a phenomenon called dual resonance occurs[5], and is defined by a cladding mode having two resonance wavelengths. This is predicted by the phase matching curves, a plot of the relationship between grating period and resonance wavelengths for each cladding mode, each of which contains a turning point, see Figure 2.6. This phenomenon is manifest in attenuation bands that display opposite sensitivities to external index of refraction[6], cladding coating thickness[7] or coating refractive index[8].

In this chapter, the dual resonance phenomenon has been explored in a number of long period gratings of different period, and the cladding mode resonances have been analysed in order to draw some conclusions on the systematic behaviour of these devices.

6.2 PHASE MATCHING CURVES

The phase matching curves generated by the solution to Equation 6.1 give a complete set of the wavelength resonances that occur in a long period grating. They can be observed in a plot of grating period verses resonance wavelength, see Figure 2.5 and 2.6, and are calculated using the method described in [9].

The phase matching curves could also be obtained experimentally by writing many long period gratings of differing period and recording the resonance frequencies, then identifying each mode and plotting the resonance wavelengths as a function of period[2].

An alternative method[2] to this has been proposed in which tilted FBGs are fabricated in optical fibre, and the core mode and the contra-propagating cladding mode resonances are identified in the reflection spectrum. From this, the effective indices can be calculated using the typical formulae that describe a tilted FBG[10]. This allows the wavelength dependence of the effective refractive index of each mode, to be plotted. Plotting these curves for the tilted FBGs allows the effective indices of the core and cladding modes within that fibre type to be determined, for all wavelengths over the measured spectrum. The effective refractive index values determined via this method

may then be used in Equation 6.1 to facilitate the plotting of the phase matching curves.

The phase matching curves can be used to great effect to show the dual resonance phenomenon. At the phase matching turning point where the gradient of grating period over wavelength equals zero, a single attenuation band appears in the transmission spectrum of the LPG. At this point, the grating is at its most sensitive to external effects (temperature, strain, ambient refractive index). This is an important consideration for sensor design[11]. Here, the extinction ratio of the attenuation band changes in response to an external perturbation, e.g. strain[12]. This subsequently splits into the dual resonance feature, see Chapter 5.

By depositing a high refractive index (HRI) coating on the fibre cladding, the response of the cladding mode to the increase in coating thickness can be monitored. The coupling wavelength of the cladding modes is dependent upon the coating thickness[13], since the addition of the coating changes the waveguiding properties of the cladding. This means that as the coating thickness is changed, the wavelength at which the phase matching between core and cladding is satisfied will also change. Cladding modes can also become guided[u] by the coating, when the coating is of sufficient optical thickness. This causes a modal redistribution of all the cladding modes[14], which exhibit a near step change in effective index, see Figure 2.3, with a corresponding change in resonance wavelength when the coated region contains an LPG. In this region, the cladding mode resonances exhibit high sensitivity to changes in the coating thickness or refractive index. If this effect is harnessed together with the dual resonance phenomenon, then optimum sensitivity can be obtained.

The results in the following sections show the transmission spectral response plotted for a number of long period gratings as a coating is gradually applied to the fibre.

6.3 EXPERIMENT FOR THE MEASUREMENT OF DUAL RESONANT LPGS

Using the predictions for the dual resonance phenomenon from the phase matching curves, long period gratings of period in the range 80μm to 180μm were fabricated, using UV inscription by the point by point technique[15]. The fibre used was hydrogen loaded single mode fibre, SM750, with cut-off wavelength 619 nm.

To characterize the long period grating response, each device was in turn coated using the Langmuir-Blodgett (LB) technique with the three materials; ω-tricosensoic acid,

[u] Or partially guided

undecyl-calix[4]resorcarene and tert-butyl-calix[8]arene carboxylic acid. See Tables 6.1 and 6.2.

Table 6.1 Fabrication parameters for three coating materials

HRI[v] Material	Chloroform Solvent Concentration (g/l)	Surface Pressure (mN/m)	Dipping Speed (mm/min)
Tricosenoic Acid	0.1-0.14	26	8-12
Calix[4]resorcarene	0.2	28-30	12-20[w]
Calix[8]arene	0.13	26	20

Each coating material was in turn dissolved in chloroform according to Table 6.1, and spread onto a pure water subphase of one compartment of a Nima Technology Model 2410A Langmuir-Blodgett (LB) trough. The material was compressed to the surface pressure recorded in Table 6.1. The dipping speed for the fibre substrate is also recorded in Table 6.1.

A tungsten-halogen lamp with a broadband spectrum extending from 550nm to 1050nm, was coupled via sma optical connectors into the fibre, and the distal end of the fibre was connected via sma optical connectors into an Ocean Optics CCD spectrometer of resolution 0.3 nm. The transmission spectrum of the fibre was recorded when the LPG was above and below the water subphase. However, the results presented in the following sections are exclusively from the air subphase i.e. above the water subphase. These have greater relevance since the work presented in Chapters 8 and 9 deals with chemical vapour sensing. In this regime of operation, the air subphase is the ambient environment of the LPG sensor in which the analyte vapour is introduced.

6.4 CHARACTERIZATION OF COATED LONG PERIOD GRATINGS

The long period gratings were dipped with alternating monolayers of the coating material to form a Y-type LB film. The dipping was fully automated to allow the deposition of coatings of thickness in excess of 1μm, and in some cases in excess of 2μm. This ensured that full development and evolution of the dual resonant attenuation bands could be observed.

[v] High Refractive Index

[w] Better results were obtained with 20mm/min. The dipping speed may affect the shape of the meniscus, which changes the angle of the orientation of the molecules. This dipping speed also determines the overall length of time of the deposition process. These factors could affect the structure of the final coating.

Table 6.2 Physical parameters of three coating materials

LPG Coating Material	Monolayer thickness (nm)	Refractive Index
ω-Tricosensoic Acid 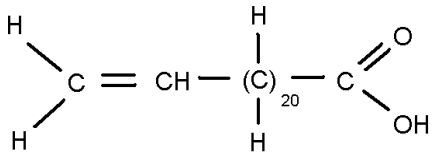	2.6[16]	1.57[16]
Undecyl-calix[4]resorcarene 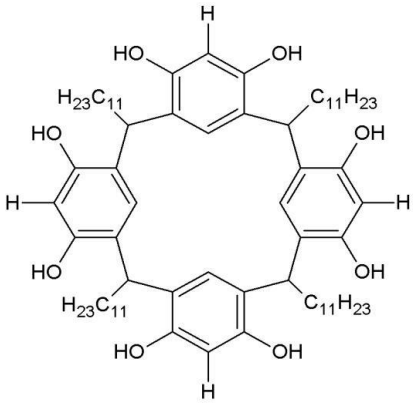	1.17[17]	1.47[17]
Tert-butyl-calix[8]arene derivative 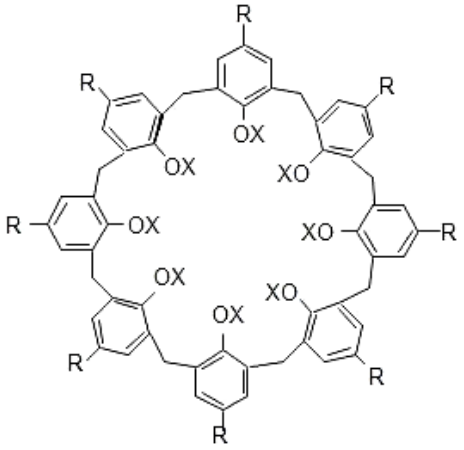 R= $C(CH_3)_3$, X=CH_2COOH	1.08[18]	1.21[18x]

[x] The quoted figure obtained using ellipsometry appears to be incorrect as the results obtained with an identical material show that the spectral response is typical of a HRI material, meaning that the refractive index must be greater than the cladding refractive index, approximately 1.45

The grey scale spectrum plots show how the attenuation bands behave with increasing coating thickness. Figure 6.2 is a typical plot, in which the dark features are the attenuation bands, which are graded with extinction with the darker regions representing higher extinction.

The mode transition region occurs when the coating is of sufficient optical thickness, and the cladding modes undergo a reorganisation when one cladding mode becomes guided[y] by the coating. This is the cause of the near step change in wavelength of the attenuations band indicated in Figure 6.2, and is notionally the first transition region, see Section 2.2. A second transition region is apparent when a further cladding mode can become guided by the coating when it has sufficient thickness or refractive index.

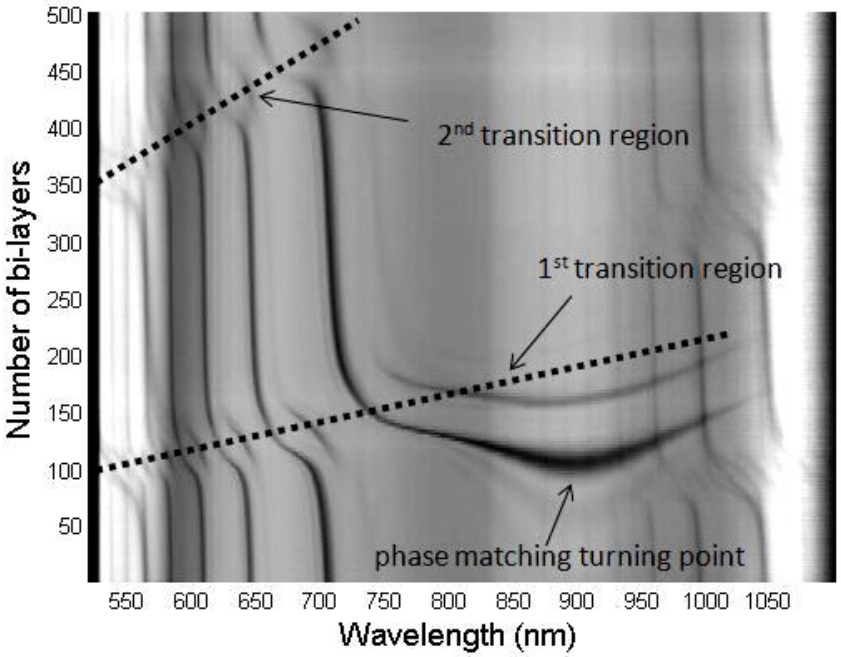

Figure 6.2 A long period grating with a coating of tert-butyl-calix[8]arene. The grating period is 180μm. The phase matching turning point is identified at approximately 900nm. The first and second transition regions are also indicated.

The phase matching turning point (pmtp) is shown occurring at 900nm. Light is coupled into a cladding mode with the development of a single broad attenuation band appearing in the transmission spectrum of the LPG. As the coating thickness is increased further, the attenuation band divides into two, the dual resonance phenomenon. Here, light is coupled into the same cladding mode at two wavelengths.

[y] Or partially guided

Since the dual resonance attenuation band is in close proximity to the transition region, this gives near optimum sensitivity to changes in the external coating of the fibre.

Four gratings of differing period were coated with tricosenoic acid. The coating thickness, as determined by the number of pairs of monolayers deposited, is indicated on the ordinate axis. It is clear from Figure 6.3 that the phase matching turning point (pmtp) increases in wavelength as the period of the grating increases[z]. It is also clear that the first transition region and the phase matching turning point coincide for grating periods of 140μm and 180μm for this coating material.

Despite using a coating material with a different refractive index and molecular length, the results presented in Figure 6.4 show many similarities with the previous set. However, the transition region and the phase matching turning point are coincident only for a long period grating of period 140μm.

The third coating material, calix[8]arene has been used to generate the grey scale plots in Figure 6.5. The images have a particular clarity meaning that the coating is free from defects that cause light scattering[19]. This amphiphilic molecule may be especially well suited to Langmuir-Blodgett deposition. The features visible in the range 900nm to 1050nm of Figures 6.5c and 6.6c are a result of a cavity formed at a mechanical splice in the system[aa].

The shape of the attenuation band centred at the phase matching turning point is clearly shown, with their subsequent evolution into dual resonant attenuation bands.

The first three transition regions are recorded in Figure 6.6. The shape of each dual resonance attenuation band changes as the coating is deposited. The loss of extinction of the attenuation bands at thicker coatings could be due to an increase in light scattering from the coating due to dislocations in the film. These will build up as more layers are deposited. Alternatively, the loss of extinction could be because the coupling to the cladding becomes more broadband in nature as the cladding waveguide becomes less well defined, either because of the presence of the coating itself or the roughness of the perimeter surface of the coating.

---

[z] For the 140μm period grating, the dual resonant attenuation band has asymmetry. The lowest layer where coupling occurs to the dual resonant attenuation band is used to the determine the λ_{pmtp} .

[aa] The bare fibre adaptors are problematic and this was overcome in the other results by splicing patch cords with sma connectors directly to the grating. This is the appropriate connectorization allowing stable and efficient coupling to the spectrometer and light source.

Coating = Tricosensoic Acid, Λ = 80μm, length = 30-35mm, $\lambda_{\text{Phase Matching Turning Point}}$ = 720nm
Coating Thickness at λ_{pmtp} = (< 0)

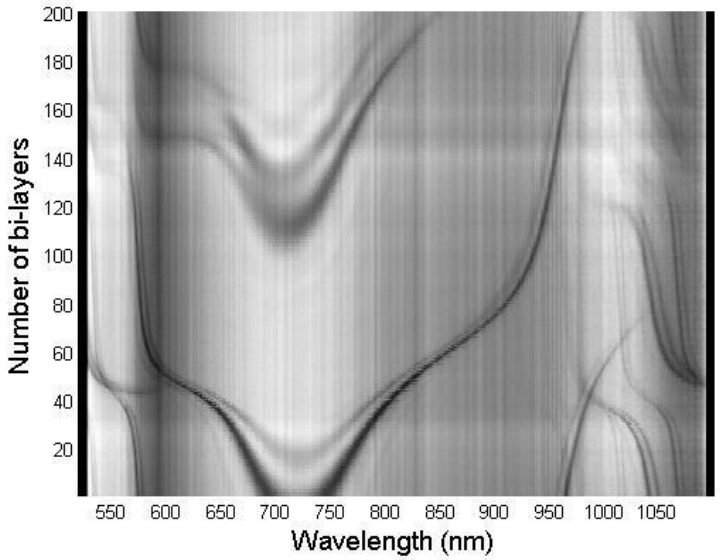

(a)

Coating = Tricosensoic Acid, Λ = 100μm, length = 30-35mm, $\lambda_{\text{Phase Matching Turning Point}}$ = 824nm
Coating Thickness at λ_{pmtp} = 234nm

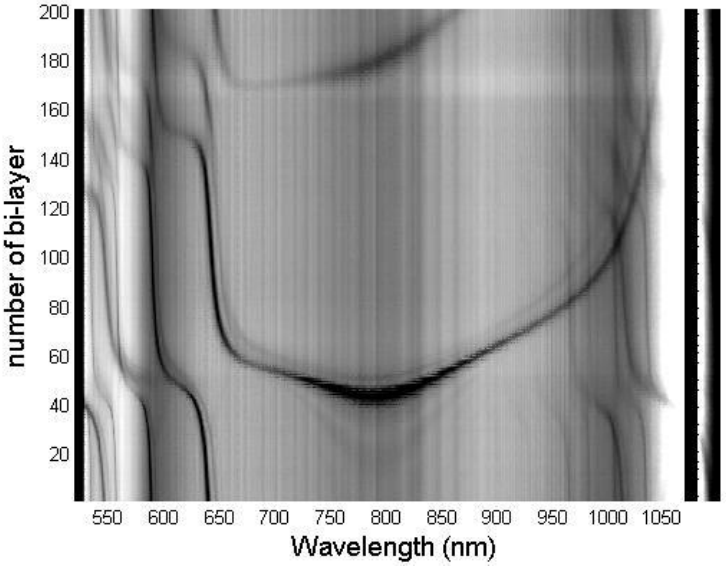

(b)

Figure 6.3 Evolution of the spectra of long period gratings with periods; (a) 80μm, (b) 100μm, coated with tricosenoic acid recorded in the air subphase, in response to the deposition of the coating.

Coating = Tricosensoic Acid, Λ = 140μm, length = 30-35mm, $\lambda_{\text{Phase Matching Turning Point}}$ = 740nm
Coating Thickness at λ_{pmtp} = 338nm

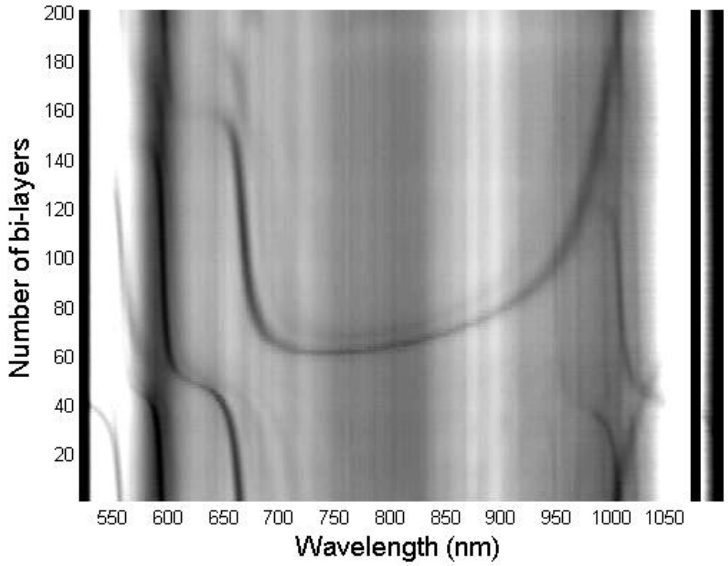

(c)

Coating = Tricosensoic Acid, Λ = 180μm, length = 30-35mm, $\lambda_{\text{Phase Matching Turning Point}}$ = 860nm
Coating Thickness at λ_{pmtp} = 364nm

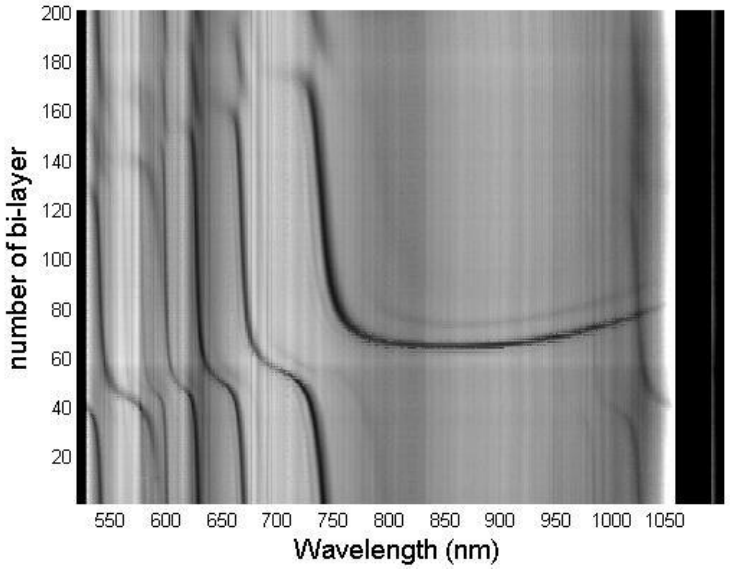

(d)

Figure 6.3 Evolution of the spectra of long period gratings with periods; (c) 140μm and (d) 180μm, coated with tricosenoic acid recorded in the air subphase, in response to the deposition of the coating.

Coating = Undecyl-calix[4]resorcarene, Λ = 80μm, length = 16mm, $\lambda_{\text{Phase Matching Turning Point}}$ = 730nm
Coating Thickness at λ_{pmtp} = (<0)

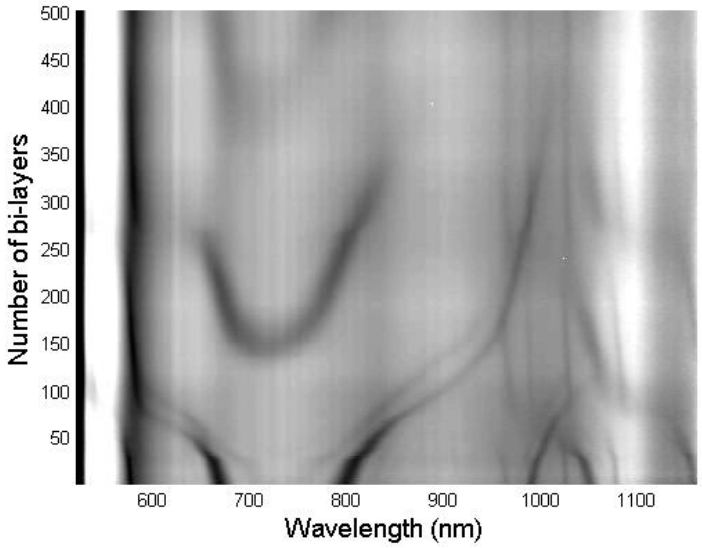

(a)

Coating = Undecyl-calix[4]resorcarene, Λ = 100μm, length = 23mm, $\lambda_{\text{Phase Matching Turning Point}}$ = 815nm
Coating Thickness at λ_{pmtp} = 316nm

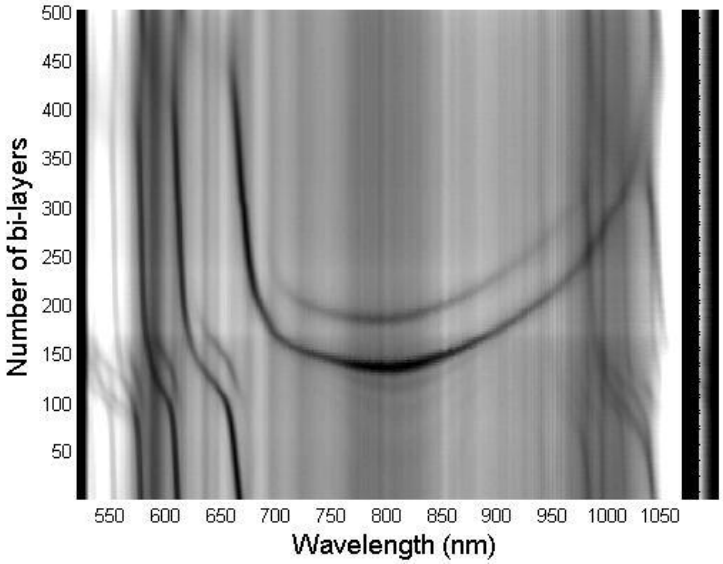

(b)

Figure 6.4 Evolution of the spectra of long period gratings with periods; (a) 80μm, (b) 100μm, coated with calix[4]resorcarene recorded in the air subphase, in response to the deposition of the coating.

Coating = Undecyl-calix[4]resorcarene, Λ = 140μm, length = 30-35mm, $\lambda_{\text{Phase Matching Turning Point}}$ = 760nm
Coating Thickness at λ_{pmtp} = 269nm

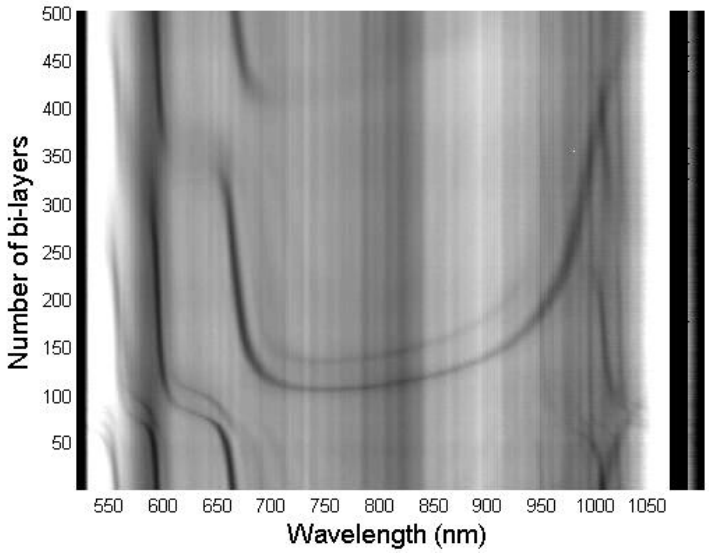

(c)

Coating = Undecyl-calix[4]resorcarene, Λ = 180μm, length = 30-35mm, $\lambda_{\text{Phase Matching Turning Point}}$ = 925nm
Coating Thickness at λ_{pmtp} = 339nm

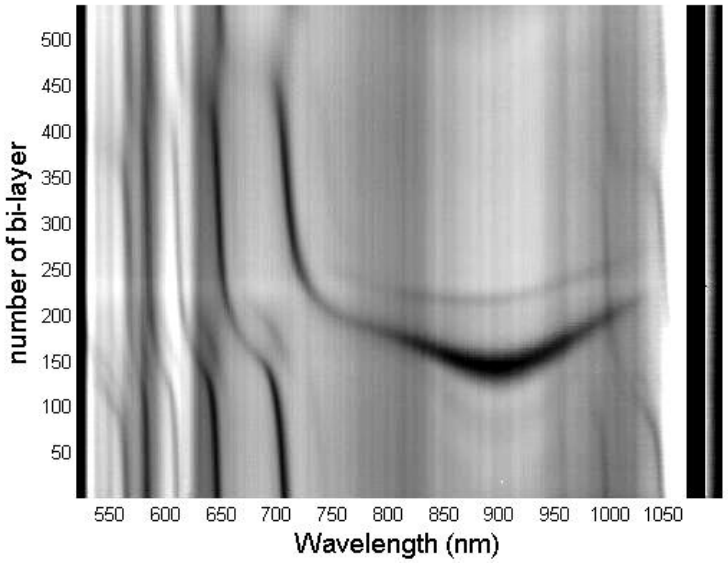

(d)

Figure 6.4 Evolution of the spectra of long period gratings with periods; (c) 140μm and (d) 180μm, coated with calix[4]resorcarene recorded in the air subphase, in response to the deposition of the coating.

Coating = Tert-butyl-calix[8]arene, Λ = 80μm, length = 16mm, $\lambda_{\text{Phase Matching Turning Point}}$ = 730nm
Coating Thickness at λ_{pmtp} = (< 0)

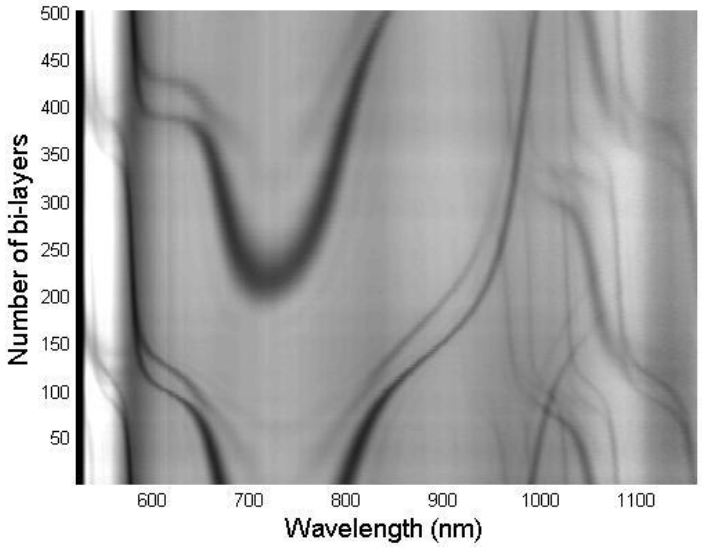

(a)

Coating = Tert-butyl-calix[8]arene, Λ = 100μm, length = 23mm, $\lambda_{\text{Phase Matching Turning Point}}$ = 831nm
Coating Thickness at λ_{pmtp} = 266nm

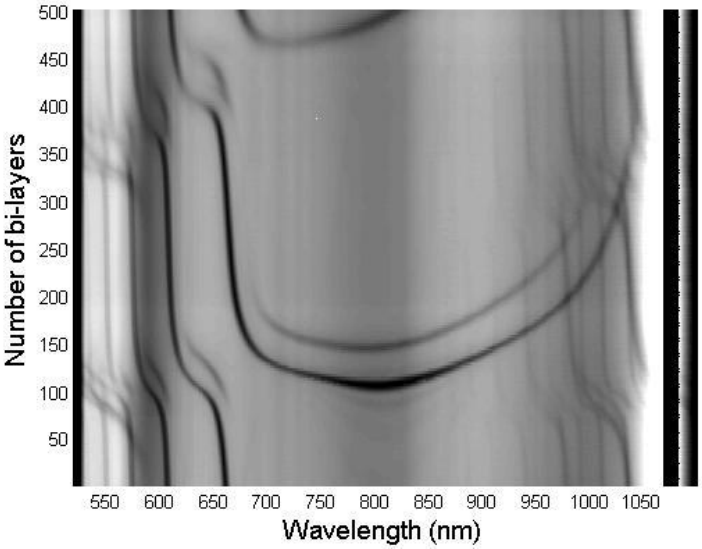

(b)

Figure 6.5 Evolution of the spectra of long period gratings with periods; (a) 80μm, (b) 100μm, coated with calix[8]arene recorded in the air subphase, in response to the deposition of the coating.

Coating = Tert-butyl-calix[8]arene, Λ = 140μm, length = 35mm, $\lambda_{\text{Phase Matching Turning Point}}$ = 930nm
Coating Thickness at λ_{pmtp} = 324nm

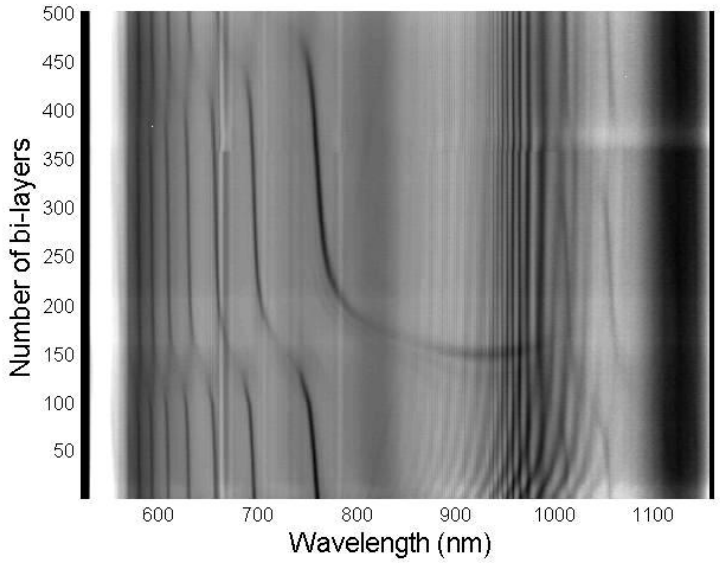

(c)

Coating = Tert-butyl-calix[8]arene, Λ = 180μm, length = 30-35mm, $\lambda_{\text{Phase Matching Turning Point}}$ = 911nm
Coating Thickness at λ_{pmtp} = 242nm

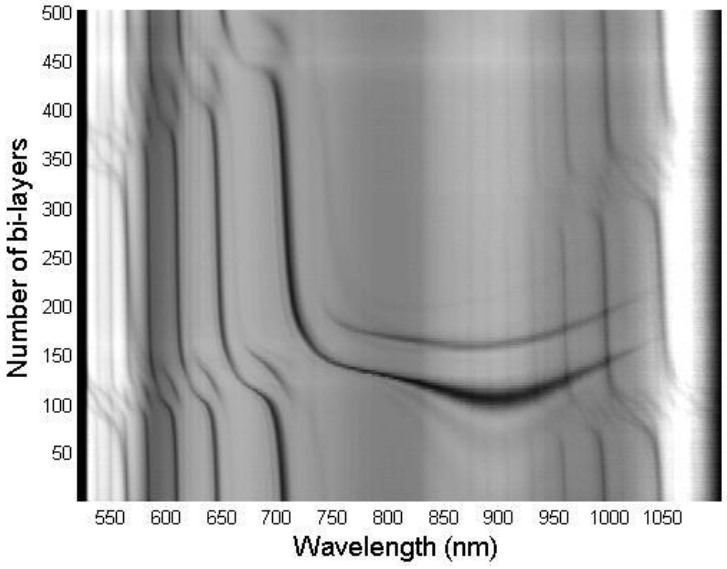

(d)

Figure 6.5 Evolution of the spectra of long period gratings with periods; (c) 140μm and (d) 180μm, coated with calix[8]arene recorded in the air subphase, in response to the deposition of the coating.

Coating = Tert-butyl-calix[8]arene, Λ = 80μm, length = 16mm, $\lambda_{Phase\ Matching\ Turning\ Point}$ = 730nm
Coating Thickness at λ_{pmtp} = (<0)

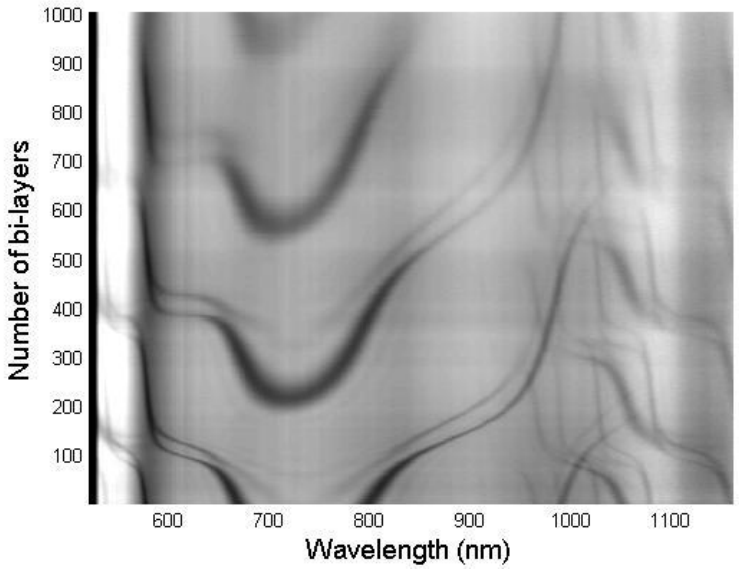

(a)

Coating = Tert-butyl-calix[8]arene, Λ = 100μm, length = 23mm, $\lambda_{Phase\ Matching\ Turning\ Point}$ = 831nm
Coating Thickness at λ_{pmtp} = 266nm

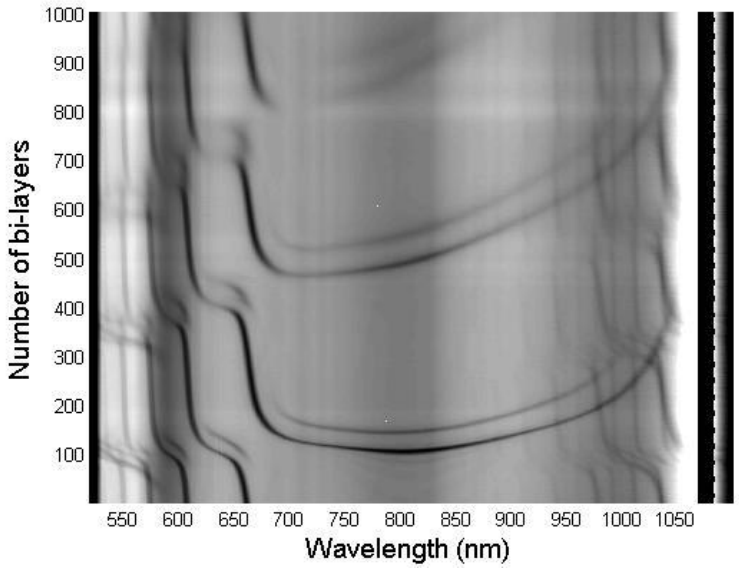

(b)

Figure 6.6 Evolution of the spectra of long period gratings with periods; (a) 80μm, (b) 100μm, coated with calix[8]arene recorded in the air subphase, in response to the deposition of the coating.

Coating = Tert-butyl-calix[8]arene, Λ = 140μm, length = 35mm, $\lambda_{\text{Phase Matching Turning Point}}$ = 930nm
Coating Thickness at λ_{pmtp} = 324nm

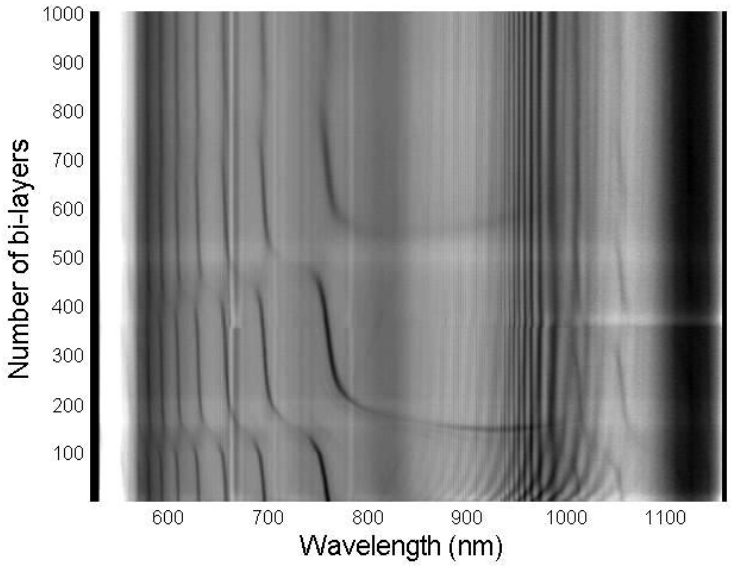

(c)

Coating = Tert-butyl-calix[8]arene, Λ = 180μm, length = 30-35mm, $\lambda_{\text{Phase Matching Turning Point}}$ = 911nm
Coating Thickness at λ_{pmtp} = 242nm

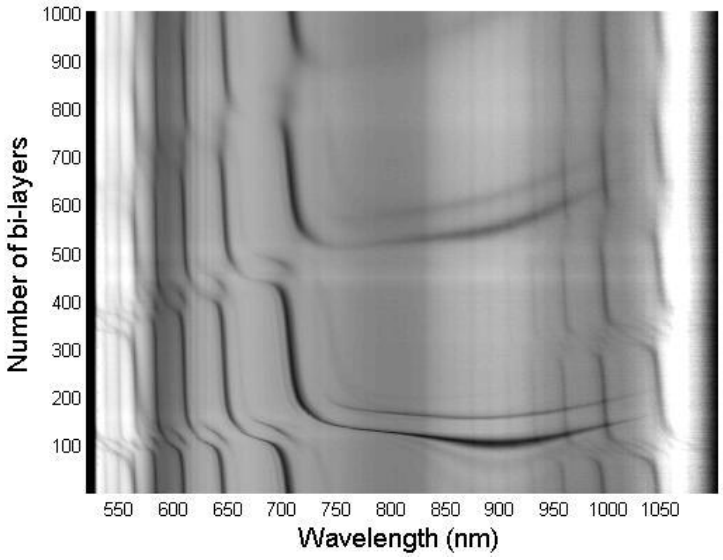

(d)

Figure 6.6 Evolution of the spectra of long period gratings with periods; (c) 140μm and (d) 180μm, coated with calix[8]arene recorded in the air subphase, in response to the deposition of the coating.

6.5 INTERPRETATION OF THE DATA

Data on long period gratings that have been fabricated in the laboratory and subsequently coated to date has been collected.

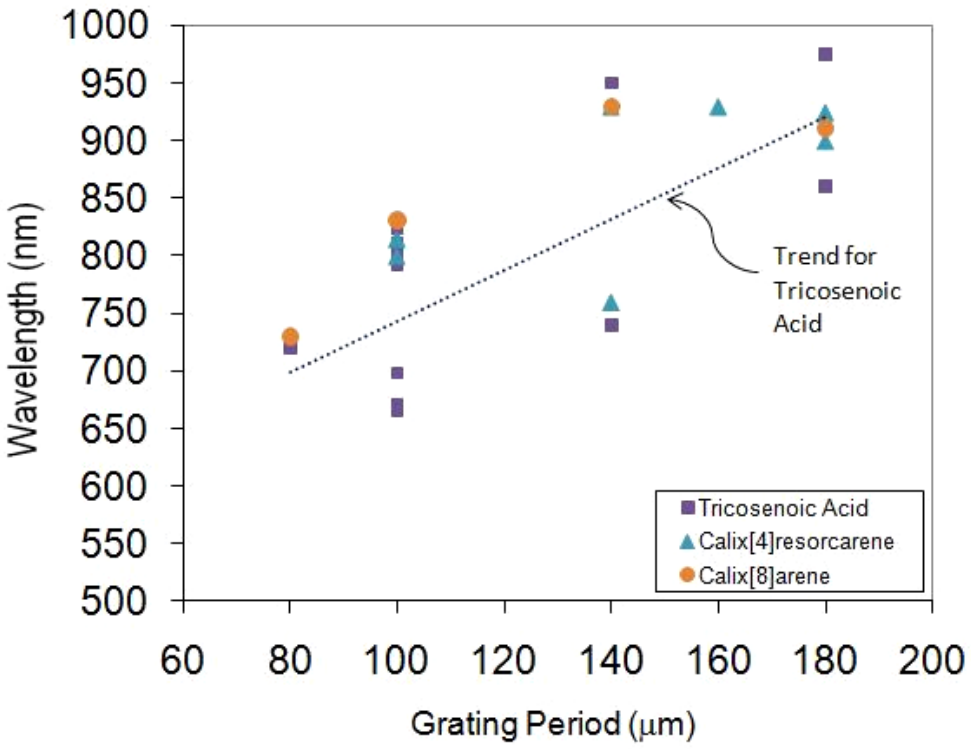

Figure 6.7 The wavelength at which coupling to a symmetric cladding mode occurs at the phase matching turning point, compared with grating period, for coated long period gratings.

The plot of the wavelength of the phase matching turning point verses the grating period for different coating materials shows that the coupling wavelength increases with grating period. The trend for tricosenoic acid in Figure 6.7 indicates this, with all three coating materials showing a similar characteristic. The phase matching curves, see Figures 2.6 and 5.1, indicate that the phase matching turning point will increase in wavelength as the period of the LPG is increased.

Next, the dual resonant phenomenon is analysed in terms of the layer thickness where coupling to a symmetric cladding mode is seen. The plot shows the coating thickness required for coupling to a symmetric cladding mode at the phase matching turning point, and is compared with the grating period, Figure 6.8.

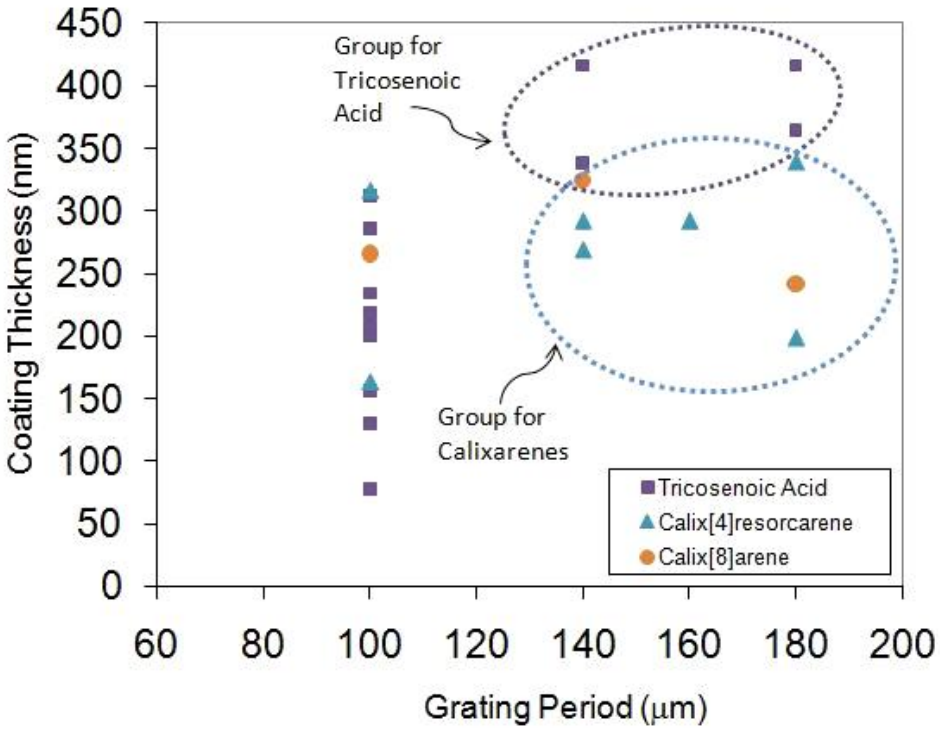

Figure 6.8 The coating thickness allowing coupling to a symmetric cladding mode at the phase matching turning point, is compared with the grating period, for many coated long period gratings.

It can also be observed that for long period grating with periods 140μm to 180μm, the coating thickness required for coupling to a dual resonant cladding mode is less for a calixarene coating than for tricosenoic acid. The groupings for gratings coated with tricosenoic acid, and either of the two calixarenes are highlighted in Figure 6.8, for the gratings with periods above 140μm. It would therefore be natural to deduce that the calixarenes deposit as a denser coating with the higher refractive index, allowing access to the dual resonant cladding mode with a thinner coating. However, Table 6.2 indicates that the tricosenoic acid has the highest refractive index and therefore the greater density.

One can question the values of refractive index recorded in the literature since it has been noted that a value recorded for the refractive index of tert-butyl calix[8]arene carboxylic acid derivative of 1.21[18] appears incorrect since our responses obtained with

this identical material shows the typical responses of HRI coatings. This means that the refractive index of this coating must be greater that the cladding refractive index, ~1.45.

It should be noted that the technique and execution of the deposition of the coating must cause the density and therefore the refractive index of the coating to vary, especially if the execution is defective in some regard. Although the figure quoted was from a coating laid down using the Langmuir-Blodgett technique, it may be the result of a different deposition speed outside the range recorded in Table 6.1. This may affect how neatly the molecules pack together, and the meshing of the alkyl chains. These considerations must clearly result in changes to the final density of the coating.

6.6 GRATING PERIOD OPTIMISATION

Different features in the transmission spectrum of the LPG arise, some of which are specific to the period of the LPG. These are identified.

At a LPG period of 80μm, the dual resonance attenuation bands appear in the spectrum of the uncoated fibre. This would allow sensors with a coating thickness of a few monolayers to be fabricated, whilst still exploiting the dual resonance attenuation bands. These sensors may have advantages of short response and recovery times. It may be necessary to fine tune the grating period to tailor the resulting transmission spectrum to one where the dual resonant attenuation bands are closer in wavelength, to achieve a spectrum resembling Figure 5.10.

A coated 100μm period long period grating develops the dual resonance attenuation band centred at a wavelength of ~800nm. This is in a region close to the cut-off wavelength of the fibre, and it is beneficial to operate at wavelengths close to the cut-off wavelength of the fibre in order to reduce the affect of bend losses.

When a coating is deposited, long period gratings with a period of 140μm have been shown experimentally in Figures 6.3 and 6.4 to be the best optimized for coincidence of the phase matching turning point and the first transition region. This was observed with an LPG deposited with a tricosenoic acid coating of thickness ~360nm, and for a calix[4]resorcarene coating with a thickness of ~280nm. If this phenomenon is harnessed, then optimized sensitivity for sensor design can be realized.

A coated LPG with a period of 180μm has been used in Chapter 8 to demonstrate chemical sensing. This grating period resulted in a transmission spectrum with the dual

resonant attenuation bands having similar extinction ratios, see Figure 8.6[bb]. A spectrum which contains attenuation bands with high extinction ratios will make the location of the centre wavelength of the attenuation bands more accurate. This is relevant for sensing applications.

6.7 CONCLUSIONS

Dual resonance in long period gratings has not been widely reported, and there has been no systematic investigation of the character and nature of these devices. With this in mind, four long period gratings have been fabricated, each of differing period in the range 80μm-180μm; this was selected to match the the operational range of a CCD spectrometer used to monitor the transmission spectrum of an LPG. Each LPG was coated with three materials, each material having a different refractive index. This is in order to observe the trends in the spectrum of the devices, and this has been illustrated in Figures 6.3 through to 6.6.

It has been learnt that if a sensor is to be made exploiting dual resonance, the selection of the grating period can determine the required coating layer thickness, the sensors operating wavelength, the sensitivity by its proximity to the transition region, or the shape of the dual banded spectrum. Although these cannot all be optmised simultaneously by controlling only the grating period, the application of the sensor may point to their respective priorities.

[bb] The grating was coated with calix[4]resorcarene

6.8 REFERENCES

1. Vengsarkar, A. M., Lemaire, P. J., Judkins, J. B., Bhatia, V., Erdogan, T. and Sipe, J. E. (1996), "Long-period fiber gratings as band-rejection filters", *Journal of Lightwave Technology,* vol. 14, no. 1, pp. 58-64.

2. Liu, Q., Chiang, K. S. and Liu, Y. (2007), "Characterization of single-mode fiber with fiber Bragg gratings for the design of long-period gratings", *Journal of Lightwave Technology,* vol. 25, no. 8, pp. 2129-2134.

3. James, S. W., Cheung, C. S. and Tatam, R. P. (2007), "Experimental observations on the response of 1st and 2nd order fibre optic long period grating coupling bands to the deposition of nanostructured coatings", *Optics Express,* vol. 15, no. 20, pp. 13096-13107.

4. Gowar, J. (1983), "Optical Communication Systems", Prentice-Hall International Series in Optoelectronics, pp. 3.

5. Shu, X., Zhu, X., Wang, Q., Jiang, S., Shi, W., Huang, Z. and Huang, D. (1999), "Dual resonant peaks of LP015 cladding mode in long-period gratings", *Electronics Letters,* vol. 35, no. 8, pp. 649-651.

6. Shu, X. W., Zhu, X. M., Jiang, S., Shi, W. and Huang, D. X. (1999), "High sensitivity of dual resonant peaks of long-period fibre grating to surrounding refractive index changes", *Electronics Letters,* vol. 35, no. 18, pp. 1580-1581.

7. Cheung, C. S., Topliss, S. M., James, S. W. and Tatam, R. P. (2008), "Response of fibre optic long period gratings operating near the phase matching turning point to the depostion of nanostructured coatings", *Journal of the Optical Society of America B,* vol. 25, no. 6, pp. 897-902.

8. Topliss, S. M., James, S. W., Davis, F., Higson, S. P. J. and Tatam, R. P. (2010), "Optical fibre long period grating based selective vapour sensing of volatile organic compounds", *Sensors and Actuators, B: Chemical,* vol. 143, no. 2, pp. 629-634.

9. Patrick, H. J., Kersey, A. D. and Bucholtz, F. (1998), "Analysis of the response of long period fiber gratings to external index of refraction", *Journal of Lightwave Technology,* vol. 16, no. 9, pp. 1606-1612.

10. Laffont, G. and Ferdinand, P. (2001), "Tilted short-period fibre-Bragg-grating-induced coupling to cladding modes for accurate refractometry", *Measurement Science and Technology,* vol. 12, no. 7, pp. 765-770.

11. Shu, X. W., Zhang, L. and Bennion, I. (2002), "Sensitivity characteristics of long-period fiber gratings", *Journal of Lightwave Technology,* vol. 20, no. 2, pp. 255-266.

12. Grubsky, V. and Feinberg, J. (2000), "Long-period fiber gratings with variable coupling for real-time sensing applications", *Optics Letters,* vol. 25, no. 4, pp. 203-205.

13. Rees, N. D., James, S. W., Tatam, R. P. and Ashwell, G. J. (2002), "Optical fiber long-period gratings with Langmuir-Blodgett thin-film overlays", *Optics Letters,* vol. 27, no. 9, pp. 686-688.

14. Del Villar, I., Matias, I. R. and Arregui, F. J. (2006), "Influence on cladding mode distribution of overlay deposition on long-period fiber gratings", *Journal of the Optical Society of America A-Optics Image Science and Vision,* vol. 23, no. 3, pp. 651-658.

15. Othonos, A. and Kalli, K. (1999), *Fiber Bragg Gratings: Fundamentals and Applications in Telecommunications and Sensing,* Artech House.

16. Skjonnemand, K. (2000), *The Optical and Structural Characterization of Ultra-Thin Films,* PhD Thesis, Cranfield University, Cranfield, UK.

17. Hassan, A. K., Nabok, A. V., Ray, A. K., Lucke, A., Smith, K., Stirling, C. J. M. and Davis, F. (1999), "Thin films of calix-4-resorcinarene deposited by spin coating and Langmuir-Blodgett techniques: Determination of film parameters by surface plasmon resonance", *Materials Science and Engineering C,* vol. 8-9, pp. 251-255.

18. Çapan, R., Ozbek, H., Goktas, H., Sen, S., Ince, F. G., Ozel, M. E., Stanciu, G. A., Davis, F. (2010), "Characterization of Langmuir-Blodgett films of a calix[8]arene and sensing properties towards volatile organic vapours", *Sensors and Actuators B: Chemical*, vol. 148, pp. 358-365.

19. Corres, J. M., Matias, I. R., del Villar, I. and Arregui, F. J. (2007), "Design of pH sensors in long-period fiber gratings using polymeric nanocoatings", *IEEE Sensors Journal,* vol. 7, no. 3-4, pp. 455-463.

CHAPTER 7: INVESTIGATION OF LENGTH APODIZED PHASE SHIFTED LPGS WITH COATINGS

7.1 INTRODUCTION

The long period grating couples light from the core into the cladding and this occurs at the Bragg resonance wavelengths, see Chapter 2. The coupling influences the transmission spectrum of the fibre, introducing drop outs or attenuation bands at the Bragg resonance wavelengths. In this way, long period gratings are inherently band-rejection devices[1; 2].

Usually, the long period grating contains a regular phase structure that forms a grating which can be described by repeating 2π phase shifts, and this is referred to as the period of the grating, Λ. Phase shifted long period gratings on the other hand contain phase shifts that deviate from 2π. A phase shifted long period grating with a single π phase shift in the centre of the grating produces a transmission spectrum in which each resonance contains a maxima at the Bragg resonance wavelength with two attenuation bands either side, a result of interference between light coupled into the cladding modes by the two sections of grating either side of the phase step. This creates a band pass response, as illustrated in Figure 7.1.

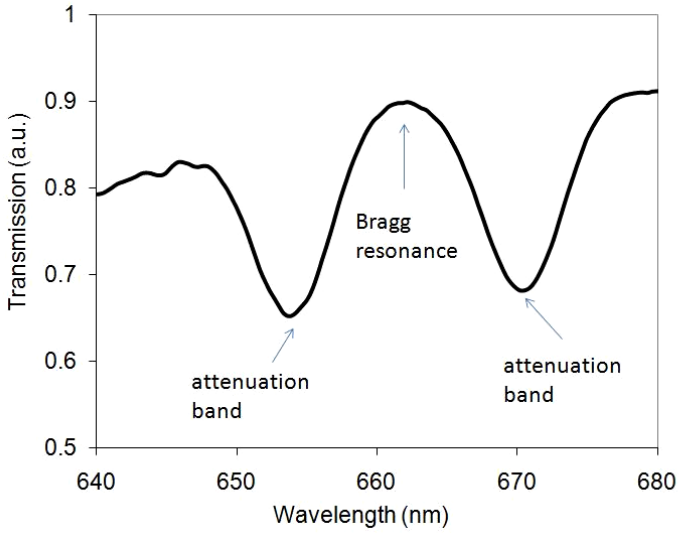

Figure 7.1. The transmission spectrum showing the attenuation bands located either side of the Bragg resonance wavelength[cc]. The two bands are the result of phase shifts in the LPG.

[cc] This plot was obtained from a length apodised phase shifted LPG of period 100μm and length 27mm

This concept can be extended by incorporating a number of equidistant π phase shifts along the grating. Here the attenuation bands become sharper with a narrower FWHM[dd] bandwidth[3]. However side lobes are introduced between the attenuation bands. Four side lobes are shown in the centre of Figure 7.2a. These are generally undesirable with regard to the passband response. For telecommunication applications, the side lobes would correspond to passband ripple in a wavelength bandpass optical filter.

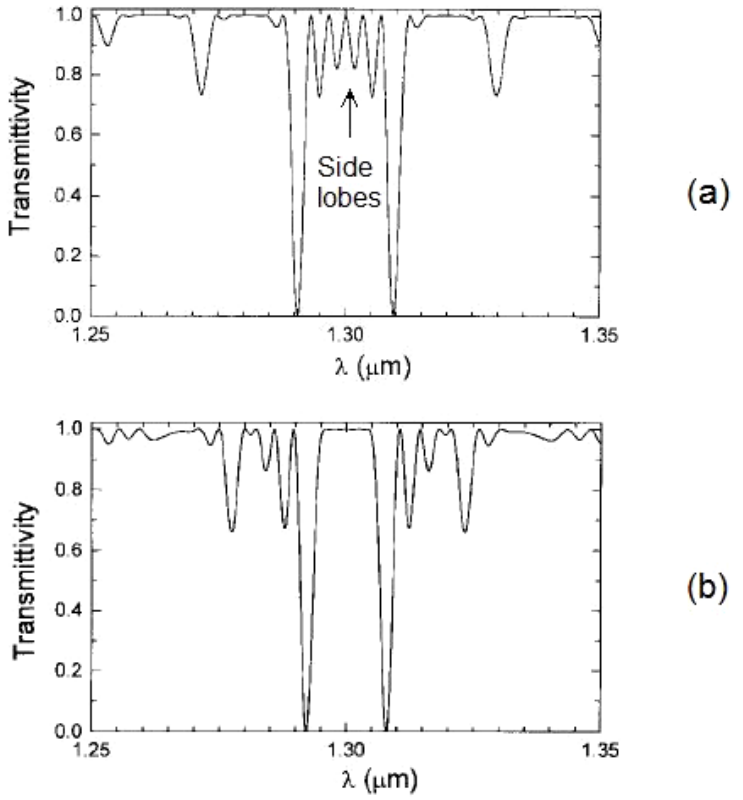

Figure 7.2 The spectral response of (a) a six section LPG with five equally spaced π phase shifts, and (b) a six section LPG with apodised π phase shifts[4]

To eliminate the side lobes, length apodization can be performed. This entails the spacing of the π phase shifts such that they located along the grating in a Gaussian distribution. In this way, the passband between the two attenuation bands can be designed to be practically free from side lobes[4]. This is illustrated in Figure 7.2b. This passband response would have uses in the construction of an optical wavelength filter for applications in dense wavelength division multiplexed fibre optic communications networks.

[dd] Full Width Half Maximum

The motivation to reproduce this phenomenon is to observe the effects of length apodization at the phase matching turning point. Here, light is coupled into the same cladding mode at two wavelengths[5], see Chapter 2. It is also known as dual resonance[6]. The interplay of dual resonance with the two attenuation bands arising from the phase shift has not been investigated before and is the subject of this Chapter.

To this end, a grey scale plot of a length apodized phase shifted LPG when coated with a high refractive index (HRI) film has be produced. The coating allows the dual resonance spectrum to be obtained, see Chapter 5. Furthermore, the effect of partially coating a length apodized phase shifted LPG has been explored. An interesting effect of *bandgaps* appearing in the attenuation bands occurs, observed in the transition region[7].

7.2 PHASE SHIFTED LONG PERIOD GRATINGS

Some studies have been reported in the scientific literature on the design of phase shifted long period gratings[2-4; 8-12]. These devices allow manipulation of the transmission response resulting from coupling to each cladding mode. Considering coupling to one such cladding mode, a centrally placed single phase shift of π gives rise to two equal attenuation bands in the spectra, Figure 7.1. This is a result of converting destructive interference into constructive interference at the Bragg resonance wavelength[4]. Here, this interference occurs between the light coupled into the cladding from the two sections of the grating, separated by the phase shift.

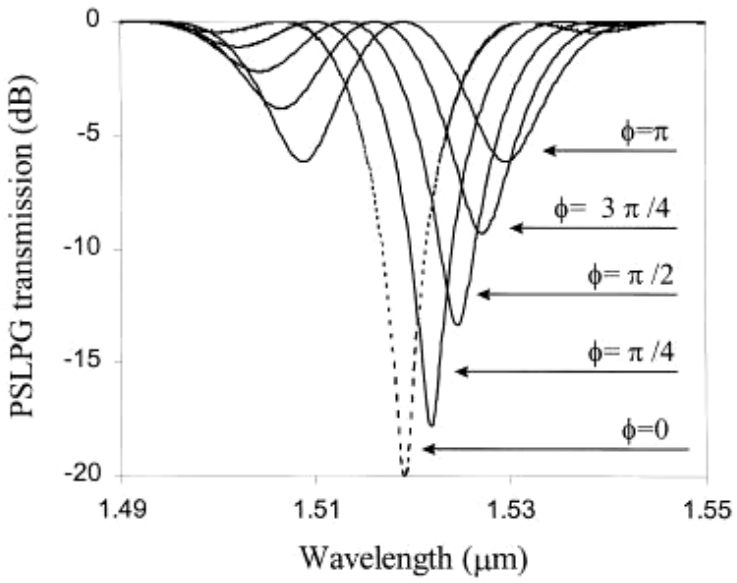

Figure 7.3 Phase Shifted PSLPG transmission for different phase shifts ϕ = 0 to π. Image from [11]

The affect of changing this phase shift from π down to $\pi/4$ has been reported[11]. Here, the attenuation bands become of non-equal extinction and the central maxima moves to shorter wavelengths, Figure 7.3.

Moving the position of the phase shift from the centre of the grating has also been investigated[4]. Here a π phase shift was located at L/5 and 2L/5 where L is the length of the grating. Here, the spectrum containing two closely spaced attenuation bands and a bandpass feature between them changes to one where the two attenuation bands coalesce, and become unresolved. This broad single attenuation band may be desirable for the design of band rejection filters.

In order to extend the design envelope further, it is necessary to introduce more than one phase shift along the length of the grating, such that the grating has multiple sections, separated by phase shifts. It has been shown that the separation of the two attenuation bands resulting from coupling to the same cladding mode is linearly proportional to the number of sections in a phase shifted LPG. For a π phase shifted LPG reported with six sections, with a grating period of 100μm and a length of 40mm, the wavelength separation of the two attenuation bands resulting from coupling to the same cladding mode is approximately 10nm. For 12 sections, the wavelength separation is 20nm[4]. The spectrum can also be modified by controlling the grating length. The FWHM bandwidth of these attenuation bands show a nearly inversely linear dependence with the grating length, with the bandwidth narrowing with greater grating length[12].

Side lobes in the frequency spectra can occur between the attenuation bands which can be removed by the technique of length apodization[3; 4]. Here, the π phase shifts are spaced in a Gaussian distribution. Again, the separation of the pair of attenuation bands resulting from coupling to a single cladding mode increases linearly with the number of phase shift sections in the grating, but is about 60% of the separation of the attenuation bands when compared to those obtained for LPGs with equidistant phase shifts[2].

Long period gratings with "*phase shifted phenomena"*[13] which contain multiple interference fringes in their spectra have also been observed for LPGs without the need to fabricate phase shifts in the grating period. Examples of these devices are cascaded LPGs that have a short separation[11; 14], LPGs in which the mark space ratio varies over the length of the grating i.e. the spatial refractive index modulation profile changes along the length of the grating[8], applying a coating with a refractive index $n_{coating}$ =1.54 to the LPG whereupon there is a partial removal of the central region of the LPG coating[13], and partial removal of the cladding through selective etching[9].

One of the advantages of introducing a band pass feature in the transmission spectrum is that it does allow these devices to operate in single-ended reflection mode by the incorporation of a mirror at the distal end[10]. In this case, the optical power received is not compromised by a high level of in-band attenuation on the forward and return transit that would occur in a sensor that utilized rejection bands.

7.3 LPG FABRICATION

Phase shifted LPGs are simply LPGs that contain one or more step changes in the phase of the grating. Here, the step change is $\Lambda/2$ in the period of the grating. They are straightforward to construct using the point by point UV inscription technique[15] by appropriate programming of the movement of the translation stage. A device has been made based on the fabrication recipe for a length apodized phase shifted LPG[3], and is defined in Figure 7.4. A period of 100μm has been chosen to obtain operation in the region of the phase matching turning point[5], see Chapter 5. The fibre used is hydrogen-loaded single mode fibre, SM750 that has a cut-off wavelength of 619nm. The fabrication recipe has been adapted to ensure that a period of 100μm resulted in a grating of length 27mm, a typical length for a regular spaced LPG of this period, see Chapter 6.

The resulting transmission spectrum, shown in Figure 7.5, was recorded using a tungsten-halogen lamp and an Ocean Optics CCD spectrometer of resolution 0.3nm. This spectrum has two attenuation bands, with a separation of about 20nm, with a fully resolved passband centred at ~660nm. All these features are a result of coupling to the same cladding mode. However an additional side-lobe located outside the two attenuation bands was present. This is a by-product of length apodization[3]. This arises from the interference of the light coupled into the cladding from each section of the grating.

These features in the spectra are repeated centred at ~610nm, resulting from coupling to a different cladding mode. These results indicate the level of resolution of the two attenuation bands that can be obtained, considering sources of imperfection that can arise in the fabrication process, e.g. tracking errors, inaccurate setting of the mark space ratio and other inconsistencies with the UV inscription experimental set up.

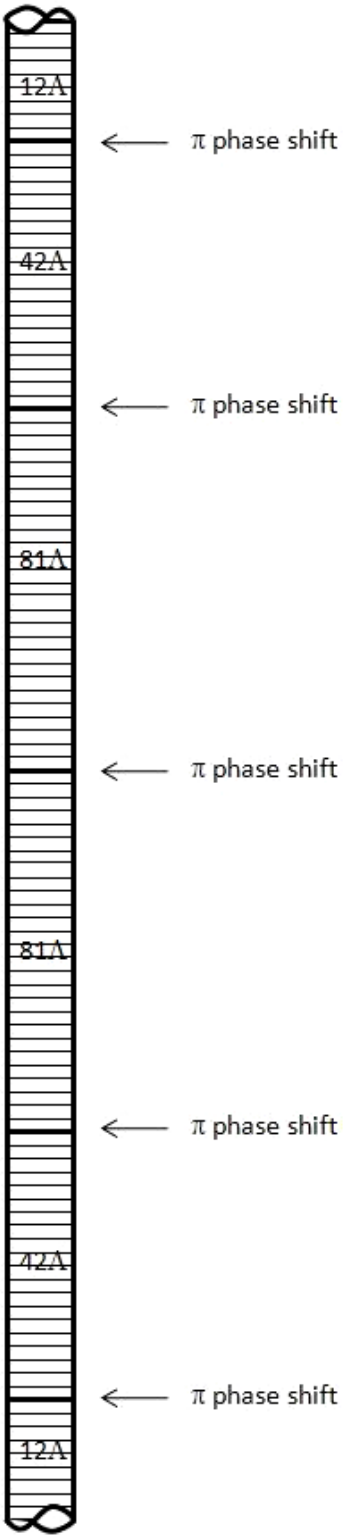

Figure 7.4 The fabrication recipe used here for a length apodised phase shifted long period grating, adapted from [3]. This is a six section device, with the number of periods, 12Λ, 42Λ, 81Λ, 81Λ, 42Λ, 12Λ, shown for each section of the grating. Between each section is a π phase shift, i.e. Λ/2.

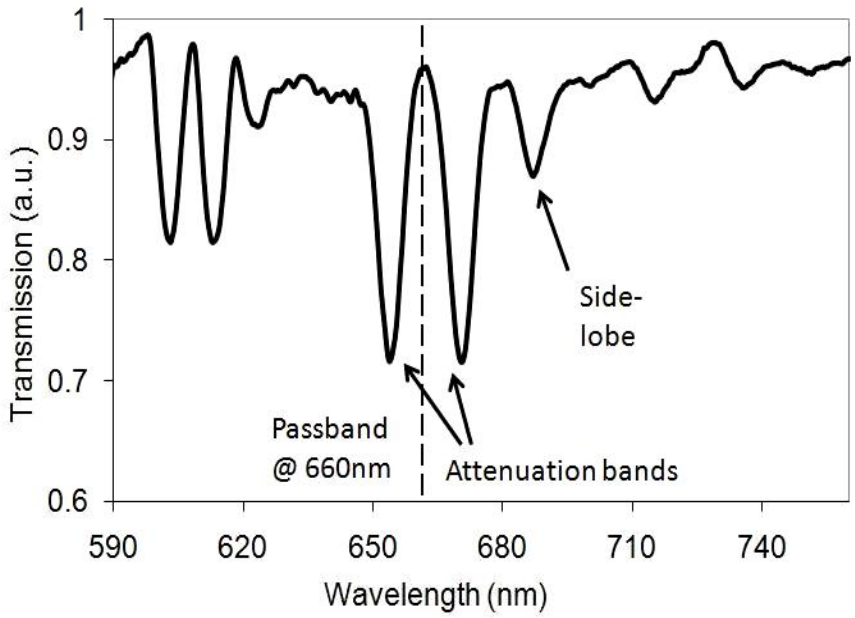

Figure 7.5 The transmission spectrum obtained from a length apodised phase shifted LPG of period 100μm and length 27mm. The two attenuation bands are the result of phase shifts in the LPG. The side-lobe as indicated is a known by-product of length apodisation[3].

7.4 COATING OF THE LPG

To investigate the affect of coatings on length apodized phase shifted LPGs, a grating coating was deposited using the Langmuir-Blodgett technique, using a Nima Technology Model 2410A Langmuir-Blodgett trough modified for use with fibre optic substrates[16]. The coating material was ω-tricosenoic acid[5] which was dissolved in chloroform at 0.14g/l. This material has a refractive index higher than the cladding, and has been used to investigate the effect of HRI coatings on the transmission spectrum of the LPG, see Chapter 5. This solution was spread onto a pure water subphase of one compartment of the trough, and was compressed to a surface pressure of 26mN/m. The transfer rate was 12mm/min.

The evolution of the transmission spectrum of the length apodized phase shifted long period grating was recorded during the coating process, in order to investigate the behaviour at the phase matching turning point. A coating thickness in excess of 0.75μm was applied to the fibre, with each layer having a coating thickness of 2.6nm, see Table 6.2. The transmission spectrum was recorded above and below the water subphase, by coupling the output from a tungsten-halogen lamp into the fibre and

connecting the distal end of the fibre to an Ocean Optics CCD spectrometer of resolution 0.3nm.

7.5 RESULTS

The transmission spectrum in Figure 7.6 shows the formation of a number of features that evolve as the coating is deposited. A single attenuation band occurs at 73 layers, and this is the single broad attenuation band that occurs at the onset of dual resonance, see Chapter 5. With the deposition of another 10 layers, the broad attenuation band splits into two resolvable attenuation bands at 83 layers. These two attenuation bands move apart in wavelength with a deposition of further layers, from 93-123 layers. So far, this is the typical dual resonant response for LPGs operating at the phase matching turning point.

However, some further spectral features are observable arising from the phase shifts present in the LPG. The spectral pattern described above repeats itself. Another single attenuation band appears at 103 layers, arising from operation at the phase matching turning point, with a further two attenuation bands developing at 113 layers. Consequently, a total of four attenuation bands are visible which proceed to diverge in wavelength between 113-123 layers.

To interpret the data further, the same transmission spectra is shown using a grey scale plot, Figure 7.7. The darker regions of the grey scale represent optical loss. The results from above the water subphase show the evolution with coating thickness of two discrete sets of dual resonance attenuation bands, identified in Figure 7.7 as (1) and (2). This is a result of the combination of both operation at the phase matching turning point, see Chapter 5, and the phase shifts present in the structure of the LPG.

The dual resonance attenuation band depicted in Figure 7.7 (2) has a closer proximity to the transition region. In Chapter 5, it was described how the proximity to the transition region results in a different sensitivity of the dual resonance attenuation band to the coating's optical properties. Therefore, the differing proximity of each dual resonance attenuation band (1) and (2) to the transition region will give differing sensitivities to the optical properties of the coating.

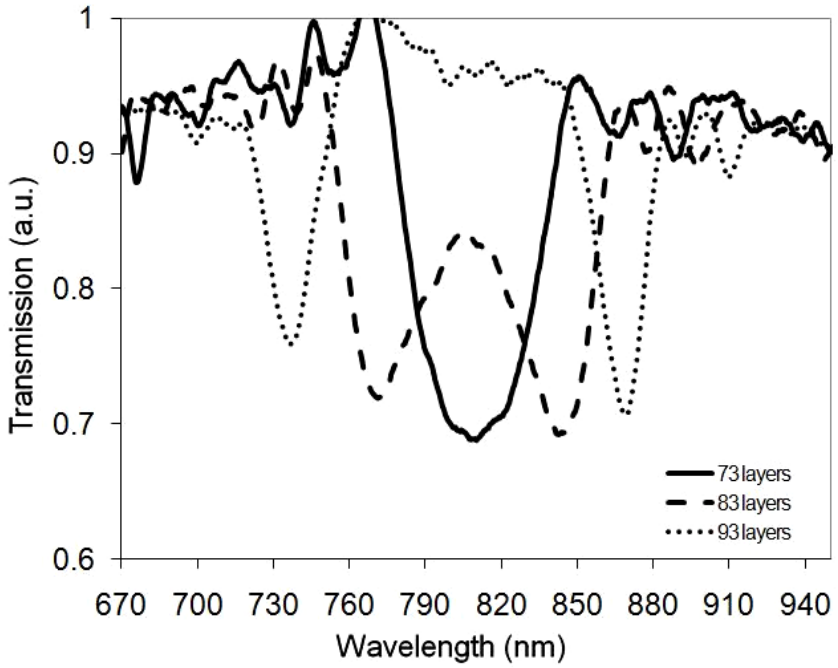

(a)

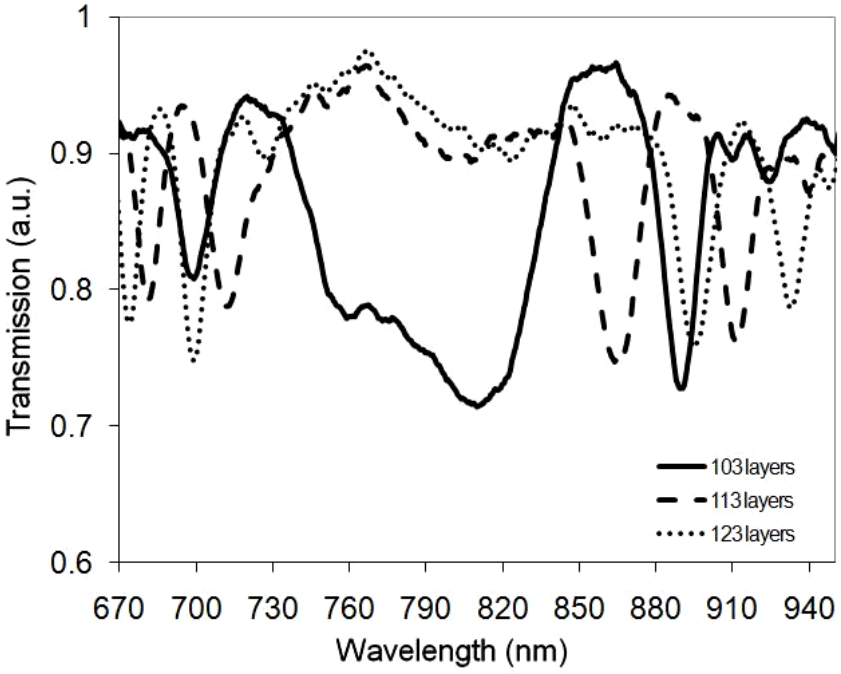

(b)

Figure 7.6 The evolution of the spectrum of a length apodized phase shifted LPG upon deposition of layers of ω-tricosenoic acid, recorded above the water subphase. (a) layers 73-93 (b) layers 103-123.

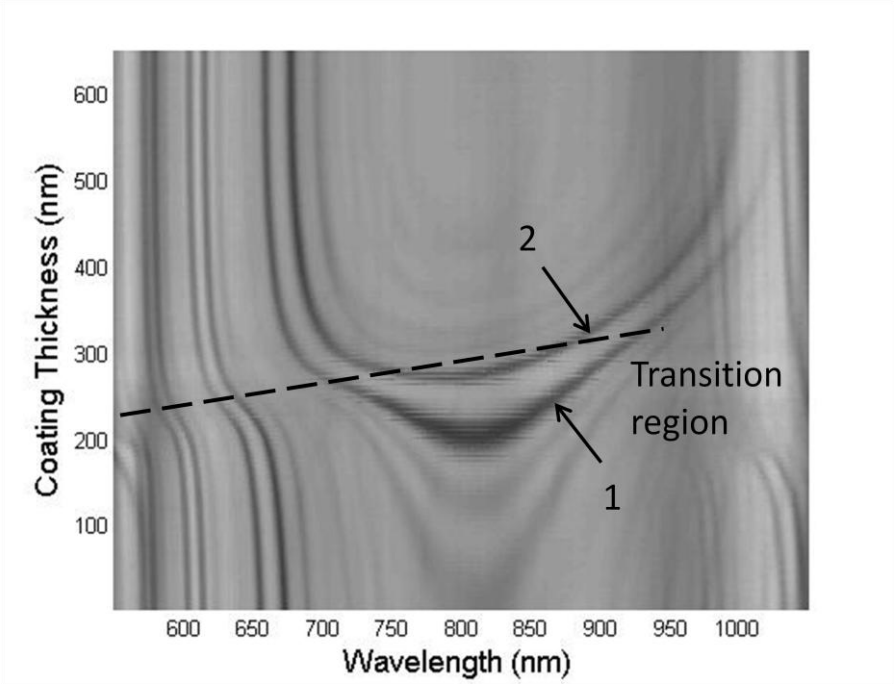

Figure 7.7 The evolution of the attenuation bands with applied coating thickness to the cladding of a length apodized phase shifted long period grating. When the coating is of sufficient thickness, ~200nm, two pairs of dual resonant attenuation bands appear, (1) and (2), at a wavelength in the region of 800nm. This spectrum was recorded above the water subphase.

7.6 PARTIAL COATING OF THE LENGTH APODIZED PHASE SHIFTED LPG

To take the investigation further, the effect of partially coating the length apodized phase shifted long period grating was studied. Starting at one end of the grating, half the grating length was coated with tricosenoic acid. The results are presented in Figures 7.8 using a grating fabricated in SM750 fibre with cut-off wavelength of 619nm, and Figure 7.9 using a grating fabricated to the same recipe, see Figure 7.4, but using another batch of fibre with a cut-off wavelength of 669nm.

When the transmission spectrum is plotted as a grey scale, it is apparent that an affect which for the purposes of this thesis are described as *bandgaps,* appear in the attenuation bands. These are a result of only coating 13.5mm of the grating, half of the length of the grating.

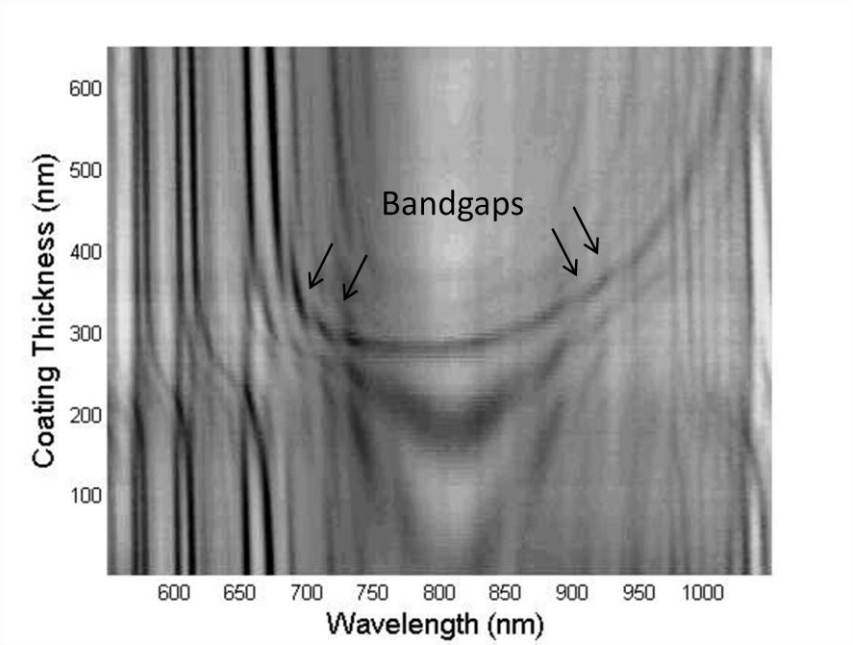

Figure 7.8 The evolution of the spectrum of a length apodized phase shifted long period grating upon deposition of layers of ω-tricosenoic acid to half the length of the grating. *Bandgaps* appear in the attenuation bands, and are clearly visible at ~700nm. This spectrum was recorded above the water subphase.

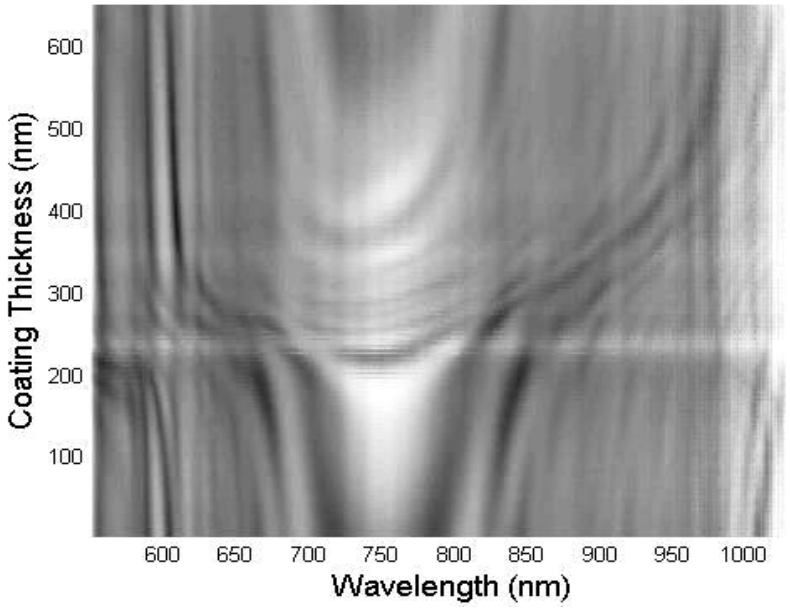

Figure 7.9 The evolution of the spectrum of a length apodized phase shifted long period grating upon deposition of layers of ω-tricosenoic acid to half the length of the grating. Bandgaps appear in the attenuation bands, and are visible at ~900nm. This spectrum was recorded above the water subphase.

The bandgaps are essentially cladding mode bandgaps where coupling is prevented from the core to the cladding mode over a narrow wavelength band. The phase shifted grating can be considered as two gratings of continuous phase that are spatially interleaved, which are referred to here as the two grating segments. By coating half the entire grating length, this is equivalent to an unequal coating applied to the two grating segments. Therefore, we would expect to see interference effects arising from a phase difference of the light coupled into the cladding, resulting from differing thicknesses of coating applied to each grating segment.

To understand this spectrum more fully, a standard 100μm long period grating was partially coated along half the grating length, Figure 7.10. Here, the spectrum from the uncoated half of the grating does not change with coating thickness, whereas the spectrum of the coated half develops in the typical dual resonant manner shown in Chapters 5 and 6. This effect can now be seen in Figure 7.8.

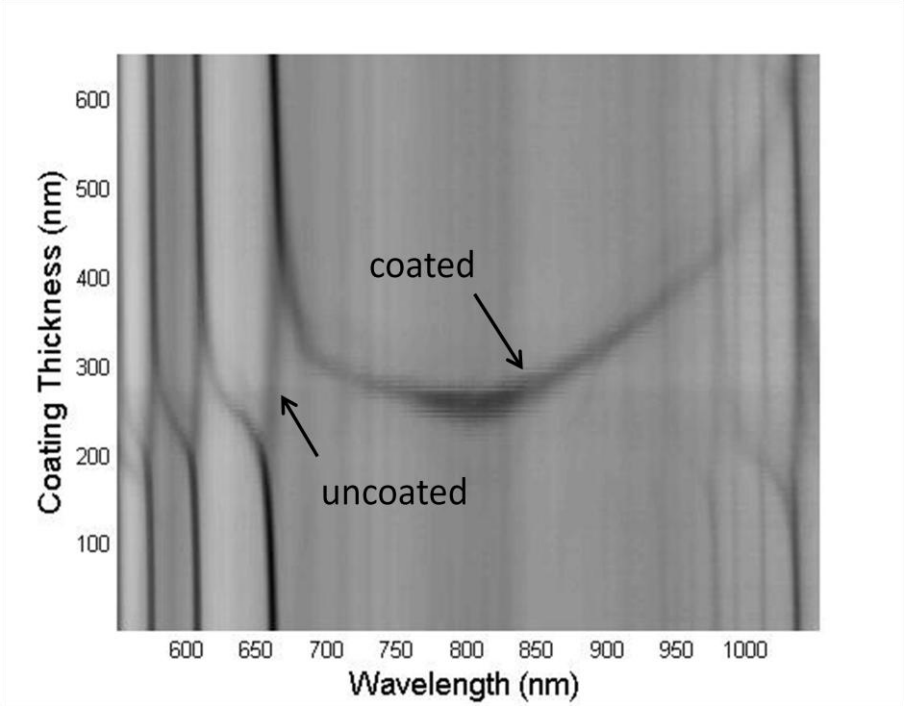

Figure 7.10 The evolution of the spectrum of a *conventional* LPG with period 100μm, with a coating of ω-tricosenoic acid applied to only half the length of the grating. This spectrum was recorded above the water subphase. No evolution of the attenuation bands occurs for the uncoated section of the grating.

The phenomenon of bandgaps may be useful since they introduce a spectral feature in the transmission response of the coated LPG that could be utilized for sensor design. Here, the attenuation bands will undergo a rapid change in extinction as well as

wavelength upon changes to the thickness or refractive index of the coating, in the region of the bandgap.

7.7 CONCLUSION

Length apodised phase shifted long period gratings have been investigated at the phase matching turning point. Two sets of dual-lobed attenuation bands occur in the spectra. Since each set has a different proximity to the transition region, the evolution of the spectra with coating thickness takes on a different form.

The response to partially coating this device has also been investigated. New features that are described here as *bandgaps* appear in the attenuation bands. It would be interesting to try to extend the bandgap region by trying different phase shifted LPG structures in conjunction with partial coatings. This will allow further analysis of this region, leading to optimization and greater definition of the bandgaps than has been achieved in this chapter. This in turn may lead to improvements in sensor design by obtaining new spectral features which can be utilised in sensor design.

7.8 REFERENCES

1. Vengsarkar, A. M., Lemaire, P. J., Judkins, J. B., Bhatia, V., Erdogan, T. and Sipe, J. E. (1996), "Long-period fiber gratings as band-rejection filters", *Journal of Lightwave Technology,* vol. 14, no. 1, pp. 58-64.

2. Chan, F. Y. M. and Chiang, K. S. (2005), "Analysis of apodized phase-shifted long-period fiber gratings", *Optics Communications,* vol. 244, no. 1-6, pp. 233-243.

3. Gu, Y., Chiang, K. S. and Rao, Y. J. (2009), "Writing of apodized phase-shifted long-period fiber gratings with a computer-controlled CO2 laser", *IEEE Photonics Technology Letters,* vol. 21, no. 10, pp. 657-659.

4. Ke, H., Chiang, K. S. and Peng, J. H. (1998), "Analysis of phase-shifted long-period fiber gratings", *IEEE Photonics Technology Letters,* vol. 10, no. 11, pp. 1596-1598.

5. Cheung, C. S., Topliss, S. M., James, S. W. and Tatam, R. P. (2008), "Response of fibre optic long period gratings operating near the phase matching turning point to the depostion of nanostructured coatings", *Journal of the Optical Society of America B,* vol. 25, no. 6, pp. 897-902.

6. Shu, X., Zhu, X., Wang, Q., Jiang, S., Shi, W., Huang, Z. and Huang, D. (1999), "Dual resonant peaks of LP015 cladding mode in long-period gratings", *Electronics Letters,* vol. 35, no. 8, pp. 649-651.

7. Del Villar, I., Matias, I. R. and Arregui, F. J. (2006), "Influence on cladding mode distribution of overlay deposition on long-period fiber gratings", *Journal of the Optical Society of America A-Optics Image Science and Vision,* vol. 23, no. 3, pp. 651-658.

8. Ke, H., Peng, J. and Fan, C. (2001), "Design of long-period fiber gratings with fast-varying parameters", *IEEE Photonics Technology Letters,* vol. 13, no. 11, pp. 1194-1196.

9. Chung, K. and Yin, S. (2005), "Design of a phase-shifted long-period grating using the partial-etching technique", *Microwave and Optical Technology Letters,* vol. 45, no. 1, pp. 18-21.

10. Falate, R., Frazão, O., Rego, G., Fabris, J. L. and Santos, J. L. (2006), "Refractometric sensor based on a phase-shifted long-period fiber grating", *Applied Optics,* vol. 45, no. 21, pp. 5066-5072.

11. Liu, Y., Williams, J. A. R., Zhang, L. and Bennion, I. (1999), "Phase shifted and cascaded long-period fiber gratings", *Optics Communications,* vol. 164, no. 1, pp. 27-31.

12. Navruz, I. and Altuncu, A. (2008), "Optimization of phase shifted long-period fiber gratings for multiband rejection filters", *Journal of Lightwave Technology,* vol. 26, no. 14, pp. 2155-2161.

13. Del Villar, I., Arregui, F. J., Matias, I. R., Cusano, A., Paladino, D. and Cutolo, A. (2007), "Fringe generation with non-uniformly coated long-period fiber gratings", *Optics Express,* vol. 15, no. 15, pp. 9326-9340.

14. Ishaq, I., James, S. W., Ashwell, G. J. and Tatam, R. P. (2005), "Cascaded long period gratings with nano-structured coatings", *Optics Letters*, vol. 30, pp. 2197-2199.

15. Othonos, A. and Kalli, K. (1999), *Fiber Bragg Gratings: Fundamentals and Applications in Telecommunications and Sensing,* Artech House.

16. Rees, N. D., James, S. W., Tatam, R. P. and Ashwell, G. J. (2002), "Optical fiber long-period gratings with Langmuir-Blodgett thin-film overlays", *Optics Letters,* vol. 27, no. 9, pp. 686-688.

CHAPTER 8: LPG BASED SELECTIVE VAPOUR SENSING OF VOLATILE ORGANIC COMPOUNDS

8.1 INTRODUCTION

The sensing of volatile organic compounds (VOCs) is of importance in a range of applications, for example, monitoring air quality in both indoor and outdoor environments, and for monitoring soil and water contamination[1]. VOCs can originate from fuel and petroleum products, from paints and inks, and from combustion processes, natural sources and farming[2]. There are a wide range of VOCs, but of particular interest are the BTEX chemicals; benzene, toluene, ethylbenzene and xylene. The ability to detect this chemical family and be able to distinguish it from the other aliphatic hydrocarbons is an important requirement for a detection system, since the aromatic hydrocarbons have a far higher toxicity.

The sensor described in this chapter utilizes calixarene to form the nanostructured coating, which is shown to facilitate the sensing of toluene and benzene, while being relatively insensitive to the aliphatic and alicyclic hydrocarbons, hexane and cyclohexane.

8.2 PHASE MATCHING CURVES

Phase matching curves generated by the solution of Equation 2.1 are an important design tool for long period gratings, allowing the calculation of a complete set of discrete wavelength resonances[3]. Figure 8.1 shows the phase matching curves predicted for a fibre of cut-off wavelength 670nm[4]. The cladding modes are numbered, corresponding to the order of each mode, and the resonant wavelengths are indicated by the intersection of the phase matching curve and a line parallel to the wavelength axis. A turning point in the phase matching curves is seen[5], making it possible to couple to the same cladding mode at two different wavelengths, producing dual resonant bands in the transmission spectrum[6].

As described in Chapter 5, optimum sensivity of the coated LPG will be accessed for the period at which the phase matching turning point and the mode transition region are coincident. This effect is illustrated in the grey scale plot shown in Figure 8.2. The resonant band corresponding to the $LP_{0\,15}$ cladding mode indicates the location of the transition region, while for the $LP_{0\,16}$ mode the transition region and the phase matching turning point are coincident in this thickness range. The increase in sensitivity for the $LP_{0\,16}$ mode is evident. Plotting the data in such a way allows the relationship of the dual resonance band with respect to the mode transition region to be observed.

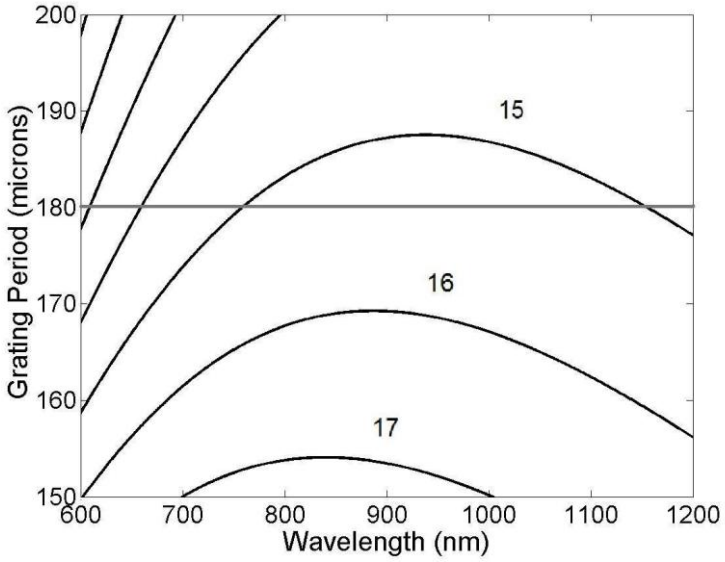

Figure 8.1 The relationship between the grating period and the wavelength at which coupling occurs to a set of symmetric cladding modes ($LP_{0\,15} - LP_{0\,17}$)[4]. The numbers refer to the order of the cladding mode, LP_{0x}. The horizontal line indicates an LPG period of 180μm.

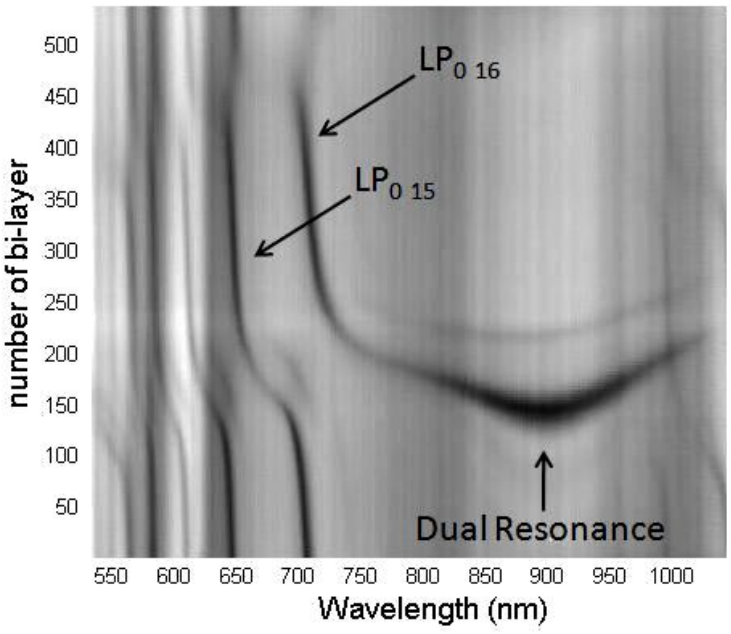

Figure 8.2 Grey scale plot illustrating the response of the transmission spectrum of an LPG of period 180μm to the deposition of a coating of calix[4]resorcarene using the LB technique. The spectra were recorded with the LPG in the air subphase. The attenuation band originating at approximately 900nm shows the development of the dual resonance effect.

8.3 COATINGS FOR SELECTIVE SENSING

Calixarene molecules are structures containing a number of phenol or resorcinol aromatic rings interconnected to form a larger ring. The calixarene used here is derived from four resorcinol aromatic rings and is referred to as calix[4]resorcarene[7]. The molecular structure is shown in Figure 8.3 and Figure 8.4. In three dimensions this is a bowl like structure[8] that has a cavity in the centre. The resorcarene cavity has an upper rim diameter of 1.32nm[9].

The eight hydroxyl groups give the resorcarene molecule a part hydrophilic nature, whereas the hydrocarbon chains are known as pendants[11] and give the molecule hydrophobicity. These long hydrophobic chains are added to make the molecule amphiphilic, such that it is part hydrophobic and part hydrophilic, which is a requirement to allow the chemical to be deposited onto the optical fibre using the Langmuir-Blodgett technique[8].

Using this technique for deposition, a coating of resorcarene consists of a matrix of nanoscale cavites formed by the resorcarene ring, and other voids generated with the alternate packing of the molecular layers of the coating[12]. The orientation of the film structure is such that the alkyl chains interdigitate, and the molecules align bowl to bowl[8].

The analyte molecule can penetrate into this matrix structure. The analyte molecule becomes temporarily entrapped in the hydrophobic resorcarene cavity and the voids. An interaction then occurs between a host molecule, resorcarene, and the analyte[1]. Weak interactions[13] occur involving the aromatic rings of the analyte and the host molecule. Since they are weak and do not involve covalent bonding, the analyte molecule is easily liberated from the cavity, and this results in a sensor whose response is reversible, an important consideration in chemical sensor development.

The size and shape of the analyte molecule determines how deeply it can penetrate the resorcarene matrix, and the chemistry of the analyte and host determines the nature of the molecular interaction when the analyte is contained in the cavity. These considerations lead to responses that have different levels of sensitivity to various analyte molecules.

The refractive index of the resorcarene coating has been measured to be 1.47 at 632nm using SPR[8], making it a suitable choice to exploit the LPG sensing principles based on nanostructured coatings. Upon adsorption of the analyte, the cavities and voids become filled with the analyte and the optical density and refractive index increases.

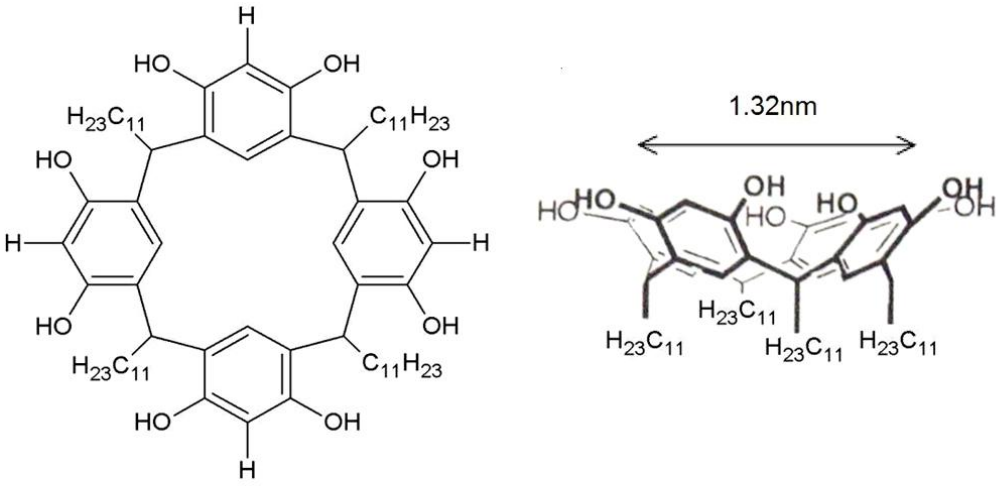

(a) (b)

Figure 8.3 (a) The resorcarene molecule, undecyl-calix[4]resorcarene used for coating the optical fibre. (b) The resorcarene cavity has an upper rim diameter of 1.32nm. The analyte molecule becomes encapsulated in this cavity[10].

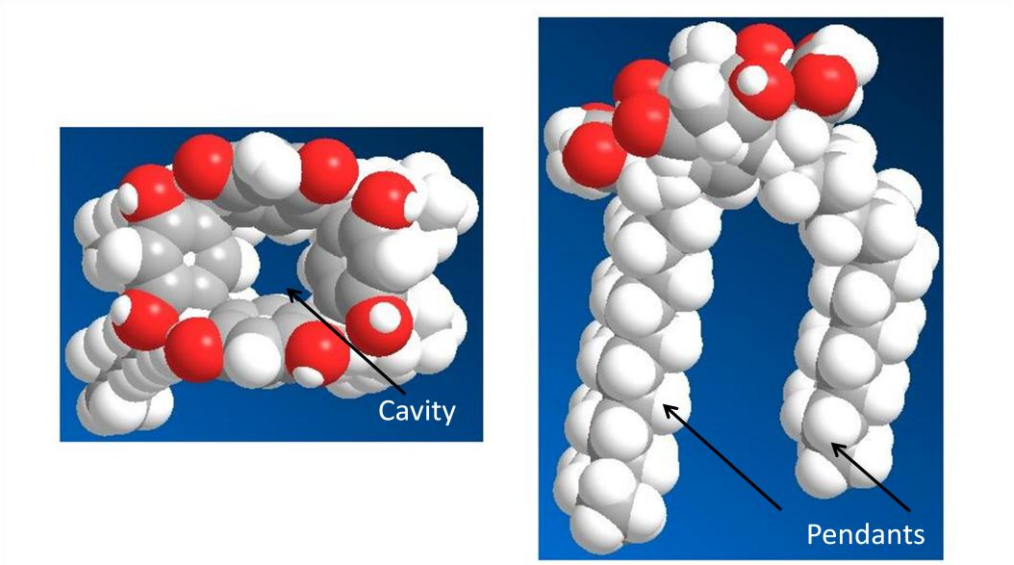

(a) (b)

Figure 8.4 Space model of the crystal structure of undecyl-calix[4]resorcarene, shown from above (a) and side view (b). KEY: White (hydrogen); Grey (carbon); Red (oxygen). The molecular cavity and alkyl pendant chains are indicated.

8.4 LPG FABRICATION

An LPG of period 180μm and length 30-35mm was fabricated in hydrogen loaded SM750 single mode fibre of cut-off wavelength 619nm, via UV inscription using the point by point technique[14]. The resorcarene was deposited using the Langmuir-Blodgett technique, see Chapter 4. The resorcarene was dissolved in chloroform at 0.2g/l, and spread onto a pure water subphase of one compartment of a Nima Technology Model 2410A Langmuir-Blodgett trough modified for use with fibre optic substrates[15]. The material was compressed to a surface pressure of 30mN/m. The dipping speed for the fibre substrate was set to 10mm/min. As the coating is deposited, Figure 8.5, the layers interdigitate giving an individual layer thickness of 1.17nm[8].

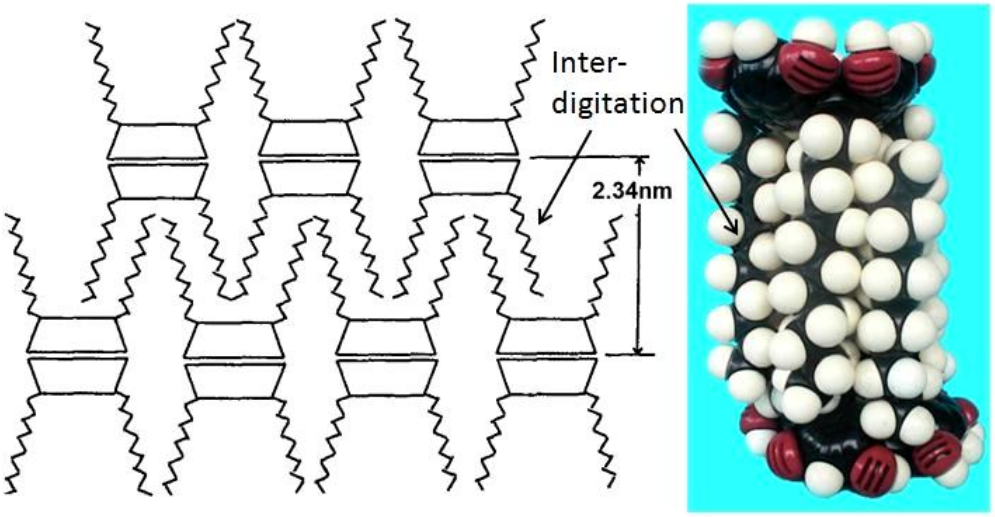

(a) (b)

Figure 8.5 (a) A schematic of the multilayer structure of resorcarene, showing the interdigitation or interleaving of the alkyl chains. This results in a bi-layer thickness of 2.34nm. (b) Space model of a resorcarene bi-layer. KEY: White (hydrogen); Black (carbon); Maroon (oxygen)[8].

The transmission spectrum of the fibre was monitored by coupling the output from a tungsten halogen lamp into the fibre and connecting the distal end of the fibre to an Ocean Optics CCD spectrometer of resolution 0.3nm. The spectrum was recorded when the LPG was above and below the water subphase. This is important, as it has been noted previously that the thickness of the coating required to access the mode transition region is dependent on the surrounding refractive index[16]. Thus for gas sensing the spectrum recorded with the LPG above the subphase was used when deciding on the optimum coating thickness.

To establish the optimum coating thickness, a thick film in excess of 1μm was deposited. This allows the grey scale plot, Figure 8.2, to be generated which shows the response of the transmission spectrum to the deposition of the coating. The LPG was then cleaned and coated with 163 layers of resorcarene, deposited as a Y-type LB film, corresponding to a calculated coating thickness of 190nm. The number of layers was chosen to ensure that a dual resonant attenuation band develops in the transmission spectrum of the fibre upon exposure to the analyte, indicating that the LPG is operating at the phase matching turning point.

8.5 EXPERIMENT

The coated LPG was placed inside a closed vessel and fixed quantities of the analyte were injected into the chamber. At room temperature and atmospheric pressure, the analyte liquid vapourized inside the chamber and the response of the sensor to the vapour concentration was monitored.

For injection of liquid toluene, the sensor took ~30 minutes to reach a steady state condition, and this incorporates the time for the solvent to evaporate, which is dependent upon the quantity of liquid injected. Benzene on the other hand took ~10 minutes to reach steady state. The difference is estimated to be a result of the solvents volatilities, see Table 8.2, and the infusion time of the analyte molecule into the multilayer film. Next, the spectrum was recorded using the CCD spectrometer. Upon opening of the closed vessel, the vapour concentration was quickly released into a fume cupboard.

The sensor was also tested with hexane, an aliphatic hydrocarbon, and cyclohexane, a hydrocarbon with a fully hydrogenated ring. This allowed for comparing the sensitivity of the device to four VOCs and determination of the selectivity of the sensor.

8.6 RESULTS AND DISCUSSION

The LPG sensor with 163 layers[ee] of undecyl-calix[4]resorcarene was tested with four organic vapours. The response of the transmission spectrum to exposure to different concentrations of toluene is shown in Figure 8.6. The initial response in air (0 ppm by volume) shows two resonant bands at 850nm and 930nm which are resolvable. The

[ee] Prior to these tests, the sensor was subject to testing with ammonia vapour. The sensor was soaked for 48 hours in ammonia vapour, and the transmission response did not return to the spectrum obtained after deposition of 163 layers, which had a single band centred at 900nm. The spectrum identified at 0 kppmv is the sensors response after the aforementioned testing, and is the baseline adopted for VOC sensing.

dual resonant bands become further resolved with increasing vapour concentrations up to the maximum used, 61.2kppmv (thousand ppm by volume), equivalent to 231g/m^3.

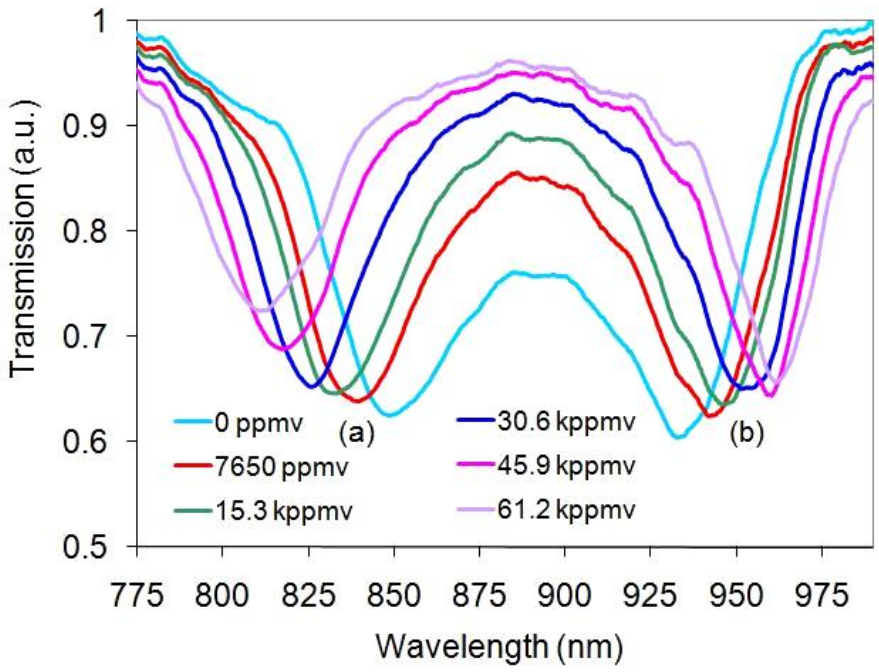

Figure 8.6 A long period grating of period 180μm fabricated in SM750 fibre coated with a resorcarene and its response to toluene vapour. The sensor was characterised at concentrations from 7650ppmv (28.9g/m^3) up to 61200ppmv (231g/m^3). The trend for increasing separation of the resonant bands labeled (a) and (b) with increasing concentration is apparent.

The response can be analysed by measuring the wavelength shifts of the two resonant bands, or by considering the change in amplitude at a fixed wavelength. The two resonant bands move apart in wavelength as depicted in Figure 8.7. The central wavelength of the attenuation bands were captured directly from the transmission spectrum, Figure 8.6. Noise and asymmetry of the attenuation band will give an error in this measurement. By curve fitting a linear trend, an average change with wavelength of 1600ppmv/nm[ff] for the shorter wavelength band and 2300ppmv/nm[gg] for the longer wavelength band has been measured, Figure 8.7. This results in a

[ff] 0.625nm/kppmv

[gg] 0.4375nm/kppmv

differential change with wavelength of 941ppmv/nm[hh]. Utilizing this differential shift gives a limit of detection of 282ppmv (1.064g/m^3) based on a spectrometer resolution of 0.3nm[ii].

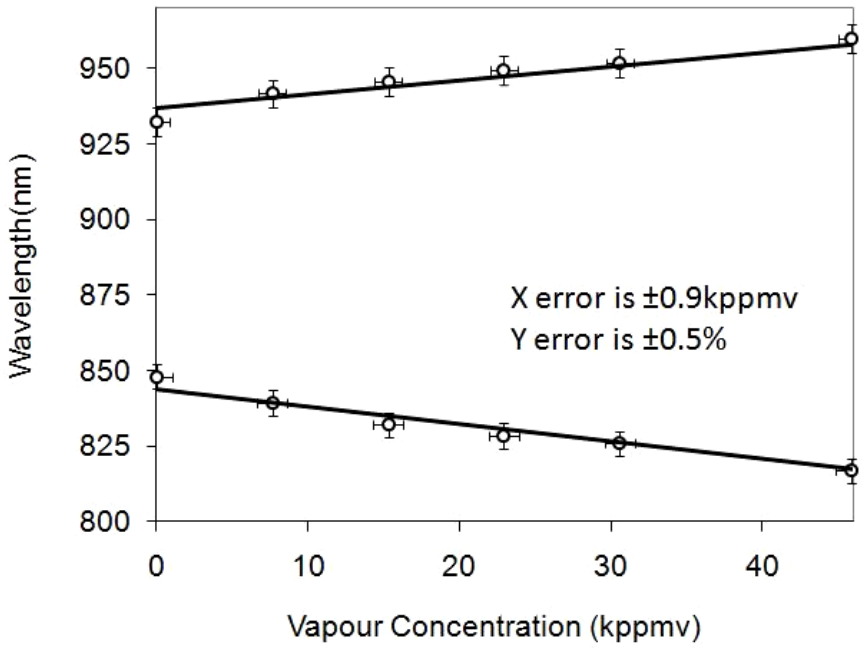

Figure 8.7 Wavelength shift of the resonant bands (a) and (b) in Figure 8.6 to increasing toluene vapour concentration. The solid lines are a guide to the eye.

These measurements were recorded in a temperature controlled environment. To utilize this level of sensitivity in a practical sensor, the temperature sensitivity of the response must also be taken into account. The temperature sensitivity for this type of sensor has been recorded in Figure 9.12. Since LPGs contain a number of attenuation bands, each with different sensitivities to temperature and other measurands, then temperature discrimination can be achieved in this device by building a mathematical model of the response of the attenuation bands under all measurement conditions. By utilizing the model in the implementation of the sensor's signal processing, discrimination between the effects of temperature and other measurands can be achieved[19].

[hh] 1.0625nm/kppmv

[ii] The sampling resolution of the spectrometer is determined by the pixel size of the CCD.

Centred at ~900nm, a broad spectral feature appears at the phase matching turning point which has a FWHM bandwidth in excess of 50nm. This is shown in Figure 8.6 between the wavelengths of 825 and 950nm. The change of transmission of the fibre at the central wavelength of this broad spectral feature could conveniently be used to develop a low cost sensor, requiring the use of only an LED of bandwidth 50nm and a photodiode to measure optical power. In a practical sensor system, a reference channel is required to compensate for the effects of source intensity fluctuations and changes in downlead losses. The reference channel would be at a wavelength where the sensor has no response to changes in analyte concentration and is therefore in a part of the spectra where there are no attenuation bands.

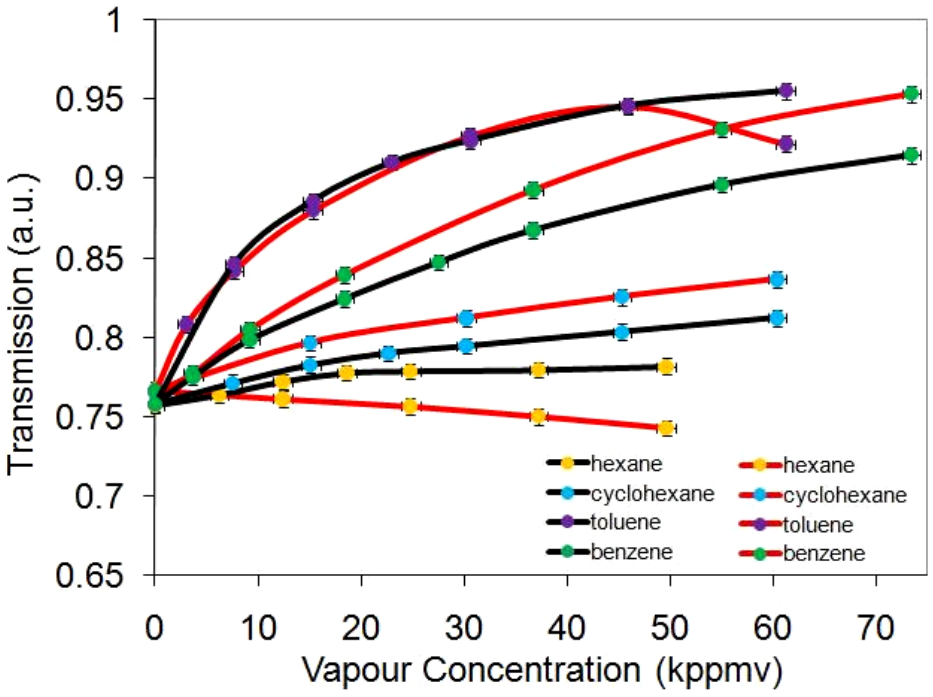

Figure 8.8 Volumetric sensitivity of the 180μm period LPG sensor (black) to the vapours toluene, benzene, hexane and cyclohexane. For comparison, a 100μm period LPG sensor coated with calix[4]resorcarene is shown (red). The transmission is monitored at 900nm (black) and 800nm (red) and an increase in transmission occurs which corresponds to the separation of the dual resonant attenuation bands. The lines are a guide to the eye.

Making use of the broad spectral feature centred at 900nm, Figure 8.6, the change in optical transmission of the LPG was measured. This is close to the centre wavelength between the two resonant bands. This was monitored as a function of the

concentration of toluene, benzene, hexane and cyclohexane, and is shown in Figure 8.8. This allows for a determination of the selectivity of the sensor. The results show that at levels up to 10 kppmv vapour concentration, the sensitivity to hexane is only 7.5% of that to toluene. For cyclohexane the sensitivity is 14.8% compared to that to toluene. This indicates that the sensor has a high selectivity for toluene.

These measurements were compared with a 100μm period LPG sensor coated with calix[4]resorcarene[jj]. In Figure 8.8, the results show that the responses to toluene, benzene and cyclohexane were similar with the exception of hexane. Hexane has shown a response of the same magnitude but with opposite polarity. This has been reported to be due to the low refractive index of liquid hexane[kk] (n_{hexane}=1.37), compared to liquid toluene ($n_{toluene}$=1.49)[12]. However, the lesser response to benzene with the highest refractive index ($n_{benzene}$=1.50) indicates that the sensing mechanism is based upon changes in the properties of the functional coating, rather than a response to the refractive index of the analyte, Table 8.1.

Table 8.1 Refractive indices for organic solvents in liquid form

Organic Solvent	Refractive Index
Hexane	1.37
Cyclohexane	1.41
Toluene	1.49
Benzene	1.50

The response of the spectrum to exposure to the analyte at the particular wavelength of 900nm, the amplitude monitored response for toluene tends towards saturation above 10 kppmv. This is a result of the increasing separation of the two attenuation bands that has decreasing influence on the transmission at 900nm the further the bands separate. However, the two resonant bands continue to diverge at the higher vapour concentrations as indicated in the wavelength response in Figure 8.7.

The relative sensitivities of the four organic compounds are evident from Figure 8.8. The size and shape of the analyte molecule can determine how deeply the analyte can move through the resorcarene matrix, and the chemistry of the host and guest determines how it becomes confined in the cavity.

[jj] 100μm period LPG with length 23mm, coated with 275 layers undecyl-calix[4]resorcarene.

[kk] The refractive index of liquid hexane is less than the coating at 1.47, thus if condensation of the analyte vapour occurs inside the coating, then this lowers the overall mean refractive index of the coating.

Hexane has a single chain molecular structure with dimensions 1.03nm x 0.49nm x 0.4nm[17] and its large size cannot enter the resorcarene cavity easily. The small response may be due to the analyte molecule filling voids between adjacent resorcarene molecules.

Cyclohexane is a ring but being fully hydrogenated is more bulky than the aromatic ring. The cyclohexane molecule has dimensions of 0.72nm x 0.64nm x 0.49nm[17]. The results indicate that there can be little molecular attraction between cyclohexane and the cavity.

Table 8.2 Boiling points for organic solvents

Organic Solvent	Boiling Point
Hexane	69^{o}C
Benzene	80.1^{o}C
Cyclohexane	80.7^{o}C
Toluene	110.6^{o}C

Benzene is the smallest molecule investigated, with dimensions 0.74nm x 0.67nm x 0.37nm[17] and the progressive response shown in Figure 8.8 indicates that it can penetrate deeper into the resorcarene film with increasing vapour concentrations. Although there is some correlation of interaction with the solvent volatility, there is also some specific interaction with aromatic molecules since benzene interacts more strongly than cyclohexane even though they have the same boiling point, Table 8.2.

The largest magnitude response is observed on exposure to toluene, which, with its methyl group, shows that this can cause a greater molecular attraction between host and guest, which is not evident for benzene. The results show that toluene is optimal above the other VOCs measured here for becoming confined in the cavity of the resorcarene matrix. The dip in the response to toluene at high concentrations shown in Figure 8.8 is due to coupling to another cladding mode, see Section 9.6.

Subsequently, exposure to xylene vapour from further testing has shown a stronger response than toluene possibly due the greater interaction of the two methyl groups of the xylene molecule with the resorcarene host matrix. However, the results were difficult to record in the format of Figure 8.8 because of the long settling time experienced, of the order of 90 minutes[II].

[II] Ammonia, formaldehyde and butanol vapour also gave strong responses but with long settling times in excess of 90 minutes, made the recording impractical.

The resorcarene coated LPG sensor was also exposed to other organic vapours. The aliphatic amines, e.g. ethylamine, diethylamine and triethylamine were tested in the chamber, and the sensor gave the strongest responses[mm] to these molecules. The sensing mechanism is the deprotonation of the hydroxyl moiety of resorcarene[18 p588]. The results proved to be of poor reversibility, and the analysis of the organic amines was not pursued for practical reasons. The same mechanism is responsible for the poor reversibility encountered when testing the sensor with ammonia vapour. This was reported in Section 8.6 with the fabrication of the sensor.

The vapour ingress times and egress times of the sensor to benzene vapour are shown in Figure 8.9, with the transmission monitored at 900nm. The vapour ingress time is dictated by the time required for the volatile solvent to vapourise. However, the vapour egress time of the order of 15 seconds shows the intrinsic speed of response of the sensor when the analyte vapour is released.

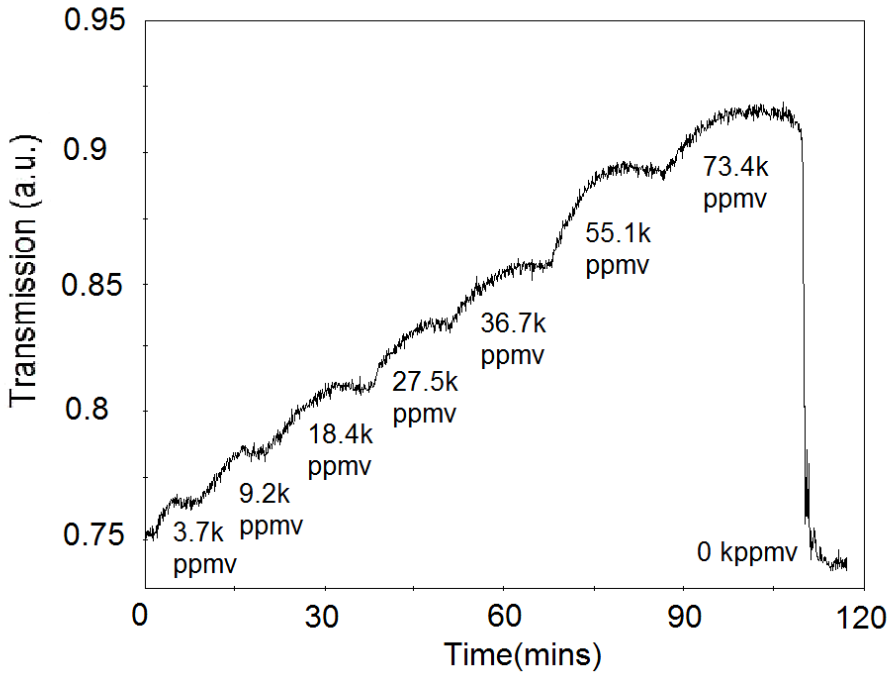

Figure 8.9 The evaporation time and the temporal response of the resorcarene coated 180μm period LPG sensor to benzene vapour, monitored at 900nm.

[mm] Stronger than the response to xylene and toluene.

8.7 CONCLUSION

It has been demonstrated that, using a fibre optic long period grating in conjunction with a functional nanostructured coating, chemical vapour sensing can be performed. Dual resonance in the spectral response of the LPG has been exploited to obtain improved sensitivity. The phase matching curves allow the grating to be designed to allow the sensor to operate within a desired wavelength range. Further tailoring of the grating period would allow the utilization of the mode transition region to attain higher sensitivities.

Using a resorcarene coating, toluene and benzene vapour sensing can be performed. Nanoscale cavities in the coating are suited to a corresponding size and shape of a particular analyte molecule. In this way, the response of the sensor is species selective. This has been demonstrated with the relative sensitivity to toluene 13 times greater than that of hexane for the same vapour concentration. Similarly, the sensitivity to toluene is over 6 times greater than cyclohexane.

A broadband spectral feature resulting from the moving apart of two attenuation bands occurs in dual resonant long period gratings. This is not due to a change in extinction ratio of the bands, but a natural result of the two bands moving apart. This feature has the potential to be utilized in conjunction with simple detection optoelectronics to implement a low cost sensor system. Such a system would need to address the noise of the signal, see Figure 8.9. The detector signal would require low pass filtering to reduce the noise. The time constant of the filter should be sufficient to have no effect on the response time of the sensor.

8.8 REFERENCES

1. Hassan, A. K., Ray, A. K., Nabok, A. V. and Davis, F. (2001), "Spun films of novel calix[4]resorcinarene derivatives for benzene vapour sensing", *Sensors and Actuators, B: Chemical,* vol. 77, no. 3, pp. 638-641.

2. Viricelle, J. P., Pauly, A., Mazet, L., Brunet, J., Bouvet, M., Varenne, C. and Pijolat, C. (2006), "Selectivity improvement of semi-conducting gas sensors by selective filter for atmospheric pollutants detection", *Materials Science and Engineering C,* vol. 26, no. 2-3, pp. 186-195.

3. Liu, Q., Chiang, K. S. and Liu, Y. (2007), "Characterization of single-mode fiber with fiber Bragg gratings for the design of long-period gratings", *Journal of Lightwave Technology,* vol. 25, no. 8, pp. 2129-2134.

4. Topliss, S. M., James, S. W., Davis, F., Higson, S. P. J. and Tatam, R. P. (2010), "Optical fibre long period grating based selective vapour sensing of volatile organic compounds", *Sensors and Actuators, B: Chemical,* vol. 143, no. 2, pp. 629-634.

5. Cheung, C. S., Topliss, S. M., James, S. W. and Tatam, R. P. (2008), "Response of fiber-optic long-period gratings operating near the phase-matching turning point to the deposition of nanostructured coatings", *Journal of the Optical Society of America B: Optical Physics,* vol. 25, no. 6, pp. 897-902.

6. Shu, X., Zhu, X., Wang, Q., Jiang, S., Shi, W., Huang, Z. and Huang, D. (1999), "Dual resonant peaks of LP015 cladding mode in long-period gratings", *Electronics Letters,* vol. 35, no. 8, pp. 649-651.

7. Gutsche, C. D. (1998), *Calixarenes Revisited,* Royal Society of Chemistry.

8. Hassan, A. K., Nabok, A. V., Ray, A. K., Lucke, A., Smith, K., Stirling, C. J. M. and Davis, F. (1999), "Thin films of calix-4-resorcinarene deposited by spin coating and Langmuir-Blodgett techniques: Determination of film parameters by surface plasmon resonance", *Materials Science and Engineering C,* vol. 8-9, pp. 251-255.

9. Collyer, S. D., Davis, F., Lucke, A., Stirling, C. J. M. and Higson, S. P. J. (2003), "The electrochemistry of the ferri/ferrocyanide couple at a calix[4]resorcinarenetetrathiol-modified gold electrode as a study of novel electrode modifying coatings for use within electro-analytical sensors", *Journal of Electroanalytical Chemistry,* vol. 549, no. SUPPL., pp. 119-127.

10. Biros, S. M. and Rebek Jr., J. (2007), "Structure and binding properties of water-soluble cavitands and capsules", *Chemical Society Reviews,* vol. 36, no. 1, pp. 93-104.

11. Davis, F. and Stirling, C. J. M. (1996), "Calix-4-resorcinarene monolayers and multilayers: Formation, structure, and differential adsorption", *Langmuir,* vol. 12, no. 22, pp. 5365-5374.

12. Nabok, A. V., Hassan, A. K. and Ray, A. K. (2000), "Condensation of organic vapours within nanoporous calixarene thin films", *Journal of Materials Chemistry,* vol. 10, no. 1, pp. 189-194.

13. Benevelli, F., Khimyak, Y. Z. and Klinowski, J. (2004), "13C and 2D WISE NMR studies of the host mobility in two aromatic complexes of p-tert-butyl-calixarene", *Journal of Inclusion Phenomena,* vol. 49, no. 3-4, pp. 211-218.

14. Othonos, A. and Kalli, K. (1999), *Fiber Bragg Gratings: Fundamentals and Applications in Telecommunications and Sensing,* Artech House.

15. Rees, N. D., James, S. W., Tatam, R. P. and Ashwell, G. J. (2002), "Optical fiber long-period gratings with Langmuir-Blodgett thin-film overlays", *Optics Letters,* vol. 27, no. 9, pp. 686-688.

16. James, S. W., Cheung, C. S. and Tatam, R. P. (2007), "Experimental observations on the response of 1^{st} and 2^{nd} order fibre optic long period grating coupling bands to the deposition of nanostructured coatings", *Optics Express,* vol. 15, no. 20, pp. 13096-13107.

17. Barrer, R. M. and Sikand, A. (1979), "Sorption of hydrocarbons and water in silanated and unsilanated partial H-forms of zeolite Y", *Journal of the Chemical Society, Faraday Transactions 1: Physical Chemistry in Condensed Phases,* vol. 75, pp. 2221-2234.

18. Hornyak, G. L., Jutta, J., Tibbals, H. F. and Rao, A. K. (2008), *Introduction to Nanoscience,* CRC Press.

19. Bhatia, V. (1999), "Applications of long period gratings to single and multi-parameter sensing", *Optics Express,* vol. 4, no. 11, pp 457-466.

CHAPTER 9: A COMPARISON OF CALIX[4]RESORCARENE AND CALIX[8]ARENE DERIVATIVE COATINGS ON LPGS

9.1 INTRODUCTION

Structured coatings of calixarenes have been reported to perform gas sensing with the infusion of BTEX analytes[1], aliphatic alcohols[2], and aliphatic amines[3], using the established techniques of surface plasmon resonance[1] and the quartz crystal microbalance[2; 3]. Here we use a long period grating (LPG) to measure the change in density and hence the refractive index of the calixarene film in response to exposure to a selection of volatile organic solvents. To achieve this, we deposit the calixarene onto the cladding of an optical fibre in the form of a multilayer coating of a few hundred nanometres in thickness, and the analyte vapour becomes adsorbed into the cavities and voids of the calixarene coating[4].

The two calixarenes, calix[4]resorcarene with a cavity size of 1.32nm in diameter[5], and a calix[8]arene derivative with a cavity nominally twice the size, have been coated onto the cladding of an optical fibre containing a long period grating. A comparison of their vapour sensing performances has been undertaken, in terms of their species selectivity and their kinetic behaviour. The analytes selected are the aromatic compounds toluene and benzene, the aliphatic compound hexane and the alicyclic compound cyclohexane. Since the molecular formulae's of these solvents are similar; toluene C_7H_8, benzene C_6H_6, hexane C_6H_{14} and cyclohexane C_6H_{12}, this allows for comparisons in behaviour in terms of the molecule size and supramolecular interactions.

9.2 PHASE MATCHING CURVES

As discussed in earlier chapters, the phase matching curves[6], Figure 9.1, give a complete set of discrete wavelength resonances that satisfy Equation 2.1. For a 100μm period LPG, the intersections with the reference line parallel to the abscissa identify the wavelengths at which energy is coupled from the core mode to a cladding mode. The cladding modes are numbered, corresponding to the order of each mode. The turning point in the phase matching curves indicates that energy can be coupled into the same cladding mode at two discrete wavelengths, and is referred to as dual resonance[7].

The phase matching curves move when either the fibre coating's refractive index or thickness is increased[9]. The grey scale plots, Figures 9.2a and 9.2b, show how the bands move upon increasing coating thickness, here the dark bands represent the resonance bands. A grading is observable where the level of darkness represents a

higher extinction ratio and lightness represents a lower extinction ratio of the resonant bands.

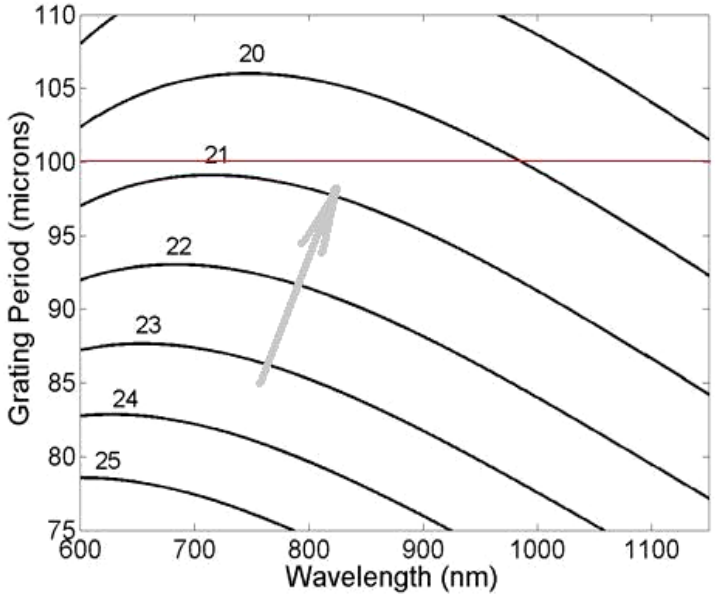

Figure 9.1 Phase matching curves for a long period grating around the period of 100μm[8]. The curves represent coupling to the 20th to 25th order cladding modes. The arrow represents the direction that the curves move upon an increase in refractive index of the coating, as occurs with the ingress of the vapour molecule into the permeable calixarene film.

For the attenuation bands labelled $LP_{0\,20}$ from Figures 9.2a and 9.2b, there is a region where there is greatest change with wavelength with coating thickness and is referred to as the transition region[10]. It has been shown in Chapter 5 that the sensitivity of these bands to changes in the coating is greatest in the transition region. The dual resonant band labelled $LP_{0\,21}$ is centred at 800nm, and the first appearance of its resonance features occurs when the thickness of the coating corresponds to that required for the transition region. Since the dual resonant band is the target region for sensing, its proximity to the transition region optimises this bands sensitivity.

In Figure 9.2a, coupling to the $LP_{0\,21}$ cladding mode causes a resonance band to occur at about 125 bi-layers (or 250 layers) whereupon this develops into two resonant bands which diverge in wavelength thereafter with increasing coating thickness. There is also coupling to another cladding mode as shown by the fainter trace shadowing the principal dual resonance band. This is perhaps due to coupling to an asymmetric cladding mode.

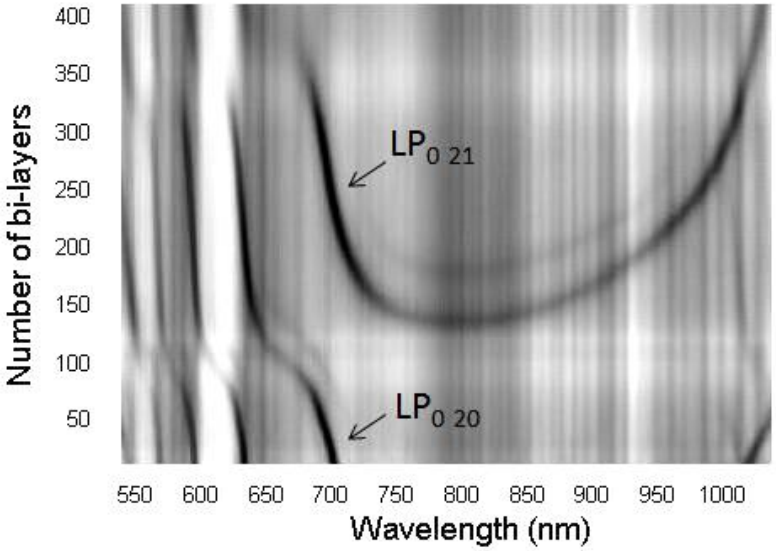

(a)

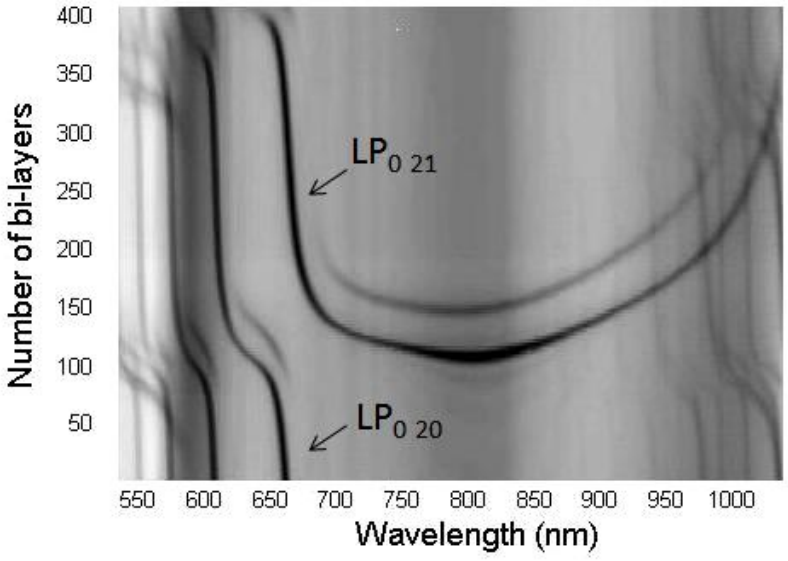

(b)

Figure 9.2 The grey scale plots showing the movement in wavelength of the resonant bands for a 100μm period LPG as (a) layers of calix[4]resorcarene, and (b) a calix[8]arene derivative are deposited.

In Figure 9.2b, the dual resonance band appears also at about 125 bi-layers , (or 250 layers), and this is the provisional target number of layers for the sensor. Another cladding mode occurring at 150 bi-layers is also clearly visible.

9.3 CALIXARENE COATINGS

The basic structure of two types of tetramer calixarene cavity is shown in Figure 9.3. For resorcarene, the bowl shape is more open. When the calixarene coating is deposited using the Langmuir-Blodgett technique, it forms a regular nanostructured film, with a Y-type orientation[11]. This matrix structure is illustrated in Figure 9.4 for the tetramer calixarenes. The cavity alignment is shown with closer alignment between the tetramer resorcarene bowl than with the tetramer calixarene bowls.

With this imperfect alignment, the multilayer calixarene coating does not contain continuous pores or channels as a porous coating would normally have. It has been suggested that for vapour sensing, lateral translation of the layers occurs such that the cavities of two adjacent layers align in the plane perpendicular to the fibre axis[12]. This enables the analyte molecule to be transported between each layer of the host molecule without the need for continuous channels. This mechanism is poorly understood but is suggested to be either analyte induced or intrinsic thermal motion[13]. It is proposed that this mechanism accounts for the long time constants of the order of hours sometimes seen with guest absorption by calixarenes[2; 4; 14; 15].

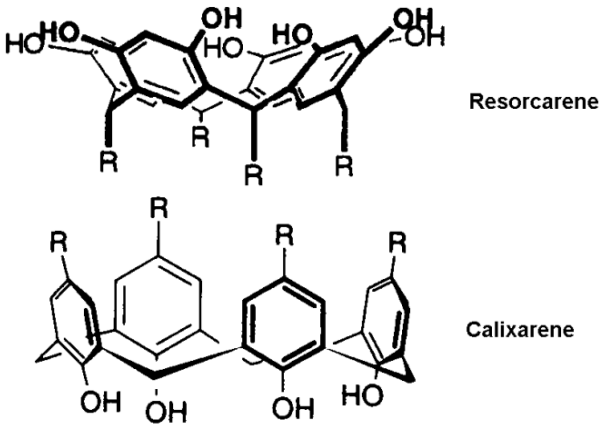

Figure 9.3. A comparison of the bowl structures for resorcarene and calixarene. The resorcarene bowl is more open[13] [17].

Calixarenes can sense organic molecules since the guest species is able to become encapsulated into the calixarene cavity. Figure 9.5 shows the inclusion complex of the

widely studied tert-butyl-calix[4]arene molecule, which can encapsulate the toluene guest. Crystallography has revealed this structure[16]. Adsorption of the guest species raises the density of the calixarene coating. Since the platform is the long period grating, this device is able to sense the change in refractive index accompanying the change in density of the LPG coating.

The calix[8]arene coating contains a large cavity in the form of a pleated loop [18]. The shape of this cavity is less well defined than the smaller cavity of calix[4]resorcarene and it has been reported that larger cavities often do not exhibit such a well defined encapsulation of chemical species[13]. The smaller cavity material calix[4]resorcarene with its long alkyl chains forms here a more regular and less densely packed multilayer structure, perhaps with closer alignment of the cavities, allowing for a simpler transport of the analyte molecule and consequently shorter response times.

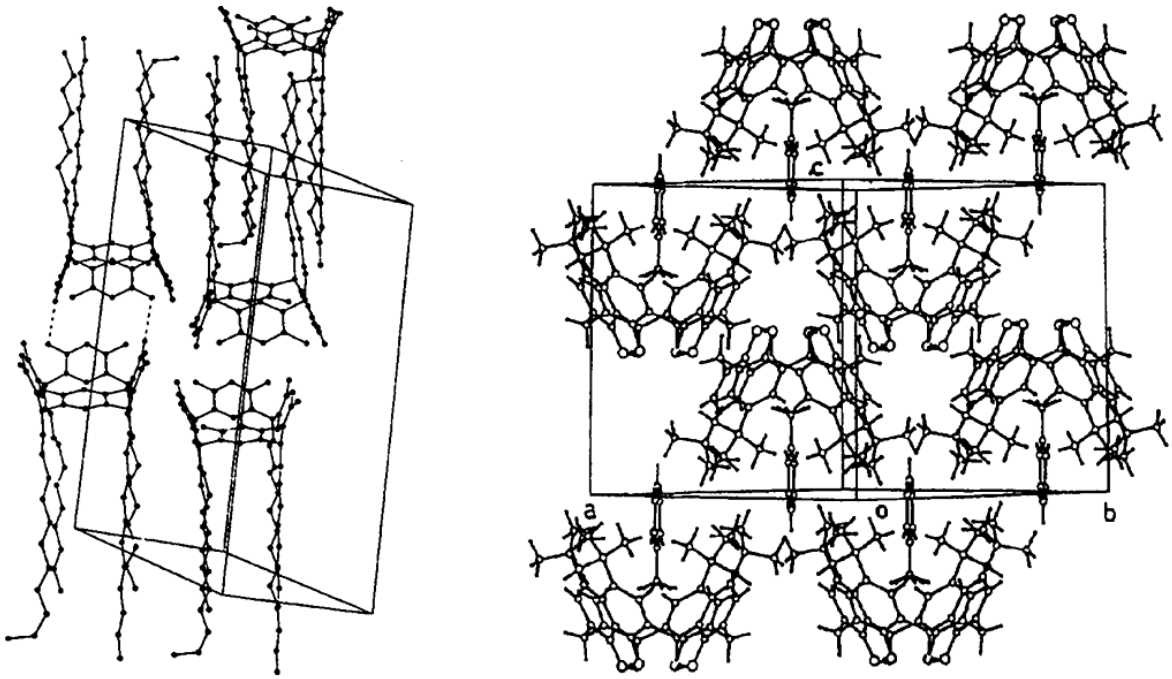

Figure 9.4 The multilayer structure of undecyl-calix[4]resorcarene and tert-butyl-calix[4]arene·toluene complex. The bowl to bowl alignment is depicted. The interdigitation of the resorcarene pendant chains is also illustrated. The 3D boxes indicate the crystalline structure[19] [20].

Selectivity is the preference the cavity has to encapsulate a particular chemical species and has been defined as "*the binding of one guest, or family of guests, significantly more strongly than others, by a host molecule*" [21 p4]. Using quartz crystal microbalance (QCM) sensors coated with a calix[4]arene derivative and a calix[6]arene derivative coating, it has been reported that differences occur in the selectivity of their response to the aliphatic amines[3]. The response to diethylamine was greater than the larger guest species of triethylamine due to steric hindrance. Furthermore, the larger cavity of calix[6]arene was found to be more favourable in accommodating these organic amines, compared to calix[4]arene.

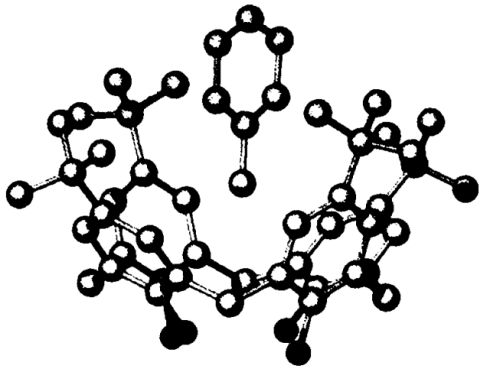

Figure 9.5 Tert-butyl calix[4]arene·toluene inclusion complex. The methyl group of the toluene molecule points into the cavity[13].

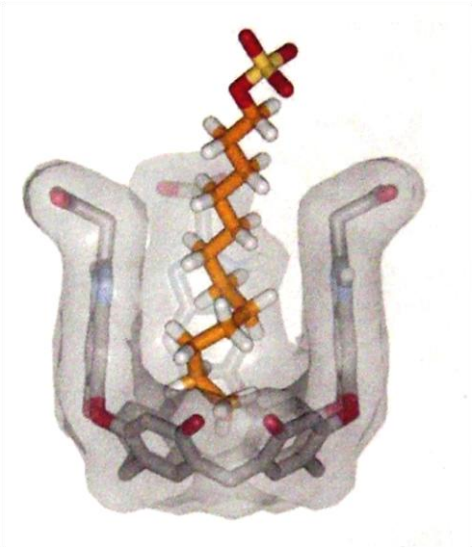

Figure 9.6 A calixarene derived cavitand encapsulating a guest molecule with a long aliphatic chain. The shape of the molecular capsule can surround the guest molecule. The electron cloud around a cavitand capsule is responsible for intermolecular bonding of the form Van der Waals and CH-π[17].

The guest species is held by interactions with the electron cloud of the cavity. This can be the electrostatic binding arising from Van der Waals interaction[22], or the CH-π bond that occurs between an aromatic group and the methyl group. The CH-π bond has been reported to occur between the aromatic moiety of the guest and the alkyl pendant chain of tert-butyl-calixarene, as would occur with the calixarene·toluene inclusion complex depicted in Figure 9.5[20; 23]. It has also been reported that this can occur between the aromatic moiety of the calixarene ring and an aliphatic guest species, as shown in Figure 9.6[24]. It is these intermolecular bonds that are the driving factor in determining species selectivity.

9.4 FABRICATION

Two LPGs of period 100μm, chosen to obtain a dual resonant response at 800nm, and with grating lengths 26mm and 23mm respectively were fabricated in hydrogen loaded single mode fibre SM750, with cut-off wavelength 619nm, via UV inscription using the point-by-point technique[25]. The attenuation bands can move in wavelength in the 48 hours after inscription, due to the out-gassing of hydrogen from the fibre causing a change of the core index modulation profile[26-28]. Often annealing techniques are used to remove any unreacted hydrogen and unstable UV induced defects[28; 29]. This is of particular importance to stabilize the spectrum where wavelength registration is required (e.g. making an optical transmission filter of a particular wavelength).

Two coating materials, undecyl-calix[4]resorcarene, Figure 9.7a, and a tert-butyl-calix[8]arene derivative, Figure 9.7b, were deposited using the Langmuir-Blodgett technique. The calix[4]resorcarene was dissolved in chloroform at 0.2g/l, and the calix[8]arene at 0.13g/l. The coating material was then spread onto a pure water subphase of one compartment of a Nima Technology Model 2410A Langmuir-Blodgett trough modified for use with fibre optic substrates[30]. The material was compressed to a surface pressure of 28mN/m for calix[4]resorcarene and 26mN/m for calix[8]arene. The dipping speed for the fibre substrate was set to 20mm/min in both cases.

The transmission spectrum of the fibre was monitored by coupling the output from a tungsten-halogen lamp into the fibre and connecting the distal end of the fibre to an Ocean Optics CCD spectrometer of resolution 0.3 nm. This was to ensure the attenuation bands acquired an extinction ratio of between 3-6dB during UV inscription, see Table 4.1, and to ensure the number of layers deposited in each case produced a spectrum with the signature dual lobed feature characteristic of dual resonant operation. In this case, the spectrum was recorded when the LPG was above and below the water subphase. As the sensors are designed for vapour sensing, the number of layers deposited were 255 and 245 respectively, Figures 9.8a and 9.8b, each

being tailored to obtain a dual resonant response in the transmission spectrum with the sensors above the water subphase.

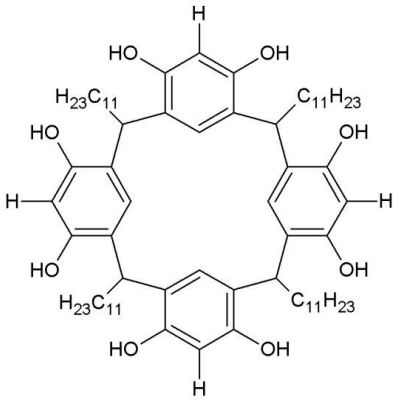

Figure 9.7a Undecyl-calix[4]resorcarene with four interlinked resorcinol molecules. The long pendant chains are undecyl ($C_{11}H_{23}$).

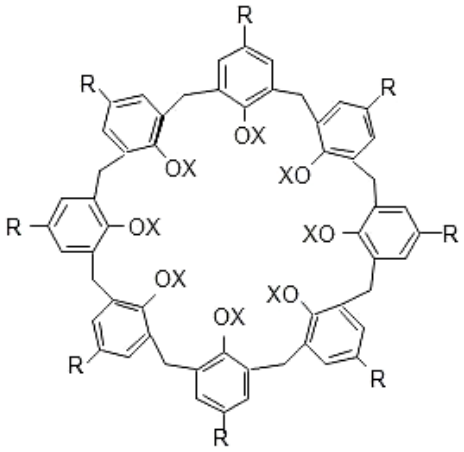

Figure 9.7b Tert-butyl-calix[8]arene derivative with a cavity comprising eight aromatic rings. The carboxyl group features on the lower rim. The short pendant chains are tert-butyl.

The fibre at this stage was removed from the trough and the film was left for 48 hours to stabilize. This is a *drying out* period whereby the characteristic transmission spectrum changes. The evolution of the spectrum over this time is perhaps due to the egress of water molecules from the film. It has been reported that water molecules can form bridges between adjacent calix[4]resorcarene molecules via hydrogen bonding[31]. This is pertinent since the trough uses water as the subphase which supports the calixarene monolayer during the fabrication process.

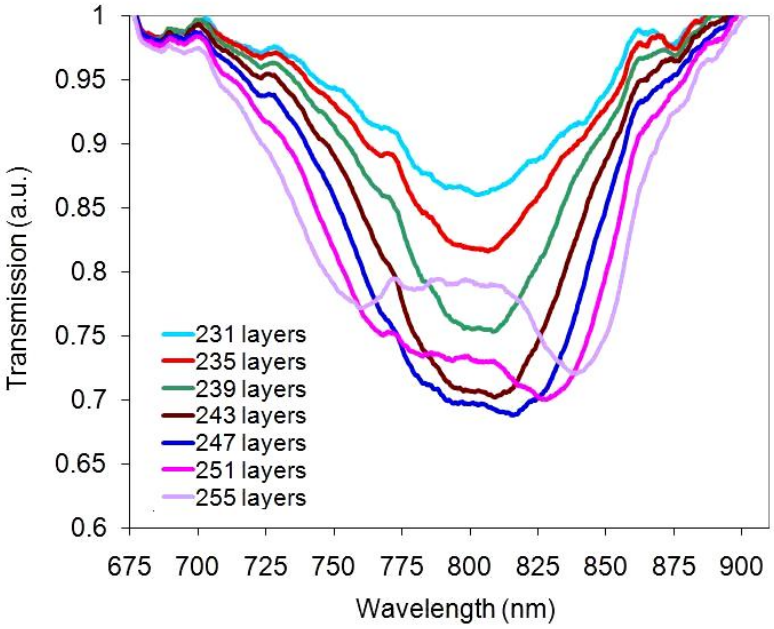

Figure 9.8a The spectrum of a 100μm period LPG fibre grating coated with calix[4]resorcarene bi-layers as depicted. The dual lobes begin to form, and the dipping of the sensor was halted at 255 layers.

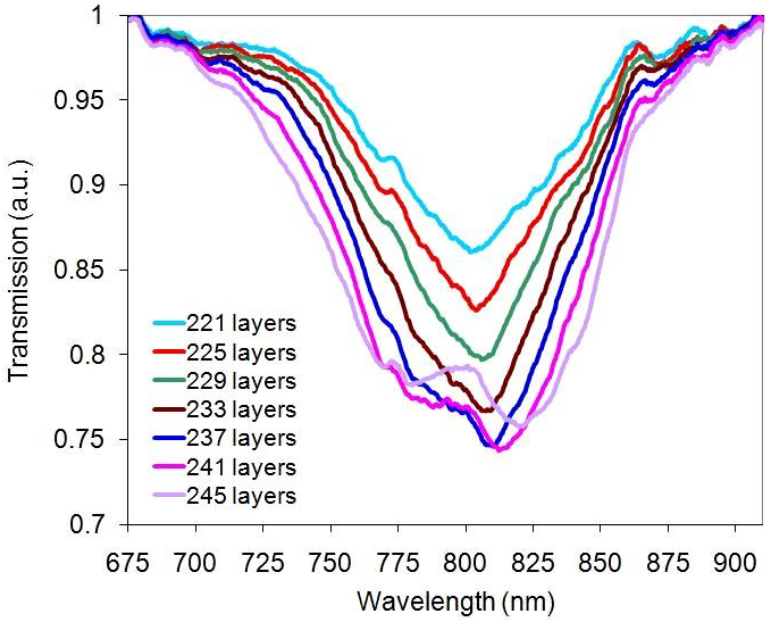

Figure 9.8b The spectrum of a 100μm period LPG fibre grating coated with between 221 to 245 layers of calix[8]arene. The dipping of the sensor was halted at 245 layers, tailored to obtain a dual resonant response in the transmission spectrum.

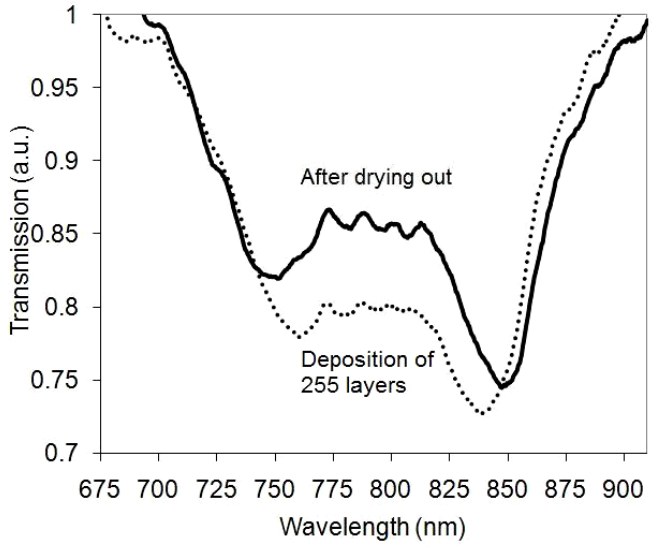

Figure 9.9a The effect of *drying out* of the newly coated film of calix[4]resorcarene on the spectrum of a 100μm period LPG. After depositing the target number of layers, 255, the spectrum evolves over the next few days. The twin lobes shown in bold are the characteristic dual resonance spectral feature.

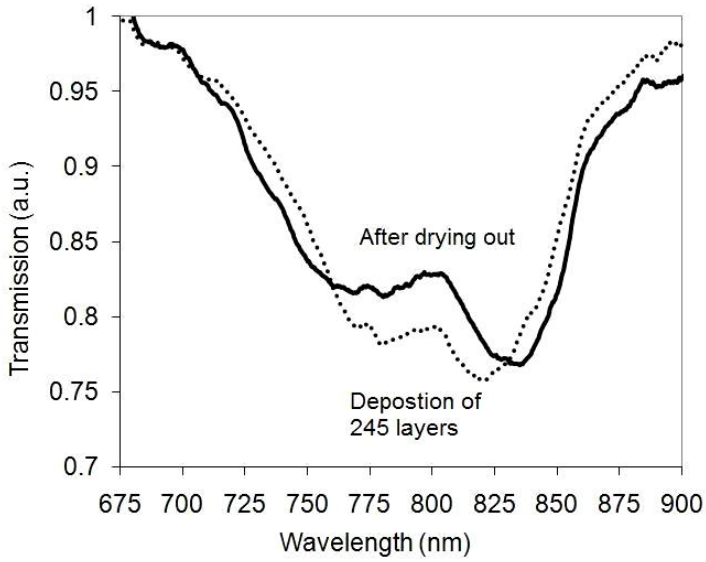

Figure 9.9b The evolution of the LPG transmission spectrum of the 100μm period LPG coated with 245 layers of calix[8]arene after *drying out*. The spectrum shown in bold is the final LPG transmission spectrum used for sensing.

The presence of water molecules between the layers of the film can be described here as a *delamination* effect. Without the water present between the layers, the film density would be greater since the layers would pack more closely. The affect of *drying*

out is therefore an increase in density and therefore refractive index of the film. This causes the LPG spectrum to evolve and in our case the dual resonant bands to become further separated. This has been observed over a few days after the coating is laid, Figure 9.9a and 9.9b. One must therefore be aware of this and factor it in to obtain an optimized sensor.

9.5 EXPERIMENT

There are three methods reported to perform vapour adsorption measurements on a permeable material inside a gas chamber; a single injection of vapours at a fixed concentration, supply of a continuous vapour flow, and injection of liquid solvent and the slow formation of vapour[4]. All three give different characteristic kinetic responses. Here, the method of injection of a volatile liquid into the gas chamber is used which gives a slow rising transient response incorporating the evaporation time and the infusion time for the analyte molecule to enter into the coating. An equilibrium condition is then reached which gives a common reference point for comparison of sensor performance. This method is in fact the closest to a real scenario where the sensor might be monitoring spillages that vapourise and enter the sensor through normal convection processes.

9.6 RESULTS

Vapour adsorption experiments were conducted and the transmission spectra of the 100μm period LPG sensor coated with calix[4]resorcarene and the calix[8]arene coated LPG sensor were recorded, Figures 9.10a and 9.10b. These show the signature response of dual resonance. The two attenuations bands diverge with increasing vapour concentration. The response progresses but a reflex is visible in the spectrum at the highest vapour concentration in the wavelength region of ~800nm, Figure 9.10a. This is perhaps due to coupling to an asymmetric cladding mode.

The selectivity of the coated LPG sensors was investigated by monitoring the change in transmission of each sensor at the centre wavelength of dual resonance, in response to a range of analytes. The signal responses were measured at 800nm, close to the centre wavelength of the dual resonant bands. Comparing the selectivities of each sensor in Figures 9.11, the results for calix[4]resorcarene and the calix[8]arene derivative coating follow the same trend. Since it was expected that cavity size would have a profound effect on chemical selectivity, then this was a surprising result. It indicates that the dominant effect must be due to common supramolecular attractions that must be present (e.g. Van der Waals, CH-π) between guests and hosts.

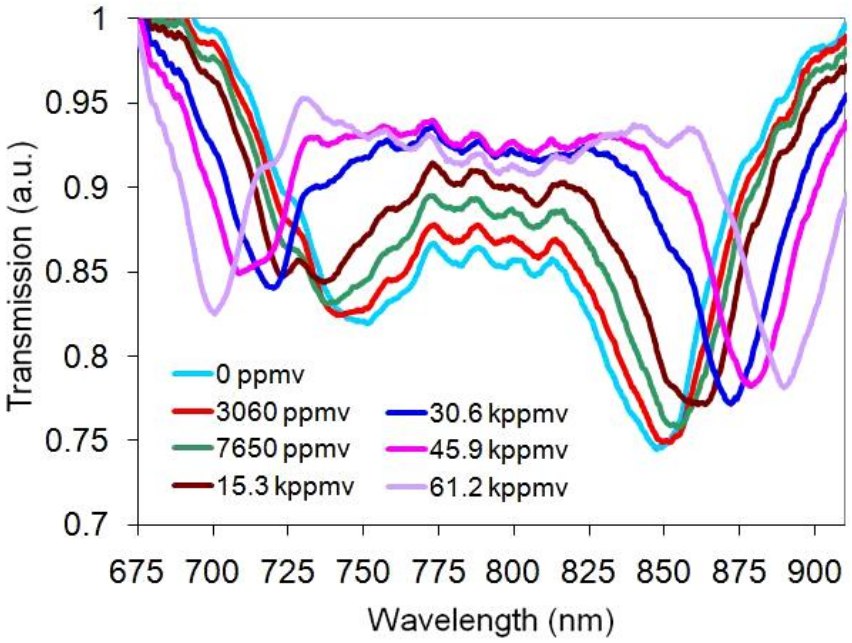

Figure 9.10a The transmission spectrum of the 100μm period LPG coated with calix[4]resorcarene. The spectrum changes with increasing toluene vapour concentrations, from 3060ppmv (11.6g/m^3) up to 61200ppmv (231g/m^3).

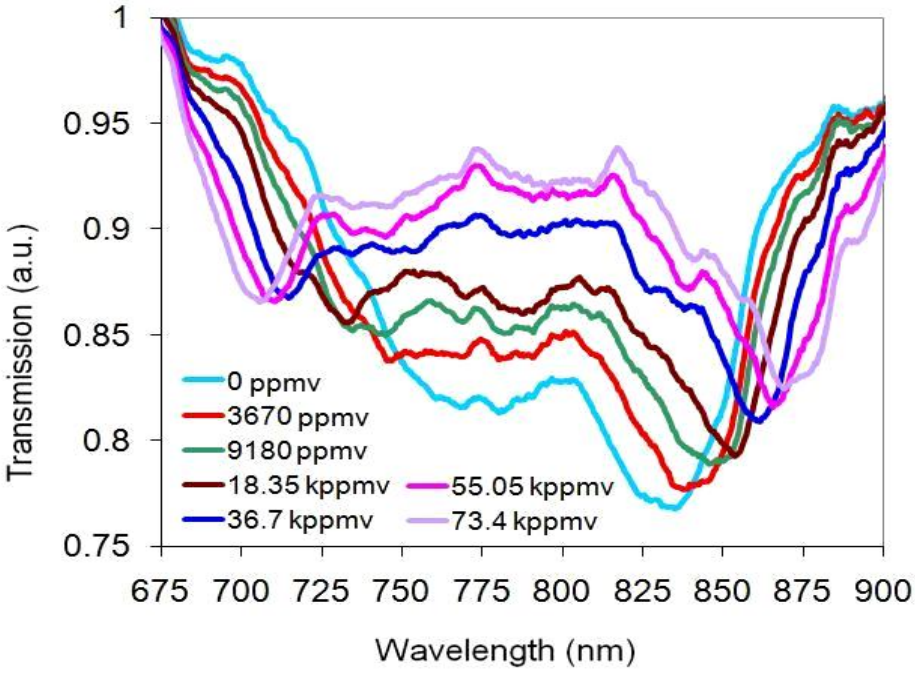

Figure 9.10b The response of the transmission spectrum of the calix[8]arene coated 100μm period LPG sensor to the changing concentration of benzene vapour at the levels indicated, from 3670ppmv (11.7g/m^3) up to 73400ppmv (234g/m^3).

Benzene and toluene gave strong responses and the increase in response with increasing vapour concentration shows that these aromatic molecules can penetrate deeper into the film at higher vapour concentrations[32]. The discrimination of aromatic compounds toluene and benzene is evident when compared to the saturated organic compounds cyclohexane and hexane, Figure 9.11. The stronger response to toluene compared to benzene indicates that the presence of the methyl group increases the intermolecular binding with the cavity. The dip in response to toluene vapour at high concentrations is due to coupling to another cladding mode.

Table 9.1 Boiling points of BTEX and other organic solvents

Solvent	Boiling Point
Hexane	69 ^{o}C
Benzene	80.1 ^{o}C
Cylcohexane	80.7 ^{o}C
Toluene	110.6 ^{o}C
Ethylbenzene	136 ^{o}C
Xylene	138.5 ^{o}C

The response to hexane showed the smallest response with the absorption of hexane into the calix[4]resorcarene coating resulting in a reduction in the refractive index and density of the film, Figure 9.11. Here the filling of cavities and voids causes a density decrease: perhaps the hexane molecule becomes adsorbed between the layers of the calixarene molecules, and causes the layers of the coating to expand and its density decreases. The response of hexane with the calix[8]arene film, Figure 9.11, shows an increase in optical density, which becomes saturated. This indicates that the hexane molecule, a pleated chain, 1.03nm x 0.49nm x 0.4nm[33], does not penetrate deeply into the film.

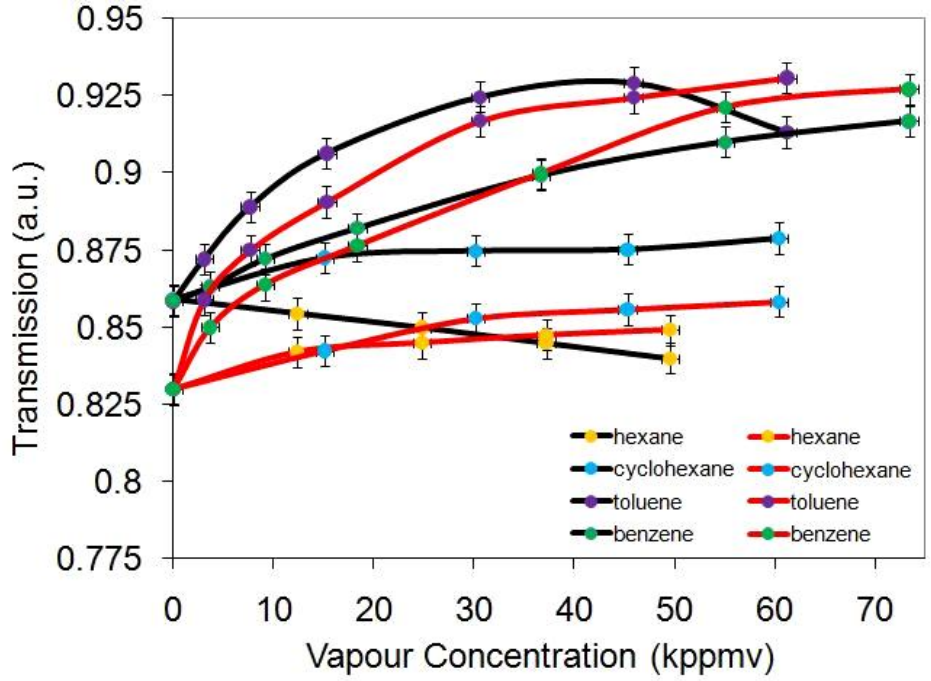

Figure 9.11 The change in optical transmission at 800nm of a undecyl-calix[4]resorcarene coated 100μm period LPG (black) and a 100μm period LPG coated with tert-butyl-calix[8]arene (red), in response to the changing vapour concentration of four guest molecules; toluene, benzene, cyclohexane and hexane.

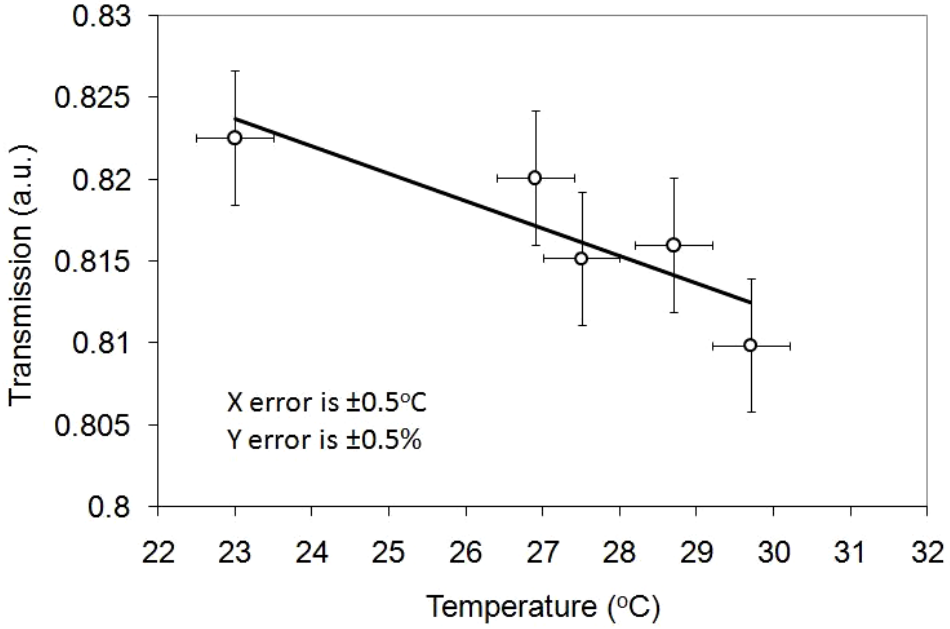

Figure 9.12 The change in transmitted optical signal strength measured at 800nm with temperature for a 100μm period LPG coated with calix[8]arene, in air. The negative temperature coefficient has a response of -0.0016 a.u./°C.

The chemical sensing presented above was conducted in a temperature controlled environment at 22^{o}C. The temperature sensitivity of the 100μm period LPG coated with calix[8]arene was characterised. The gas chamber was placed on a hot plate, and a thermocouple was used to monitor the temperature change inside the gas chamber. The results shown in Figure 9.12 are captured directly from the transmission intensity data at 800nm, Figure 9.10b. The intensity noise on this signal is averaged by plotting a linear trend. A negative temperature coefficient of -0.0016 a.u./^{o}C was observed. The behaviour was found to be reversible, and showed a normal cooling transient when the hot plate was switched off. However, when the sensor was heated to 40^{o}C, an irreversible change was observed, and the sensor did not return to its original calibration point. A form of thermal annealing of the coating may have taken place.

Although the two sensors gave broadly similar levels of discrimination, the two coating materials of the sensors could be distinguished by the large differences in their response times to changing vapour concentration. In this regard, the results are presented for cyclohexane and benzene. Both these solvents have near identical volatilities since their boiling points are 80.7^{o}C and 80.1^{o}C respectively, Table 9.1.

In response to cyclohexane, Figure 9.13a, with molecular dimensions 0.72nm x 0.64nm x 0.49nm[33], the response time with increasing vapour concentration was ~15 times longer with calix[8]arene compared to calix[4]resorcarene.

In response to benzene, Figure 9.13b, with a molecular volume of 0.74nm x 0.67nm x 0.37nm[33], the response time with decreasing vapour concentration was about 40 times longer with the sensor with the calix[8]arene coating than with the calix[4]resorcarene coating.

For the vapour ingress times, the evaporation time of the solvent is incorporated in both plots which must be the same time in both cases. The large difference seen here must therefore be due to the difference in infusion times of the cyclohexane molecule into the host matrix. For the vapour egress times, there is no evaporation time to take into account. The large difference indicates the different egress times of benzene from the two types of host matrix.

The reason for this is attributed to the different permeability's of the two coating materials. The larger cavity material would be expected to give the greater porosity. However it is the other way around. Therefore one must appeal to the packing structure of a multilayer matrix formed from such materials.

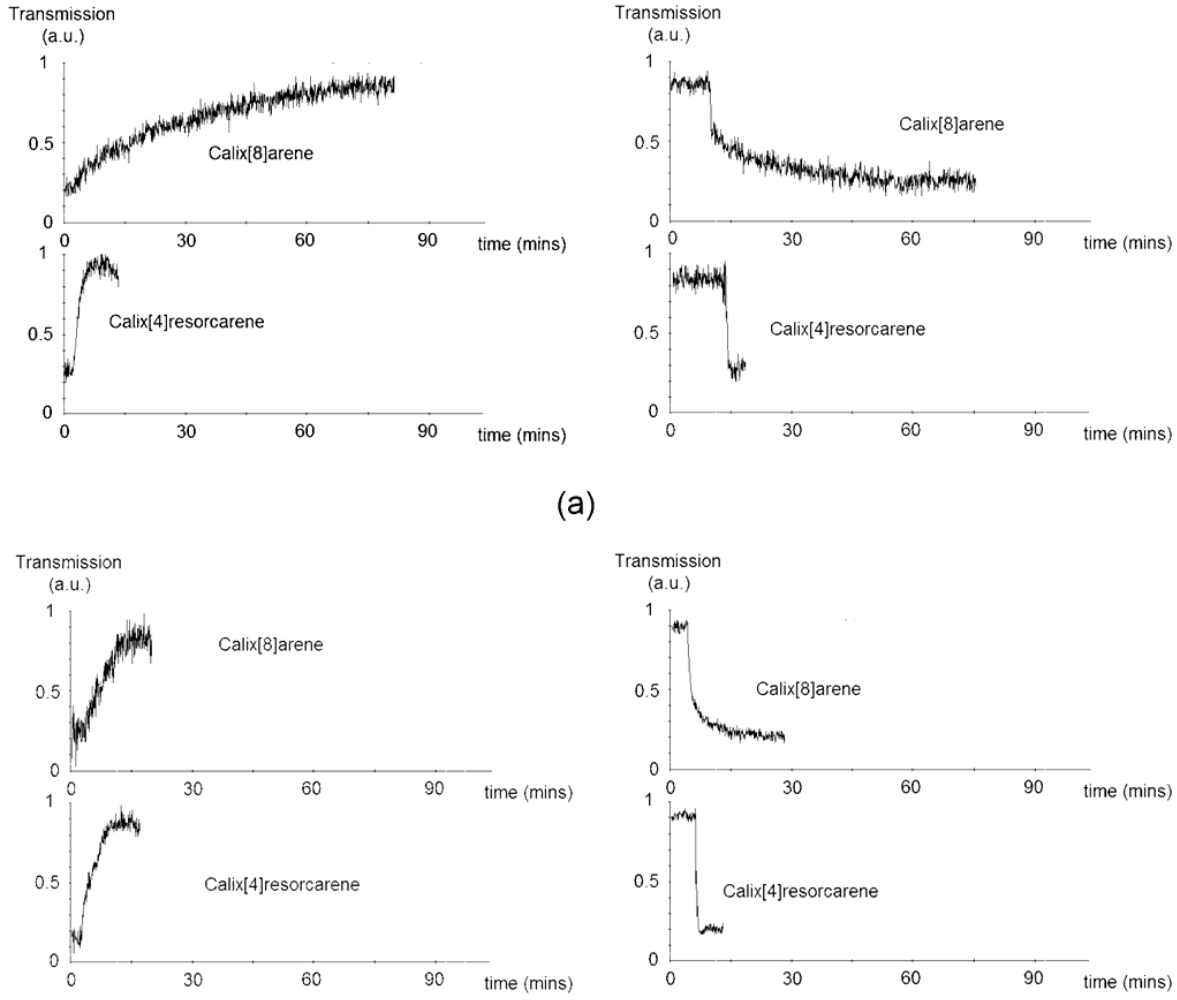

Figure 9.13 Response times of 100μm period LPG sensor coated with calix[8]arene and calix[4]resorcarene to (a) cyclohexane vapour and (b) benzene vapour.

Work on quartz crystal microbalance (QCM) sensors has lead to the following findings in relation to calixarene coatings. It has been noted that the long pendant alkyl chains lead to highly permeable thin films for gas sensors[34]. It has also been reported that the tert-butyl pendant chain gives poorer reversibility compared to the long alkyl chains when using calix[8]arene for measuring chloroform and trichloroethane in water solution[15]. The length of the pendant chain determines the packing density of the coating and hence its permeability[2]. Drawing on these same conclusions, the calix[4]resorcarene has a relatively long undecyl pendant chain ($C_{11}H_{23}$) compared to the calix[8]arene coating with the shorter tert-butyl chain, this would imply the greater density of the latter, offering less permeability.

Apart from packing density, the regularity of the calix[4]resorcarene multilayer structure or the alignment of the cavities between layers would lend itself to easier transport of the guest molecule from layer to layer[12]. These factors determine the transient response times.

9.7 CONCLUSION

A comparison between the responses of LPGs coated with two different materials has been completed. The two materials are calix[4]resorcarene with a cavity size of 1.32nm in diameter[5], and a calix[8]arene derivative with a cavity nominally twice that size. The two coatings exhibit similar species selectivity, with the results showing that supramolecular forces rather than the cavity size is the dominant affect for molecular recognition for the host and guest molecules investigated here.

There was however a significant difference in the measured response times to vapour concentration changes, and this is because the permeability of the two coatings differ. The reason for this is put down to the packing structure of the two coatings which is determined when the multilayer film is deposited. Here we used the Langmuir-Blodgett technique for depositing the calixarene coating onto an optical fibre. Although calix[8]arene has the larger cavity, the packing structure in terms of its regularity, alignment of cavities in the plane perpendicular to the fibre axis, and the higher packing density with its shorter pendant chains is thought to be responsible for its poorer porosity.

9.8 REFERENCES

1. Hassan, A. K., Ray, A. K., Nabok, A. V. and Wilkop, T. (2001), "Kinetic studies of BTEX vapour adsorption onto surfaces of calix-4-resorcinarene films", *Applied Surface Science,* vol. 182, no. 1-2, pp. 49-54.

2. Koshets, I. A., Kazantseva, Z. I., Belyaev, A. E. and Kalchenko, V. I. (2009), "Sensitivity of resorcinarene films towards aliphatic alcohols", *Sensors and Actuators, B: Chemical,* vol. 140, no. 1, pp. 104-108.

3. Liu, Y., You, C., Kang, S., Wang, C., Chen, F. and He, X. (2002), "Synthesis of novel β-cyclodextrin and calixarene derivatives and their use in gas sensing on the basis of molecular recognition", *European Journal of Organic Chemistry,* , no. 4, pp. 607-613.

4. Nabok, A. V., Hassan, A. K. and Ray, A. K. (2000), "Condensation of organic vapours within nanoporous calixarene thin films", *Journal of Materials Chemistry,* vol. 10, no. 1, pp. 189-194.

5. Collyer, S. D., Davis, F., Lucke, A., Stirling, C. J. M. and Higson, S. P. J. (2003), "The electrochemistry of the ferri/ferrocyanide couple at a calix[4]resorcinarenetetrathiol-modified gold electrode as a study of novel electrode modifying coatings for use within electro-analytical sensors", *Journal of Electroanalytical Chemistry,* vol. 549, no. SUPPL., pp. 119-127.

6. Liu, Q., Chiang, K. S. and Liu, Y. (2007), "Characterization of single-mode fiber with fiber Bragg gratings for the design of long-period gratings", *Journal of Lightwave Technology,* vol. 25, no. 8, pp. 2129-2134.

7. Shu, X., Zhu, X., Wang, Q., Jiang, S., Shi, W., Huang, Z. and Huang, D. (1999), "Dual resonant peaks of LP_{015} cladding mode in long-period gratings", *Electronics Letters,* vol. 35, no. 8, pp. 649-651.

8. Cheung, C. S., Topliss, S. M., James, S. W. and Tatam, R. P. (2008), "Response of fiber-optic long-period gratings operating near the phase-matching turning point to the deposition of nanostructured coatings", *Journal of the Optical Society of America B: Optical Physics,* vol. 25, no. 6, pp. 897-902.

9. James, S. W., Cheung, C. S. and Tatam, R. P. (2007), "Experimental observations on the response of 1^{st} and 2^{nd} order fibre optic long period grating coupling bands to the deposition of nanostructured coatings", *Optics Express,* vol. 15, no. 20, pp. 13096-13107.

10. Del Villar, I., Matias, I. R. and Arregui, F. J. (2006), "Influence on cladding mode distribution of overlay deposition on long-period fiber gratings", *Journal of the*

Optical Society of America A: Optics and Image Science, and Vision, vol. 23, no. 3, pp. 651-658.

11. Petty, M. C. (2008), *Molecular Electronics: From Principles to Practice,* John Wiley & Sons Ltd.

12. Atwood, J. L., Barbour, L. J., Jerga, A. and Schottel, B. L. (2002), "Guest transport in a nonporous organic solid via dynamic van der Waals cooperativity", *Science,* vol. 298, no. 5595, pp. 1000-1002.

13. Steed, J. W. and Atwood, J. L. (2009), *Supramolecular Chemistry,* Second Edition, John Wiley & Sons, Ltd.

14. Filenko, D., Gotszalk, T., Kazantseva, Z., Rabinovych, O., Koshets, I., Shirshov, Y., Kalchenko, V. and Rangelow, I. W. (2005), "Chemical gas sensors based on calixarene-coated discontinuous gold films", *Sensors and Actuators, B: Chemical,* vol. 111-112, no. SUPPL., pp. 264-270.

15. Roesler, S., Lucklum, R., Borngraeber, R., Hartmann, J. and Hauptmann, P. (1998), "Sensor system for the detection of organic pollutants in water by thickness shear mode resonators", *Sensors and Actuators, B: Chemical,* vol. B48, no. 1 -3 pt 4, pp. 415-424.

16. Andreetti, G. D., Ungaro, R. and Pochini, A. (1979), "Crystal and molecular structure of cyclo{quater[(5-t-butyl-2-hydroxy-1,3- phenylene)methylene]} toluene (1 : 1) clathrate", *Journal of the Chemical Society, Chemical Communications,* , no. 22, pp. 1005-1007.

17. Biros, S. M. and Rebek Jr., J. (2007), "Structure and binding properties of water-soluble cavitands and capsules", *Chemical Society Reviews,* vol. 36, no. 1, pp. 93-104.

18. Gutsche, C. D., Gutsche, A. E. and Karaulov, A. I. (1985), "Calixarenes 11. Crystal and molecular structure of p-tert-butylcalix[8]arene", *Journal of Inclusion Phenomena,* vol. 3, no. 4, pp. 447-451.

19. Davis, F. and Stirling, C. J. M. (1996), "Calix-4-resorcinarene monolayers and multilayers: Formation, structure, and differential adsorption", *Langmuir,* vol. 12, no. 22, pp. 5365-5374.

20. Arduini, A., Caciuffo, R., Geremia, S., Ferrero, C., Ugozzoli, F. and Zontone, F. (1998), "Temperature dependence of the weak host-guest interactions in the p-tertbutylcalix[4]arene 1:1 toluene complex", *Supramolecular Chemistry,* vol. 10, no. 2, pp. 125-132.

21. Steed, J. W., Turner, D. R. and Wallace, K. J. (2007), *Core Concepts in Supramolecular Chemistry and Nanochemistry,* John Wiley & Sons, Ltd.

22. Notestein, J. M., Katz, A. and Iglesia, E. (2006), "Energetics of small molecule and water complexation in hydrophobic calixarene cavities", *Langmuir,* vol. 22, no. 9, pp. 4004-4014.

23. Andreetti, G. D., Pochini, A. and Ungaro, R. (1983), "Molecular inclusion in functionalized macrocycles. Part 6. The crystal and molecular structures of the calix[4]arene from p-(1,1,3,3-tetramethylbutyl) phenol and its 1:1 complex with toluene", *Journal of the Chemical Society, Perkin Transactions 2,* , no. 9, pp. 1773-1779.

24. Nishio, M., Umezawa, Y., Honda, K., Tsuboyama, S. and Suezawa, H. (2009), "CH/π hydrogen bonds in organic and organometallic chemistry", *CrystEngComm,* vol. 11, no. 9, pp. 1757-1788.

25. Othonos, A. and Kalli, K. (1999), *Fiber Bragg Gratings: Fundamentals and Applications in Telecommunications and Sensing,* Artech House.

26. Fujita, K., Masuda, Y., Nakayama, K., Ando, M., Sakamoto, K., Mohri, J., Yamauchi, M., Kimura, M., Mizutani, Y., Kimura, S., Yokouchi, T., Suzaki, Y. and Ejima, S. (2005), "Dynamic evolution of the spectrum of long-period fiber Bragg gratings fabricated from hydrogen-loaded optical fiber by ultraviolet laser irradiation", *Applied Optics,* vol. 44, no. 33, pp. 7032-7038.

27. Jang, J. N., Kim, H. G., Shin, S. G., Kim, M. S., Lee, S. B. and Kwack, K. H. (1999), "Effects of hydrogen molecule diffusion on LP0m mode coupling of long-period gratings", *Journal of Non-Crystalline Solids,* vol. 259, no. 1-3, pp. 156-164.

28. Vasil'ev, S. A., Medvedkov, O. I., Bozhkov, A. S., Korolev, I. G. and Dianov, E. M. (2006), "Modification of cladding-mode fields upon fibre loading with H2 and its influence on the spectral characteristics of long-period gratings", *Quantum Electronics,* vol. 36, no. 1, pp. 61-66.

29. Guan, B., Tam, H., Chan, H. L. W., Choy, C. and Demokan, M. S. (2001), "Growth characteristics of long-period gratings in hydrogen-loaded fibre during and after 193 mn UV inscription", *Measurement Science and Technology,* vol. 12, no. 7, pp. 818-823.

30. Rees, N. D., James, S. W., Tatam, R. P. and Ashwell, G. J. (2002), "Optical fiber long-period gratings with Langmuir-Blodgett thin-film overlays", *Optics Letters,* vol. 27, no. 9, pp. 686-688.

31. MacGillivray, L. R. and Atwood, J. L. (1997), "A chiral spherical molecular assembly held together by 60 hydrogen bonds", *Nature,* vol. 389, no. 6650, pp. 469-472.

32. Nabok, A. V., Lavrik, N. V., Kazantseva, Z. I., Nesterenko, B. A., Markovskiy, L. N., Kalchenko, V. I. and Shivaniuk, A. N. (1995), "Complexing properties of calix[4]resorcinolarene LB films", *Thin Solid Films,* vol. 259, no. 2, pp. 244-247.

33. Barrer, R. M. and Sikand, A. (1979), "Sorption of hydrocarbons and water in silanated and unsilanated partial H-forms of zeolite Y", *Journal of the Chemical Society, Faraday Transactions 1: Physical Chemistry in Condensed Phases,* vol. 75, pp. 2221-2234.

34. Pinalli, R., Suman, M. and Dalcanale, E. (2004), "Cavitands at Work: From Molecular Recognition to Supramolecular Sensors", *European Journal of Organic Chemistry*, no. 3, pp. 451-462.

CHAPTER 10: CONCLUSION AND PROPOSALS FOR FUTURE WORK

10.1 LONG PERIOD GRATINGS AT THE PHASE MATCHING TURNING POINT

Long period fibre gratings are structured in principally two ways; a square wave modulation[1; 2] of the refractive index in the core of the fibre, or by mechanical inducing an equivalent change by etching the cladding or physical deformation of the fibre[3]. The grating period is of the order of hundreds of microns. This induces a coupling of energy from the core to a subset of the cladding modes, at wavelengths that satisfy the phase matching condition, Equation 2.1[4].

The energy transfer from core to cladding modes results in drop outs in the transmission spectrum of the optical fibre, referred to as attenuation bands. The central wavelengths of these bands are dependent not only on the ambient index of the medium surrounding the fibre, but also on the refractive index or thickness of a coating applied to the fibre in the region of the LPG, and can be seen to retune in wavelength upon perturbation in the ambient index[5], or that of the coating[6].

The operation of these devices at the phase matching turning point has been investigated in Chapters 5 and 6, which is indicated by two resonant bands appearing in the transmission spectrum of the fibre. These dual resonant bands have opposite sensitivities to the thickness of the coating applied to the fibre, and this has been demonstrated by obtaining data showing the evolution of the optical spectrum with applied coating thickness in Figures 5.3 and 5.5.

It has been shown that appropriate selection of the period of the LPG and the refractive index of the coating material can ensure that the phase matching turning point of the LPG coincides with the mode transition region. This ensures optimum sensitivity of the device to the coating's optical properties. It has also been shown in Chapter 6 that the selection of the grating period can determine the optimum coating layer thickness, the sensors operating wavelength, the sensitivity by its proximity to the mode transition region, or the symmetry of the dual banded spectrum.

In order to extend the design envelope further, phase shifted LPGs have been explored in Chapter 7. This device has two dual resonant attenuation bands, with different proximities to the mode transition region. Here, the evolution of the attenuation bands in Figure 7.7 indicate that the dual resonant band with closer proximity to the mode transition region has greater sensitivity.

Some new results have been obtained by coating half the length of the phase shifted LPG, with the evolution of the attenuation bands not showing the smooth progressive

response to coating thickness. This feature has been referred to here as a *bandgap*, Figures 7.8 and 7.9. This phenomenon has not been reported before.

10.2 NANOSTRUCTURED CALIXARENE COATINGS

In Chapters 8 and 9, four organic chemical sensors have been presented based on a long period grating (LPG) formed in an optical fibre, see Figure 8.8 and Figure 9.11. A calixarene coating of thickness of several hundred nm's has been applied to the region of the fibre containing the LPG sensor. An interaction takes place between the sensor and the environment by adsorption of the organic analyte molecule, and the transmission response of the LPG is changed. The four sensors presented show a chemical selectivity towards aromatic molecules which is a function of the calixarene coating, which avail different levels of binding or complexation compared to other non-aromatic molecular species.

The determination of complexation and selectivity for guest adsorption of calixarene can be summarised in the following way. At the individual molecule level, calixarenes have been described as scaffolding structures[7] which allow the guest molecule to interact with functional groups in the concerted way. In our case, the functional groups of the host are particularly the aromatic rings of the calixarene cavity, and methyl groups on the pendant chains. Here, the calixarene structure allows the inclusion of a guest species, which through these functional groups can maximise in terms of strength and number the formation of intermolecular bonds of the form CH-π, Van der Waals and π-π.

The 3D structure of the calixarene molecule forms a matrix structure upon deposition, and by having a regular periodic arrangement allows the guest molecule to freely penetrate the multilayer structure. It is logical that the size of the cavity relates to the maximum size that a guest molecule can freely penetrate the multilayer structure. It has been reported using calixarene coated QCM sensors that the larger cavity of calix[6]arene was found to be more favourable in forming complexes with organic amines, compared to calix[4]arene[8]. For the two coatings, the smaller guest species of diethylamine gave a greater response than the larger guest species of triethylamine due to steric hindrance. Furthermore, the binding of these guests favoured the larger cavity of calix[6]arene.

It has been found that for larger guest molecules a reduction in porosity has been observed, and this is manifested in a lengthening of the absorption time. For the larger analyte molecules tested, the long settling time for the uptake of xylene for the host molecule undecyl-calix[4]resorcarene points to the relative sizes of the cavity and analyte molecule in determining the porosity. Moreover, the long settling time for the

uptake of xylene and cyclohexane for the larger cavity material tert-butyl-calix[8]arene, points to the multilayer structure as well in determining the porosity.

However, the cavity size is not the driving force behind determining the selectivity of calixarene to a particular chemical species, as a *lock and key* description would imply. The ability for calixarene to encapsulate a guest molecule is driven by the strength and number of intermolecular bonds that can occur and this is shown by the similarity in results[nn] for species selectivity for the two calixarenes investigated, which had different cavity sizes, but similar chemistries. This is the simplest interpretation of the results given the set of data presented in this thesis.

This leads to the question of what are the intermolecular bonds involved: the specific mechanism is difficult to pinpoint since the literature is often contradictory. They are most often referred to by three types of bonds, Van der Waals[7], CH-π[9] and π-π[10].

Van der Waals is the most widely cited and is a weak electrostatic attraction arising from polarisation of the molecules electron cloud[11]. This can occur at multiple points and is proportional to the surface area of contact between the host and guest molecules. It has been reported that the tert-butyl groups on the upper rim of the calixarene bowl forms multiple Van der Waals contacts with the guest molecule, compared to the weaker complexation observed with a calixarene host without the tert-butyl group on the upper rim[7].

CH-π is most often cited referring specifically to the binding between the methyl group in an aliphatic pendant chain of tert-butyl-calixarene and the aromatic ring of an aromatic guest molecule e.g. toluene[9; 12]. It has not been quoted referring to the methyl group of a toluene guest and the aromatic ring of the host for calixarene·toluene complexes. However, for a wider set of calixarene derived hosts, the CH-π has been cited in relation to the methyl group of the guests and the aromatic groups of the calixarene host cavity[13]. The results in Chapters 8 and 9 show that the methyl group of the toluene guest molecule does increase the affinity to form inclusion complexes when compared to the guest molecule benzene, with no methyl group. Furthermore, CH-π bonding between the methyl group of the guest and the aromatic groups of the host could also apply to the inclusion of non-aromatic guests

[nn] The signal magnitudes recorded for vapour sensing were determined by the extinction of the dual resonant bands of the sensor, which are a result of the deposition process. The basis for reporting the similarity of species selectivity is therefore not based on comparing absolute signal magnitudes across different sensors, but on the ability of the sensor to discriminate between the guest molecules. This discrimination was found to be similar for sensors using both reported calixarene materials.

e.g. hexane and cyclohexane, although complexation was weaker with aliphatic and alicyclic guests.

π-π clearly refers to binding between an aromatic ring in the guest with an aromatic ring in the host. Although cited for the interaction between the calix[8]arene host and a toluene or benzene guest[10], this bond is the least commonly referred to in the literature in relation to complexation in calixarene hosts.

So selectivity is determined by the nature of the intermolecular bonds, and the presence of an aromatic moiety on the analyte molecule has been shown through the results presented in this thesis to give a stronger adsorption into the calixarene cavity. The adsorption of toluene has been demonstrated to be 13 times greater than hexane, and six times greater than cyclohexane, either which have no aromatic moiety.

10.3 APPLICATIONS

Selectivity does not however allow the identification of a particular chemical species, in an environment which contains many different chemical vapours. To overcome this, it has been reported that the development of multisensory arrays with sufficiently graded responses in their selectivity could be used for the discrimination of different types of vapours[14]. For the deployment of the sensor in a chemical plant, factory or manufacturing environment where many species could be encountered, it would be necessary to implement a multisensory approach for this situation.

A single sensor could however be used for detecting vapour within an environment targeted for a limited set of known chemical species. This could be for example an aircraft cabin, where the pollution of fumes from the engine could enter the aircraft through the compressed air system and pollute the inside area where occupants are situated. The petrochemical based organic species could be detected, with the sensors selectivity providing a preference for the more toxic species i.e. the aromatic molecules. In such an environment, it is unlikely that the sensor would give a false positive from detecting for example, ammonia or organic amines, since these chemical species will not occur in this situation. Indeed, the detection of other chemical species in this environment may indicate the presence of homemade bombs.

For the LPG sensors described in Chapters 8 and 9, toluene concentrations from 3060ppmv (11.6g/m^3) up to 61200ppmv (231g/m^3) have been investigated. This is above the levels reported in Chapter 1 for traffic pollution at kindergarten sites[15], at photocopier centres[16] or in the workplace[17]. This indicates that the sensor would only be useful in higher toxicity environments. There is a need for the LPG based sensor described in this thesis to be made more sensitive.

The LPG based sensors reported in Chapter 5 and 8 have given levels of sensitivity of 1600ppmv/nm for toluene vapour and -0.55pH/nm for pH. These sensitivity figures show a need for improvement. Reduction of the fibre cladding radius from 125μm to 35μm has been shown to improve LPG sensitivity threefold[18]. A closer alignment of the dual resonant attenuation band and the transition region, which occurs using LPGs with a period of 140μm will also increase sensitivity, Chapter 6. The introduction of other hypothetical coatings that give a larger refractive index change in relation to adsorption of analyte vapours would also boost sensitivity.

The levels of sensitivity stated above are based of wavelength detection where the central minimum of an attenuation band is measured. This can be done by a peak detection process, and is limited by intensity noise, asymmetry of the attenuation band, and the resolution of the spectrometer, see Sections 5.7 and 8.6. The accuracy of wavelength measurement can be improved by using polynomial curve fitting techniques where an 'n' order polynomial is fitted to the measured data, the measured data is discarded, and the central wavelength is read from the minimum of the polynomial function, see Section 5.4. By interpolating between data points, this technique allows for enhanced resolution.

Wavelength detection requires the use of a spectrometer or optical spectrum analyser. For a lower cost implementation of a sensor system, intensity detection is an alternative approach. The dual resonant spectrum obtained in Figure 8.6 contains a broad spectral feature that would result in the modulation of light in the fibre by the measurand. The use of a photodiode to detect optical power and a simple transimpedance amplifier to convert the photocurrent into voltage, followed by further amplification is a typical implementation of an intensity detection system[20].

Amplifier systems are generally ac-coupled to circumvent the problems of biasing and drifts associated with temperature and power supply variations. Since ac-coupled amplification does not pass any low frequency electrical signal, it would be necessary to optically modulate the sensor signal at the source. The use of a semiconductor light source, e.g., LED or laser diode, permits electrical modulation of the light source by an RF signal. The amplifier system can then be designed around the electrical signal frequency. Filtering the broadband noise using electrical filters outside the passband of the signal would improve the sensitivity of this approach. Finally the signal can be demodulated by a simple peak detector.

Therefore, building a low cost sensor system for *in the field* deployment may be implemented with low cost optoelectronics by using intensity detection. An appropriate reference channel is required, see Section 8.6. A suitable jig to hold the LPG sensor must be designed to prevent fibre bending as well as an enclosure that

allows for chemical vapour ingress and egress. This solution would of course be competing with the existing technology and the principal technologies for detecting hydrocarbons are spectroscopic methods and photoionization detectors.

Molecular species absorb IR or UV at different wavelengths and spectroscopic sensors detect this unique signature. For example, hexane absorbs IR light at ~3.4μm[21 p595]. The aromatic organic compounds have absorption spectra in the UV region, benzene absorbs at ~250nm[22]. The Lambert Beer law states that the absorbance is proportional to the chemical concentration. Gas detectors are built around these principles and are commercially available e.g. General Monitors Model IR400. This unit is specified for the chemical species methane, propane, ethane, ethylene, butane, hexane, pentane and benzene. This technique yields ppm sensitivity levels[22].

For greater sensitivity, the photoionization detector (PID) techniques uses UV light to ionize a gas, forming positively charged ions that can be detected by the arising electrical current formed between two electrodes. This technique has little selectivity, determined by the ionization potential (IP) of the gas. Typically organic aromatic compounds have IP's of ~9.5eV whereas aliphatic compounds have IP's of ~10.6eV. The UV lamp must be selected with adequate ionization energy and therefore a 10.6eV rated lamp is often used to detect most VOC's[21 p585]. Such a device is the Rae Systems Model ppbRAE 3000 portable handheld VOC monitor. This unit offers ppb (parts per billion) levels of sensitivity.

Since both these examples are complex instruments, an LPG based sensor system as outlined here can compete in terms of cost. Sensitivity of the LPG solution is an issue and further developments of this technique must be made. Selectivity falls between the spectroscopic and the PID techniques. However, the LPG as a platform will be able to make use of new materials that are developed in the future with exceptional chemically selective properties.

10.4 FINAL REMARKS

In closing, the use of materials that change their properties to chemical species, and have a strong preference for certain chemical species allows chemically selective optical sensors to be realized, based on the long period grating. The exploitation of dual resonance in long period gratings allows a sensitivity improvement over long period gratings that operate away from the phase matching turning point, and broadband responses in the transmission spectrum allow for straightforward optical intensity monitoring methods of detection to be employed.

Four calixarene coated LPG sensors have been characterized in Chapters 8 and 9 of this thesis. The results show that these LPG sensors are most suitable in environments with a limited variety of chemical species since calixarenes have a cross-sensitivity to many chemical species. Also, the levels of sensitivity obtained show that this sensor is suitable for environments with very high levels of analyte concentration. These shortcomings may be overcome with their use in multisensor arrays and the further development of the technology.

_____

The following section outlines the next steps for developing this technology and some possible future developments.

10.5 FURTHER WORK

- The next logical step for this work is the construction of a constant vapour flow set up[19] to permit repetitive testing of the vapour sensing capabilities for the LPG sensors. This would allow kinetic measurements to be undertaken, with an in-depth analysis of drifts and hysteresis, as well as transient response times. With the sensor remaining in-situ, and with the vapour flow being modulated by a valve, the problem of disturbing the fibre and the accompanying change in bend losses could be surmounted.
- A strong direction in the understanding of the underlying behaviour of calixarenes could be gleaned by working with monolayers or multilayer films say less than 10 layers. At the monolayer level, the quintessential behaviour of the calixarene cavity could be investigated without complications arising from a multilayer structure. An 80μm long period grating has been fabricated that contains dual resonant bands in the spectrum in its uncoated state, Figure 5.2. Further tailoring of the grating period would create a spectrum where the dual resonant attenuation bands are conjoined. Such a device could be deposited with a few layers to achieve a spectrum that is similar to Figure 8.6. The sensing characteristics in terms of magnitude of response from just a few layers would give strong indicators of the mechanisms behind guest encapsulation with calixarene. Also, the response time could be expected to be far shorter for absorption to reach a saturation condition.
- The characterization work that has been conducted on calixarene coated LPGs with period 180μm (Chapter 8) and 100μm (Chapter 9) could be repeated with an LPG with period 140μm. This would allow the sensitivity improvement by operating closer to the transition region to be gauged.
- Further investigation can be done into the effect of temperature on the calixarene coating. Whilst a small temperature dependence has been measured for these devices up to 30^{o}C which was reversible, it has been observed that elevating the temperature of the coating to 40^{o}C led to an irreversible change in the spectral response of a long period grating device using a calix[8]arene coating, Chapter 9. Here, the refractive index of the calix[8]arene coating increased. This is possibly an annealing effect, perhaps the matrix or lattice of the calixarene coating forms itself into a more regular arrangement with lateral movement of the calixarene molecules. A permanent change may take place to effect the bowl to bowl alignment, with a consequence on the porosity of the

coating. The new response of this modified coating needs to be fully characterised.

- Operating the sensor at elevated temperature would also allow a determination of the mechanisms behind the sensor's selectivity. This would be very interesting since it has been reported that the Van der Waals bond weakens with increasing temperature, whilst the CH-π bond strengthens with temperature[9]. This test would give a strong indication of the identity of the intermolecular bond responsible for molecular encapsulation, something that has been difficult to determine from the literature.
- A move from chemical sensors to biochemical sensors would allow higher selectivities to be obtained since the nature of biological molecular interactions in more specific. Indeed, species specific bio-sensors may be realisable.
- Translating the work done here onto other fibre types is a natural extension of the work. Imprinting long period gratings onto tapered fibres and photonic crystal fibre is a likely next step in this vein of research.
- New coating materials for LPG's, e.g. porphyrines could be researched, allowing the detection of nitrous oxides or other chemical species. The crossover in nanotechnology with coatings which incorporate nanospheres or other nanoparticles is an avenue that may lead to simpler manufacturing processes for such sensors. Here, simple dipping methods and a low layer counts are the likely benefits.
- A prototype sensor could be demonstated with low cost optoelectonics using a LED and a photodiode to show how the broadband spectral response of dual resonance could be usefully employed in a low cost sensor system. By incorporating appropriate low-pass electrical filtering, one could experimentally determine the level of sensitivity that could be achieved with this mode of detection.
- The work on phase shifted LPG's with partial coatings described in Chapter 7 is not exhaustive, and other constructions could be investigated, e.g. starting with a grating with a single π phase shift in the centre. It would be interesting to try to enlarge the bandgap observed in the spectra, Figure 7.8. This will allow further analysis of the bandgap region, leading to optimization and greater definition of the bandgaps. It is hoped that this may lead to improvements in sensor performance by obtaining new spectral features which can be utilised in sensor design.

10.6 REFERENCES

1. Mizunami, T. and Fukuda, T. (2005), "Hydrogen diffusion in fabrication processes of long-period fiber gratings: Measurement and finite-element-method analysis", *Proceedings of WFOPC2005 - 4th IEEE/LEOS Workshop on Fibres and Optical Passive Components* vol. 2005, Article number 1462128, pp. 198-203.

2. Fujita, K., Masuda, Y., Nakayama, K., Ando, M., Sakamoto, K., Mohri, J., Yamauchi, M., Kimura, M., Mizutani, Y., Kimura, S., Yokouchi, T., Suzaki, Y. and Ejima, S. (2005), "Dynamic evolution of the spectrum of long-period fiber Bragg gratings fabricated from hydrogen-loaded optical fiber by ultraviolet laser irradiation", *Applied Optics,* vol. 44, no. 33, pp. 7032-7038.

3. James, S. W. and Tatam, R. P. (2003), "Optical fibre long-period grating sensors: Characteristics and application", *Measurement Science & Technology,* vol. 14, no. 5, pp. R49-R61.

4. James, S. W., Cheung, C. S. and Tatam, R. P. (2007), "Experimental observations on the response of 1st and 2nd order fibre optic long period grating coupling bands to the deposition of nanostructured coatings", *Optics Express,* vol. 15, no. 20, pp. 13096-13107.

5. Patrick, H. J., Kersey, A. D. and Bucholtz, F. (1998), "Analysis of the response of long period fiber gratings to external index of refraction", *Journal of Lightwave Technology,* vol. 16, no. 9, pp. 1606-1612.

6. Rees, N. D., James, S. W., Tatam, R. P. and Ashwell, G. J. (2002), "Optical fiber long-period gratings with Langmuir-Blodgett thin-film overlays", *Optics Letters,* vol. 27, no. 9, pp. 686-688.

7. Notestein, J. M., Katz, A. and Iglesia, E. (2006), "Energetics of small molecule and water complexation in hydrophobic calixarene cavities", *Langmuir,* vol. 22, no. 9, pp. 4004-4014.

8. Liu, Y., You, C., Kang, S., Wang, C., Chen, F. and He, X. (2002), "Synthesis of novel β-cyclodextrin and calixarene derivatives and their use in gas sensing on the basis of molecular recognition", *European Journal of Organic Chemistry,* , no. 4, pp. 607-613.

9. Arduini, A., Caciuffo, R., Geremia, S., Ferrero, C., Ugozzoli, F. and Zontone, F. (1998), "Temperature dependence of the weak host-guest interactions in the p-tertbutylcalix[4]arene 1:1 toluene complex", *Supramolecular Chemistry,* vol. 10, no. 2, pp. 125-132.

10. Çapan, R., Ozbek, H., Goktas, H., Sen, S., Ince, F. G., Ozel, M. E., Stanciu, G. A., Davis, F. (2010), "Characterization of Langmuir-Blodgett films of a calix[8]arene and sensing properties towards volatile organic vapours", *Sensors and Actuators B: Chemical*, vol. 148, pp. 358-365.

11. Steed, J. W. and Atwood, J. L. (2009), *Supramolecular Chemistry,* Second Edition, John Wiley & Sons, Ltd.

12. Andreetti, G. D., Pochini, A. and Ungaro, R. (1983), "Molecular inclusion in functionalized macrocycles. Part 6. The crystal and molecular structures of the calix[4]arene from p-(1,1,3,3-tetramethylbutyl) phenol and its 1:1 complex with toluene", *Journal of the Chemical Society, Perkin Transactions 2,* , no. 9, pp. 1773-1779.

13. Nishio, M., Umezawa, Y., Honda, K., Tsuboyama, S. and Suezawa, H. (2009), "CH/π hydrogen bonds in organic and organometallic chemistry", *CrystEngComm,* vol. 11, no. 9, pp. 1757-1788.

14. Hassan, A. K., Ray, A. K., Nabok, A. V. and Wilkop, T. (2001), "Kinetic studies of BTEX vapour adsorption onto surfaces of calix-4-resorcinarene films", *Applied Surface Science,* vol. 182, no. 1-2, pp. 49-54.

15. Rehwagen, M., Schlink, U., Herbarth, O. and Fritz, G. J. (1999), "Pollution profiles at different kindergarten sites in Leipzig, Germany", *Environmental toxicology,* vol. 14, no. 3, pp. 321-327.

16. Lee, C., Dai, Y., Chien, C. and Hsu, D. (2006), "Characteristics and health impacts of volatile organic compounds in photocopy centers", *Environmental research,* vol. 100, no. 2, pp. 139-149.

17. Angerer, J., Schildbach, M. and Krämer, A. (1997), "S-p-Toluylmercapturic acid in the urine of workers exposed to toluene: A new biomarker for toluene exposure", *Archives of Toxicology,* vol. 72, no. 2, pp. 119-123.

18. Yang, J., Yang, L., Xu, C. and Li, Y. (2007), "Optimization of cladding-structure-modified long-period-grating refractive-index sensors", *Journal of Lightwave Technology,* vol. 25, no. 1, pp. 372-380.

19. Nabok, A. V., Hassan, A. K. and Ray, A. K. (2000), "Condensation of organic vapours within nanoporous calixarene thin films", *Journal of Materials Chemistry,* vol. 10, no. 1, pp. 189-194.

20. Senior, J. M. (1992), *Optical fiber communications : principles and practice,* Second Edition, Prentice Hall.

21. Fraden, J. (2010) *Handbook of Modern Sensors : Physics, Designs and Applications,* Fourth Edition, Springer.

22. Patterson, B. A., Lenney, J. P., Sibbett, W., Hirst, W., Hedges, N. K., Padgett, M. J. (1998) "Detection of benzene and other gases with an open-path, static Fourier-transform UV spectrometer", *Applied Optics*, vol. 37, no. 15, pp. 3172-3175